Analysis and Synthesis of Aircraft Engine Fan Noise for Use in Psychoacoustic Studies

Matthew Paul Allen

Thesis submitted to the faculty of the
Virginia Polytechnic Institute and State University
in partial fulfillment of the requirements for the degree of

MASTER OF SCIENCE

in

Mechanical Engineering

Ricardo A. Burdisso, Chair
Stephen A. Rizzi
Christopher R. Fuller

April 18th, 2012
Blacksburg, Virginia

Keywords: Turbofan Noise, Complex Analysis, Tonal Synthesis, Broadband Synthesis, Psychoacoustics

ANALYSIS AND SYNTHESIS OF AIRCRAFT ENGINE FAN NOISE FOR USE IN PSYCHOACOUSTIC STUDIES

Matthew Paul Allen

ABSTRACT

Community noise impact is an important factor in design of current generation aircraft, especially when considering projected trends in flight volume and urbanization. Simulation is a useful tool to evaluate the human annoyance response due to both current and proposed aircraft, and it has some advantages over field studies or playback of recordings. However, current simulation methods which are based on time-averaged prediction methods do not include short term fluctuations observed in recordings of real aircraft engines. Those fluctuations in both tonal and broadband sources provide psychoacoustic clues to listeners when evaluating flyover noise realism. When those short-term fluctuations are not included, simulation realism may suffer and evaluation results might not be applicable to real aircraft.

This thesis presents work to analyze and model fluctuations in aircraft engine fan noise, using an existing set of static turbofan engine recordings. The inclusion of the observed fluctuations, which are unaccounted for in many current prediction and simulation routines, was expected to increase the perceived realism of simulated flyover events. The analysis of tonal fluctuations was performed by utilizing the complex-valued analytic signal to extract instantaneous amplitude and frequency. A simple parametric model was developed to represent each measured fluctuation using its spectral bandwidth and variance. The model was then used to generate new fluctuations which were perceptually similar to the original. Tonal synthesis was performed as the sum of many amplitude- and frequency-modulated tones. Analysis was also performed on the broadband fan noise component, which used output from the Short-Time Fourier Transform was used to characterize fluctuations in third-octave band SPL. Those fluctuations were not modeled as in the case of tonal fluctuations and were directly reproduced using an overlap-add synthesis tool.

A subjective listening test was then conducted to evaluate the perceptual similarity between synthesized and recorded fan noise. That test concluded that synthesized tonal noise which included short-term fluctuations was perceived as more realistic than noise without. It also concluded that the addition of broadband fan noise components tended to mask tonal fluctuations.

Acknowledgments

I am very thankful to my advisory committee for providing support and guidance on the various stages of this thesis research. Working with them for the past two years on a wide range of topics has had a profound influence on my development as a scientist and a researcher. I'd like to specifically thank my NASA mentor, Dr. Steve Rizzi, for many long discussions and for always pushing me to improve myself.

I would like to thank Aric Aumann for his contributions to the synthesis aspects of this thesis, and for working through my confusing MATLAB code so that I could see my results in use. Dr. Selen Okcu provided wonderful support through my second year, both as a research partner for subjective evaluations and as an encouraging voice while writing the thesis itself. Finally, I'd like to express my gratitude to the researchers in the Structural Acoustics Branch at NASA Langley Research Center, who have all provided me with valuable insight in one way or another.

I also wish to acknowledge Honeywell Aerospace for their role in producing the high quality data set required for this work. Specifically, I'd like to thank Don Weir for his helpful discussions regarding measured data and for evaluating the accuracy of corresponding predictions.

This work was supported by the Subsonic Fixed and Subsonic Rotary Wing Projects of the National Aeronautics and Space Administration (NASA) Fundamental Aeronautics Program, through a cooperative agreement (NNL09AA00A) with the National Institute of Aerospace (NIA) entitled "Analysis and synthesis of tonal noise sources for fixed and rotary wing aircraft" (NIA Activity Number 4740-009). I am greatly indebted to both organizations for their financial support.

Table of Contents

List of Figures

List of Tables

1 Introduction

Fixed and rotary wing aircraft operations can have a significant impact on communities in proximity to airports. Continuing trends in urbanization and flight volume will serve to increase annoyance responses in the future, unless accompanied by reduced noise impact. The US Federal Government regulates the allowable community noise impact of commercial aircraft operations through the Federal Aviation Administration (FAA), which has instituted noise standards for in-service aircraft. Those standards are implemented according to methods described in Federal Air Regulations. Noise prediction and simulation routines allow manufacturers to estimate the noise impact of a proposed aircraft or operation during the design stages. Feedback for those prediction routines is often generated by annoyance evaluation of in-service aircraft.

Traditionally, recordings of flyovers are presented to listeners for annoyance evaluation. Synthesized flyover noise has advantages over recordings since it is much less expensive, allows more control over experimental variables, and can be used for unconventional designs where current metrics may not accurately capture annoyance response. However, current simulation methods do not account for all observed qualities of engine noise, namely short term fluctuations which contribute significantly to perceived realism. This chapter details historical motivations for regulating, predicting, and simulating aircraft flyover noise, as well as how those simulations may be improved through the addition of short-term fluctuations.

1.1 Community Noise Impact

Aircraft flyovers can have a significant noise impact, especially on residential and business communities in proximity to airports. That impact is heightened when take-off and approach operations occur at low elevations. This section describes regulations applicable to aircraft flyover noise, detrimental effects of that noise, and industry forecasts which show that community noise will continue to play a large role in aircraft certifications.

1.1.1 Noise Standards

The FAA has historically maintained noise standards which govern the allowable community noise impact of in-service aircraft. Guidelines for calculating the noise impact according to those standards are expressed in Title 14 of the Code of Federal Regulations (CFR), and are known as

Federal Air Regulations (FAR). FAR part 36 and FAR part 150 are the sections which deal most directly with the community impact of aircraft flyover noise [1, 2]. The FAR 36 standard specifies what metrics apply to various aircraft categories, and mandates conditions under which the applicable noise measurements must be acquired. Metrics relevant to the FAR 36 standard take into account psychoacoustic research which relates qualities of measured noise to human annoyance response. Common metrics include Effective Perceived Noise Level (EPNL), tone-corrected perceived noise level (PNLT), and Sound Exposure Level (SEL), which include adjustments for the duration and tonal content of flyover events as measured at several points in the community [3, 4]. The FAR 150 guideline defines precise calculations and limitations for allowable noise levels in certain zones surrounding airports. As part of certification according to the FAR 150 standard, noise exposure maps are generated for each airport which describe noise contours for A-weighted sound pressure levels, as well as day-night adjusted levels.

The FAR 36 guidelines have been amended several times to provide for and mandate decreasing noise emissions from commercial aircraft. A plot which shows the decreasing trend in the community noise impact of in-service aircraft relative to FAA guidelines is shown in Figure 1. The vertical axis represents average margins with respect to three certification points (at takeoff, cutback, and approach). The "Stage 2" standard, instituted in 1969, was developed to set limits on newly designed aircraft, and was eventually replaced by the "Stage 3" standard in 1977. As aircraft noise impact decreased further, the guidelines became stricter; "Stage 4" standards were instituted in 2004 to reflect that trend. Also shown in Figure 1 (as yellow diamonds) are entry-into-service (EIS) goals from several recent NASA research projects conducted to investigate integrated technologies for aircraft noise reduction. Each EIS goal also lists the corresponding cumulative margin which would result if the reduction goal was achieved at each certification point.

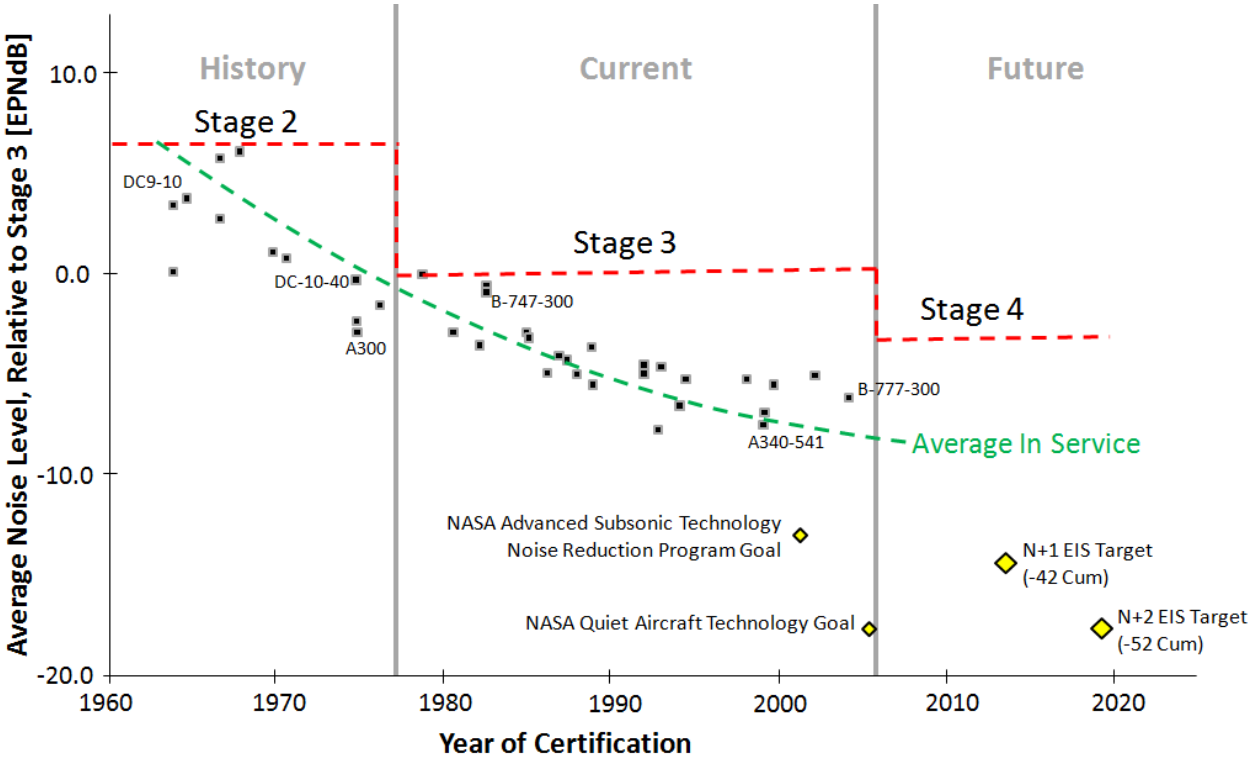

Figure 1. Progress in in-service aircraft noise reduction with respect to FAA noise level standards, with several aircraft labeled. Adapted from [5].

1.1.2 Annoyance to Flyovers

Community noise reduction efforts date back to at least the 1950's when the National Advisory Committee for Aeronautics (NACA) initiated preparations for the forecasted entrance of turbojet engines into commercial service [6, 7]. The development of turbofan engines, while driven primarily by fuel efficiency concerns, had the added benefit of significant noise reduction over turbojet engines in service at the time. However, the addition of the fan itself at the engine intake added several new noise generation mechanisms, among them significant tonal components which contribute to increased annoyance. Military vehicles also benefitted from the introduction of the turbofan engine, both by reduced fuel consumption and by reduced noise signature during operations.

Current generations of commercial aircraft, while significantly quieter overall than 1950's era turbojet-powered vehicles, maintain significant annoyance levels in communities surrounding airports. Adverse effects resulting from flyovers in populated areas have been well documented and include loss of sleep and reduction of speech intelligibility, in addition to general feelings of discomfort and annoyance [8]. In some extreme cases, compensation is paid to residents whose

homes fall inside of certain noise map contours. The reader is referred to ref. [8] for a summary of past work relating to adverse effects of flyover noise.

To reduce perceived aircraft noise and thus address community annoyance to frequent flyover events, several funded activities are in progress by government organizations in partnership with industry groups. One example is the NASA Environmentally Responsible Aviation project (ERA), which seeks to develop simultaneous aircraft noise and emissions reduction for aircraft two generations ahead of those currently in service. The ERA goal for cumulative noise reduction is 42 dB below the FAA stage 4 standard (52 dB below Stage 3), relative to a large twin aisle reference configuration [9].

1.1.3 Air Traffic Forecasts

In general, air traffic is projected to increase significantly over the next several decades when evaluated according to several metrics, most notably Revenue Passenger Kilometers (RPK). Historically, air traffic has doubled by that measure every 15 years since 1976 and current data shows this trend continuing [10]. By 2025, Airbus projects that North America and Europe will see nearly double the amount of air traffic relative to 2010 levels. Total plane movements (both passenger and freight) will also double in that time period according to the Airports Council International [11]. Factors driving the increase in demand for air travel worldwide include a larger trend in urbanization, the expanding global middle class, and a demand for access to flight in emerging economies. This growth is anticipated to lead to substantial increases in orders for new aircraft, specifically in the mid-size commercial category. For example, according to Airbus and Boeing reports, about 70% of new aircraft deliveries over the next 20 years will be single-aisle, utilizing turbofan engines in the 7,000 to 9,000 lb thrust category [10, 12]. Annoyance problems due to an increase in air traffic will thus be compounded by increasing population density near airports without further source noise reduction.

1.2 Flyover Noise Prediction

The aircraft flyover noise problem represents a significant factor in the design process for commercial vehicles, for the reasons mentioned earlier. In order to measure the impact before production, noise emissions which will result from vehicles or operations in the design stages must be evaluated according to the relevant community noise metrics. Of course, for designs where no

working prototype exists, noise evaluations must be based on some prediction or characterization. Aircraft flight operations which are not currently in use (such as continuous descent approach) must also use predictions to evaluate their community noise impact. This section details the historical motivation and outcomes of aircraft noise prediction efforts.

1.2.1 Historical Background

Many noise reduction efforts before 1950 were motivated by military concerns, and typically addressed turbojet, ramjet, pulsed jet, or rocket sources [6, 13]. In the late 1950's, turbofan engines emerged as a fuel efficient replacement for turbojet engines, with the added benefit of a large reduction in overall noise emission. With the introduction of the first commercial turbofan engines, turbomachinery and the relevant noise generation mechanisms rapidly became topics of interest. Work was initiated to predict propagating duct modes, identify and characterize important tonal and broadband noise sources, and predict total source noise generation based on engine geometry and performance specifications [14, 15]. Particularly about 1960, work began to identify relationships between engine parameters and the resulting noise. Due to the complicated nature of turbomachinery noise and the inadequacy of available numerical techniques, many approaches at this time were empirically based, fitting analytical models to observed data. Work performed by independent teams was summarized in 1971, and subsequent attention was turned primarily toward identification of mechanisms producing broadband and multiple-pure-tone noise (MPT, also known as "buzz-saw") [15]. However, assessing the accuracy of predictions was difficult since the available data only represented a small subset of the turbofan engines in service. Where data was available, its quality was often low, making it unsuitable for comparison.

For the purpose of combining existing results and directing future research, the National Aeronautics and Space Administration (NASA) formed the Aircraft Noise Prediction Office (ANOPO) at NASA Langley Research Center in 1973. ANOPO was designed to be the "focal point" for NASA aircraft source noise prediction activities [16].

1.2.2 Aircraft Noise Prediction Program (ANOPP)

A major task of ANOPO was the development of a comprehensive Aircraft Noise Prediction Program (ANOPP) [17]. The effort had the goals of identifying major noise sources and desired levels of prediction fidelity while keeping a focus on practical implementation. As part of ANOPP development, several investigations into specific noise sources and radiation effects were completed,

such as low frequency core noise, fan and compressor noise, jet noise, and externally blown flap noise [16]. In addition, flow field noise, duct acoustics, and noise propagation were identified as areas for improvement in the understanding and prediction of flyover noise.

Since the initial release of ANOPP and its subsequent adoption by commercial vendors for prediction of flyover noise, periodic comparisons to modern measurements and corresponding updates to empirical methods have been made. Notably, in 1996, modifications to all components resulted in the "Improved NASA-ANOPP Code" [18]. The most current version of ANOPP includes options to perform fan noise prediction in three different fashions, corresponding to updated methods. A second-generation code (ANOPP2) is currently under development [19].

1.3 Simulation and Synthesis

Just as advances have been made over several decades in the ability to predict aircraft noise, corresponding advances have been made in the methods available which present that noise to listeners for evaluation. Since metrics were originally developed through correlation with human annoyance responses, it can be beneficial to present noise directly to listeners. For unconventional aircraft, such as the hybrid wing-body configuration under evaluation by the ERA project, it may even be more desirable to directly evaluate annoyance. This section describes how simulations of aircraft noise may be advantageously used in a simulated outdoor environment to gauge human annoyance response to proposed designs.

1.3.1 Comparison with Other Methods

The three traditional methods of evaluating flyover annoyance are field studies with actual flyovers, playing recordings of actual flyovers in a laboratory environment, or simulating the entire flyover event [20]. Field tests are understandably expensive, as are obtaining and playing back quality recordings of actual flyovers. In addition to expense, the usefulness of a given recording may be limited because it represents only one flight trajectory and one set of ambient conditions. Specific flyover events are prohibitively difficult to replicate, since small changes in atmospheric conditions can result in large differences in noise received by the listener [8]. Furthermore, exactly what each listener is hearing during a flyover is unknown and may vary considerably even between listeners in close proximity.

For these reasons, playback of recorded flyovers in a laboratory environment is generally preferable to presenting them in the field. In the laboratory, the same flyover event may be presented multiple times in exactly the same way. Additionally, the same flyover may be presented at different levels [21]. However, even recordings of actual flyovers are met with severe limitations. First, recordings require that a working prototype exists and is available for testing. Once a recording is made, the noise still represents only a single set of conditions. Whatever atmospheric or listener effects were present when the recording was produced will be present when it is reproduced. Studies which might investigate the effects of including or excluding various atmospheric factors on the perceived noise are not possible.

Presentation of simulated noise thus gives the researcher the most control over experimental conditions. Evaluations may be conducted at a wide variety of conditions and presented multiple times in exactly the same way. For example, various weather conditions may be directly evaluated for their effect on annoyance. However, the increase in experimental control places a different sort of burden on the researcher, depending on the presentation environment and desired accuracy of the result. Researchers must ensure that each phase of the simulation process is a realistic analog of the real-world effect. For example, ground reflections are an important part of most simulations, since they result in a comb-filter characteristic which listeners tend to associate with real flyover noise. Effects due to frequency-dependent attenuation in the atmosphere or complicated wind and temperature gradients must also be accurately modeled and reproduced. Playback systems designed to simulate the total environment must have memory and processing power capable of executing multiple time-domain processing routines, which imposes significant hardware investments. This list is not exhaustive; it only serves to illustrate that the advantages of using virtual simulations of aircraft flyovers demand a high level of attention to a variety of problems.

1.3.2 Previous Simulation Efforts at NASA Langley

NASA Langley Research Center has been pursuing efforts to simulate realistic flyover noise since the creation of ANOPO. The first simulation effort was called the Aircraft Noise Synthesis System (ANOSS), developed by Time/Data Corporation beginning in 1976. ANOSS was capable of presenting a simulated flyover event to the listener in one of several laboratory environments, and included support for broadband, narrowband, and pure-tone spectral components. In addition, the system handled realistic propagation effects including Doppler shift, atmospheric effects, and ground

reflections [22]. Flyover noise synthesized using ANOSS was typically presented either over headphones or over a loudspeaker system.

In the late 1980's, a second generation Aircraft Noise Synthesis System (ANOSS II) was developed due to limitations in the original system [20]. Specifically, there were doubts about the ability of the system to translate input spectra into output time histories, as well as support for a limited number of synthesized tones. The second-generation system addressed these concerns, as well as adding capabilities which allowed more complete specification of flight trajectories. In addition, ANOSS II improved modeling capabilities for source directivity patterns, atmospheric effects, and ground reflections.

Work on flyover noise simulation was initiated again in 2003, using more detailed synthesis and rendering technology. The focus at that time was broadband noise (primarily radiated from jet noise sources), and subsequent attention has been focused on improvements to tonal source noise synthesis techniques. Broadband synthesis included unsteady characteristics which were observed in real data but not accounted for in jet noise predictions. A real-time digital signal processor simulated Doppler shift, spherical spreading loss, atmospheric attenuation, and ground plane simulation over multiple surfaces. Head-tracking and HRTF filtering allowed test subjects to become fully immersed in the three-dimensional virtual environment. The environment also included visualizations which were rendered over head-mounted display while audio was presented over headphones. Those synthesis and rendering systems are in use currently, and are described in detail in the next section.

1.3.3 The Source/Propagation/Receiver Paradigm

The current simulation system used to generate and present noise to subjects has two parts, designated as the Aircraft Source Noise Generator (ASoNG) and the Community Noise Test Environment (CNoTE). Figure 2 shows a top-level summary of the simulation paradigm. Practically, the simulation process can be viewed in three sections: source noise synthesis, propagation through the environment, and rendering at the listener. ASoNG handles pre-processing and generation of multiple noise components at the source, while CNoTE is responsible for applying realistic propagation and receiver characteristics to the simulated source noise.

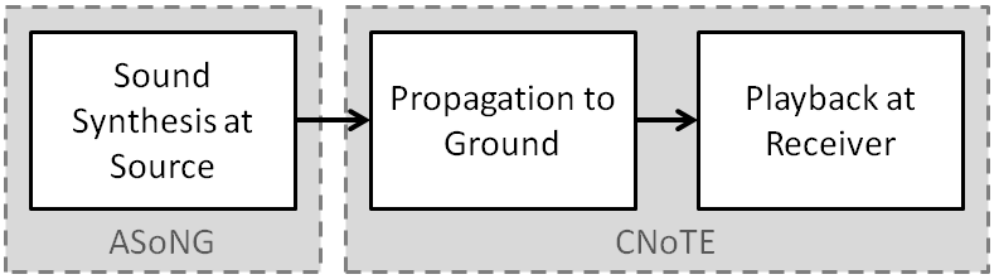

Figure 2. Synthesis and rendering procedure used in the current simulation paradigm.

A detailed flowchart describing ASoNG operation is shown in Figure 3. ASoNG begins with whatever prediction methods are desired or necessary to characterize noise at the source. This characterization may be provided in the form of directionally dependent pressure-time histories (as provided by some computational aeroacoustics routines) or time-averaged frequency spectra (typically provided by ANOPP) [17]. Source noise characterizations are obtained during a pre-processing stage for each component and are evaluated at points on a hemispherical grid around the source. Currently, a straight line path is assumed between source and observer. The intersection of the straight line path and the prediction hemisphere determines the appropriate emission angle at each point in the simulated vehicle trajectory. Source noise may be generated according to several methods, including frequency domain methods for either broadband or tonal types. Additionally, time-domain methods are available which accept direct specification of pressure-time history segments at relevant gridpoints. A given component may consist of one or more noise types, which are then mixed at each trajectory point.

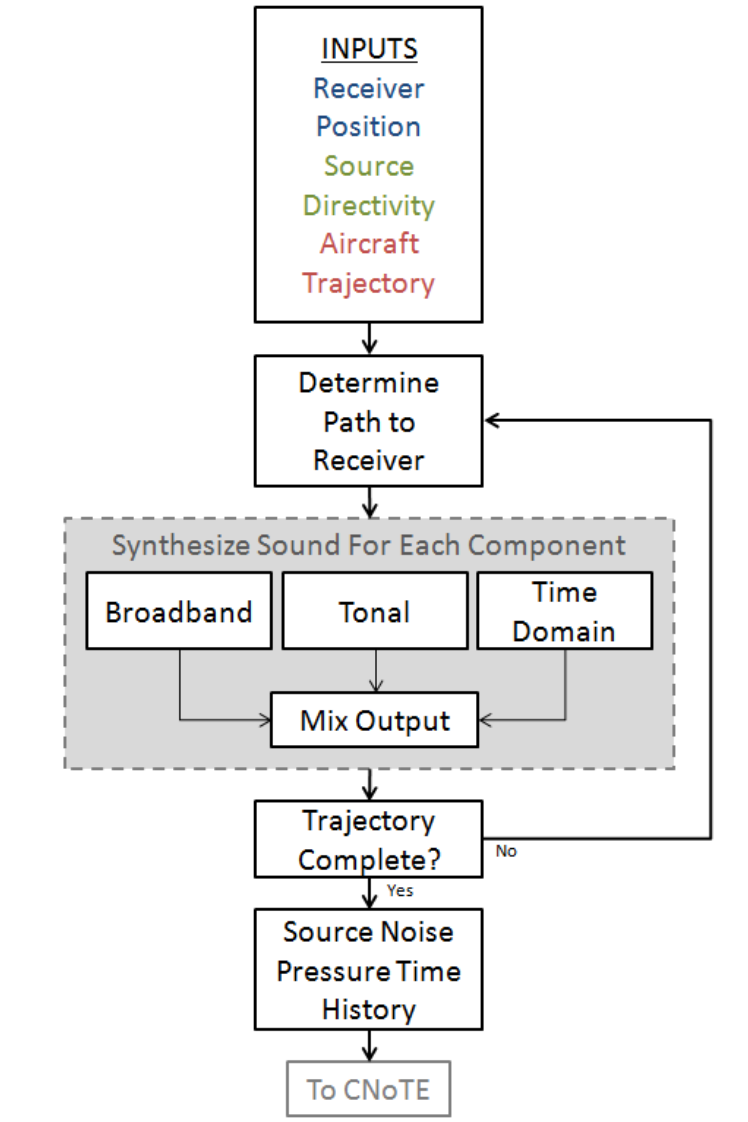

Figure 3. Description of ASoNG source noise generation process for a given vehicle trajectory.

While ASoNG carries out generation of source noise, CNoTE handles application of propagation and receiver effects. A flowchart detailing the operation of CNoTE can be seen in Figure 4. CNoTE begins with the source pressure-time history along the specified trajectory as calculated by ASoNG. Next, a variety of path-dependent effects are applied to the source noise. Currently, the system applies a time-dependent gain for spherical spreading loss, as well as time-dependent filtering to account for atmospheric attenuation and ground reflections. Ground reflections arise when source noise reaches the listener's ears along several paths. One of these paths directly reaches the listener, while the other reflects off the ground plane before reaching the listener after a short delay. Time-domain finite impulse response (FIR) filters are generated and applied depending on the ground

plane impedance model in use. At each time step, an absolute time delay is calculated for propagation time to the receiver; this has the benefit of inherently handling effects of Doppler shift due to a moving source.

Finally, the simulation system renders the propagated source noise to the listener. For binaural playback over headphones, an appropriate Head Related Transfer Function filter is employed to approximate attenuation and diffraction around the listener's head. When the signal is presented via three-dimensional speaker array, a process called Vector-Base Amplitude Panning (VBAP) is used [23]. Similar to left-right stereo panning in a typical playback system, VBAP varies the gains of three speaker elements at once to place the simulated source in three-dimensional space.

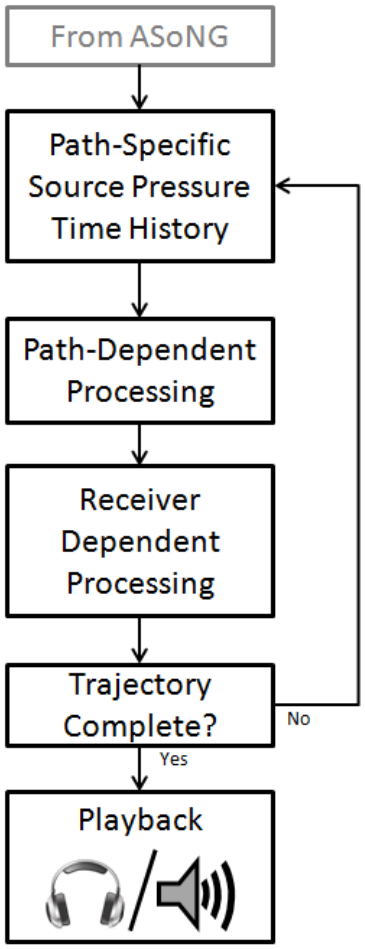

Figure 4. Simulation of propagation and receiver characteristics inside CNoTE.

1.3.4 Time-Invariant Simulation

Current simulation methods begin with source noise predictions. Those predictions, whether obtained from ANOPP or other computational routines, usually use time-invariant source noise parameters[1] which are derived from long-term averages of measured data. However, noise sources are not completely characterized by time-invariant parameters, since they include short-term fluctuations which were not captured by long-term averages. One specific area of interest to this investigation where this is the case is in tonal noise predictions. Tonal effects have been identified as a factor affecting annoyance response for several decades, while recent work noted the lack of time variations in synthesized source noise that were observed in recordings [24, 25]. Available evidence suggested that short-term fluctuations in both tonal and broadband noise sources contributed to the perception of source noise realism, while the absence of fluctuations damaged that perception. Psychoacoustic literature shows that time-domain fluctuations in source noise can be a significant discriminator for subjects [4].

1.4 Objectives and Problem Statement

The importance of evaluating the community impact of aircraft flyover noise during the design stage continues to grow. Flyover simulation is a useful tool to evaluate that annoyance by providing synthesized noise directly to listeners. However, simulation realism can suffer when using time-invariant predictions as the basis for source noise synthesis, since listeners use short-term fluctuations as psychoacoustic clues. The main aim of the work in this thesis is to increase the realism of simulated aircraft flyover noise. To that end, three main objectives were defined.

The first objective was the extraction of the described short term fluctuations using an existing set of engine recordings. For tonal noise, both the amplitude envelope and instantaneous frequency were of interest. The broadband noise source also contained short-tem fluctuations in third-octave band SPL. Tools were developed which used the complex-valued analytic signal to extract tonal parameters, and used the short-time Fourier transform to measure broadband fluctuations. The analysis tool developed is also applicable to general aircraft noise sources to improve its future usefulness. A simple parametric model was developed to represent each measured tonal fluctuation based on its spectral bandwidth and variance.

[1] Specifically: third-octave band SPL for broadband noise, amplitudes and frequencies for tonal noise.

A second objective was the development of synthesis tools capable of reproducing general time-varying tonal and broadband noise sources. Those synthesis tools do not operate in real-time, but should be easily modified to do so. It is the objective of NASA to integrate these tools into the broadband and tonal synthesis stages of ASoNG, as shown in Figure 3. Inputs to the synthesis routines could either be generated according to the model or directly supplied from measurements. Model parameters could be tied to engine power setting and emission angle when synthesizing the fan noise source for any arbitrary aircraft operation.

The final objective was the psychoacoustic evaluation of synthesized fan noise to verify that the inclusion of short-term fluctuations produced a more realistic result. A set of subjective listening tests was conducted with members of the surrounding community. Participants were asked to rate the similarity between noises synthesized according to current (time-invariant) methods, synthesized according to the proposed (time-varying) method, and actual engine recordings. Several engine power settings, emission angles, and types of spectral content were targeted by those evaluations. Results demonstrated that inclusion of short-term fluctuations which were modeled and synthesized according to the methods developed here improved the perceived realism of the tonal noise source. That improvement is diminished by the inclusion of a synthesized broadband noise source.

This document is structured as follows. Chapter 2 is dedicated to a general description of turbofan engine operation and noise emissions. It also describes specifics of the ANOPP prediction method for fan noise sources, and how those predictions relate to the set of recordings used for subsequent analysis and modeling. Chapter 3 describes the underlying theory of the analysis methods chosen, as well as how those methods were applied directly to recorded data for both tonal and broadband components. Chapter 4 first details the model used to describe extracted tonal fluctuations, then the synthesis tools developed to reproduce each source. Chapter 5 is included to describe the design and implementation of subjective listening tests which evaluated the analysis and synthesis methods. Finally, Chapter 6 sums up the work and examines the application of results to other noise sources and conditions.

2 Turbofan Noise Overview

Fan noise analyzed in this work was measured directly from an existing set of recordings made on a full-scale turbofan engine. Turbofan noise sources are temporally and spectrally complex, and consist of the combined emission from multiple generation mechanisms. This section provides an overview of turbofan engine operation, noise sources typically radiated from turbofan engines, as well as how those sources were observed and accounted for in measured data. Prediction methods inside ANOPP are discussed and related to recordings.

2.1 Turbofan Engine Operation

Turbofan engines are based on the operational principles of turbojet designs, which produce thrust using a multistage system made up of three general parts; compressor, combustion chamber, and turbine. Those three stages are collectively referred to as the "core." The major distinction of turbofan designs is the addition of the large fan at the engine inlet, which accelerates a portion of the incoming air through the core stages and diverts the rest through a duct around the outside (called the bypass section). Two axial shafts are generally used in turbofan engines; one shaft links the high-pressure turbine and the high-pressure compressor while another links the low-pressure turbine stages with the low-pressure compressor and fan rotor. Stationary airfoils called stators are installed between each stage to ensure that the flow maintains kinetic energy axially, rather than rotationally.

Thrust in turbofan designs is generated through a combination of air accelerated through the bypass and fuel-air mixture directed through the jet discharge nozzle. The proportion of air mass which is diverted around the core to the proportion of air mass which passes through the core is called the bypass ratio. By increasing the fan diameter and bypass ratio, manufacturers were able to generate more thrust, consume less fuel in the core, and lower the net exit velocity of the flow. Modern high-bypass turbofan engines increase fuel efficiency significantly by using bypass ratios of around ten, a benefit which is usually at a maximum for travel at high subsonic speeds.

A diagram of typical turbofan machinery is shown in Figure 5, with important sections labeled. The bypass and core air streams are usually then recombined at the engine discharge.

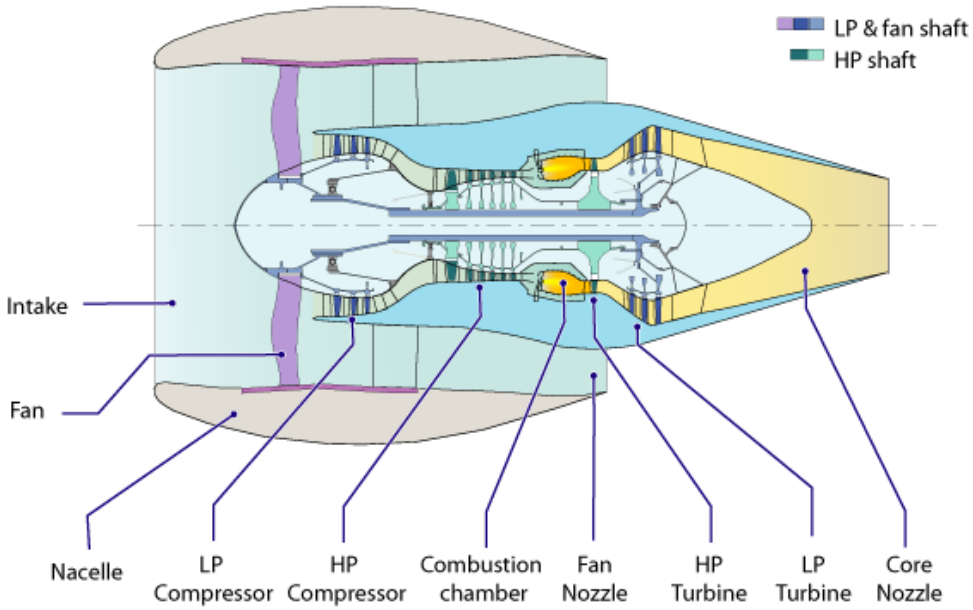

Figure 5. Schematic diagram illustrating the operation of a two-spool, high-bypass turbofan engine [26].

2.2 Noise Generation Mechanisms

Each stage of turbofan propulsion generates significant noise. An outline of a typical high bypass turbofan engine and major noise components is shown in Figure 6. The ovals show significant directivity regions and relative contributions from each component. The fan, through interaction with the stator vanes, produces noise which tends to be tone-dominated and radiated primarily forward. To a lesser degree, these fan "rotor-stator interaction" tones are transmitted through the bypass duct and out the engine discharge. Since it is the primary focus of this investigation, fan noise sources and the specific related mechanisms are discussed in greater detail in Section 2.3.

Noise radiating from each compressor stage also contains a significant tonal component. It should be noted that since the high-pressure compressor is attached to a different shaft and has a different number of blades than the fan, the tonal content it generates has a different fundamental frequency. Compressor noise is typically radiated forward. The low pressure turbine stages each have a different number of blades, so their tonal content also occurs at several frequencies. Turbine noise is mainly radiated to the rear of the engine.

Broadband noise from several sources is also an important part of the overall turbofan source, and often obscures tonal noise (especially in the aft arc). Noise from fuel burn inside the combustion

chamber represents a significant broadband noise source, along with jet noise caused by high-velocity flow at the discharge. Those sources generally contain energy concentrated in the range below 500 Hz. The radiation of jet noise to the far-field is greatly reduced relative to turbojet designs due to the addition of the mid-velocity bypass stream.

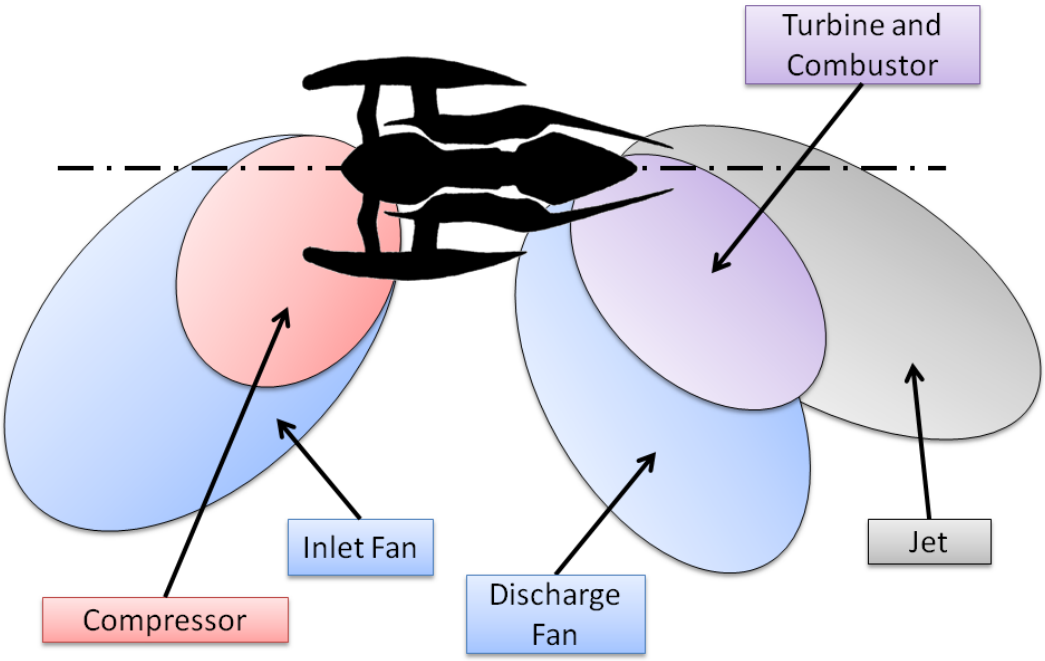

Figure 6. Diagram of a turbofan engine along with major noise components.

2.3 Heidmann Fan Noise Prediction Method

The fan noise prediction module inside of ANOPP is based on a model originally developed in the mid-1970's by Boeing in conjunction with NASA Ames Research Center [15, 27]. The so-called "Heidmann Fan" method consists of analytical functions whose major parameters were adjusted to fit available data. The analytical equations use mass flow rate and temperature rise across the fan stage as correlating factors to mechanical power and specific work. The model assumes that a small fraction of total engine power is converted to output sound power. Prediction of noise according to the Heidmann method and its subsequent updates takes into account operational factors such as forward flight Mach number and the presence of inlet flow distortions [18, 28].

The Heidmann Fan Module predicts five components of radiated fan noise; three inlet-radiated components and two discharge-radiated components. From the engine inlet, the Heidmann method predicts the radiation of a broadband component, a discrete tone component, and (at high

power settings) a multiple-pure-tone (MPT) component. The mechanism of generation for the broadband component is likely the sum of many sources "which are random in both time and location" [29]. Discrete tones are generated at multiples of the fan blade passage frequency (BPF) due to lift fluctuations on each blade and interactions between the fan rotor wakes and stator vanes. For this reason, tones at the fan BPF are often called "rotor-stator interaction" tones. Fan BPF tones are also predicted to propagate through the bypass duct and result in the discharge-radiated fan discrete-tone source.

MPT noise appears in measured spectra when the fan blade relative velocities are supersonic. At these conditions, shock waves form at leading edges of fan rotor blades and coalesce into a sawtooth pattern pressure wave. That wave then propagates upstream, out of the engine inlet, and to the far-field[2]. The sawtooth pattern displays periodicity associated with the rotational speed of the fan shaft, since small blade-to-blade manufacturing and installation differences diverted some energy away from the BPF and onto shaft order frequencies. The cut-on point for MPT noise in the Heidmann method is set at a relative flow Mach number of 1.05.

Each of the five noise components described are predicted by the Heidmann method as sound pressure levels at a user-specified radius around the engine. The predicted SPL for each component varies as a function of third-octave band frequency and emission angle. Practically, the Heidmann method specifies spectral shape, spectral level, and far-field directivity pattern for each noise component directly as a function of geometric and operational parameters. Noise components are then combined on an energy basis to obtain the total emission pattern as a function of third-octave band center frequency. The total fan component may then be combined with turbine, jet, compressor, and core components to obtain the total turbofan engine noise source. The total engine source may then be combined with other vehicle noise sources such as airframe noise generated by landing gear and high-lift devices.

Figure 7 shows one such Heidmann fan noise prediction[3] for a low engine power setting in the forward arc. The prediction was calculated for the TECH977 demonstrator engine; those tests are described in further detail in Section 2.4. Note that at low power settings, the MPT component is not predicted. Further, both the tonal and broadband inlet-radiated sources are dominant on the forward

[2] "Far-field" defines a radius sufficiently far from the source that all noise reaching the observer arrives at essentially one angle. The source radiation pattern is independent of distance in the far-field.
[3] Heidmann fan noise predictions shown in this thesis were calculated using the 1996 "Small Fan" update at a forward flight Mach number of 0 [28] .

arc. The total noise source, as combined from all predicted components, is shown in black. Figure 8 shows a fan noise prediction at another forward emission angle at a high power setting. The MPT source has cut on, and is shown by red diamonds as a dominant spectral feature. Once again, discharge radiated broadband and rotor-stator interaction tones are not a significant part of the total fan noise source in the forward arc. A fan noise prediction at the same high-power engine setting in the aft arc is shown in Figure 9. The forward-radiated MPT component remains dominant, though now the discharge-radiated broadband and rotor-stator interaction tones play a significant role in the total source. Figure 10 shows the total fan noise component as related to the other noise generation mechanisms in turbomachinery [30]. Note that, at the 60° emission angle pictured, forward-radiated fan and jet noise are predicted to be the dominant noise sources. Fan noise is the most significant component in the frequency range above about 1,000 Hz, while jet noise is most significant below that limit. Turbine and combustion components are not predicted to dominate the spectrum, with the exception of the turbine BPF tone which makes a contribution in the 6,300 Hz band.

The quantities predicted by Heidmann fan are time-averaged; that is, they are based on semi-empirical fits of available fan noise data measured over long time periods. For broadband noise, the third-octave band sound SPL is predicted to be one value for all time. Tones arising from rotor-stator interaction at the fan BPF are predicted to have a single frequency and pressure amplitude. Multiple pure tone noise is predicted with even less precision. The total energy contribution in each third-octave band from all shaft-order tones in that band is returned by the Heidmann Fan prediction. Assumptions must be made about the distribution of energy to specific tones if pressure amplitudes are to be obtained on that basis. The frequencies of fan shaft-order tones are also not returned specifically, but may be inferred if the fan shaft rotational speed is available. That inference is detailed in Section 2.6.

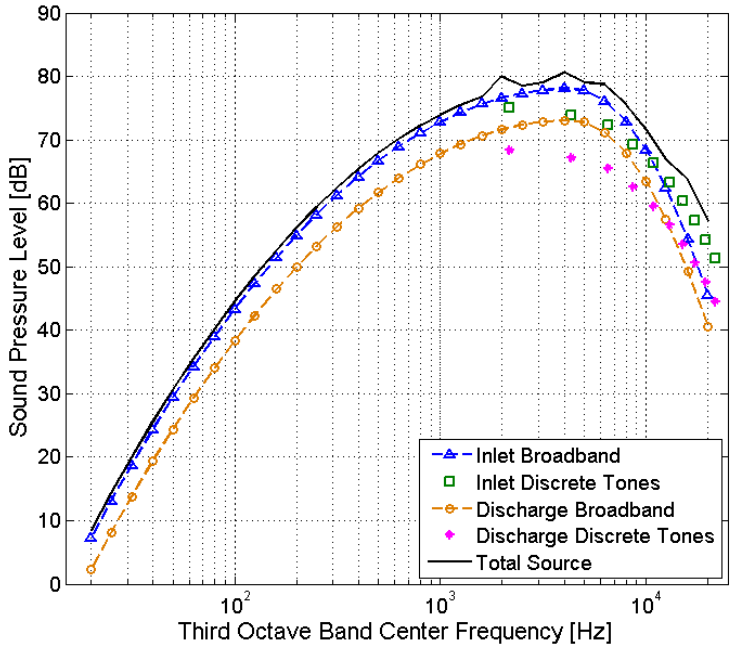

Figure 7. Heidmann Fan noise prediction for TECH977 engine at a low power setting in the forward arc (54% power setting, 20° emission angle).

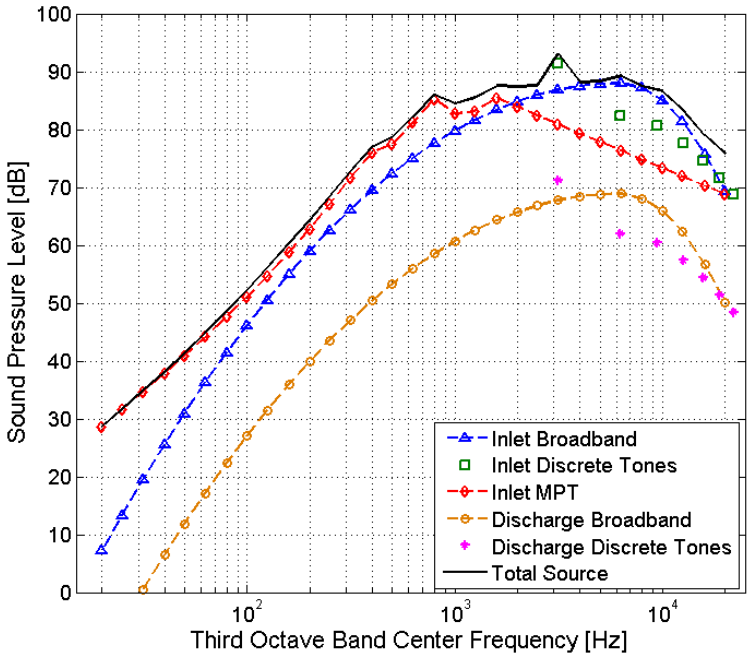

Figure 8. Heidmann Fan noise prediction for TECH977 engine at a takeoff power setting in the forward arc, containing a significant MPT component (87% power setting, 30° emission angle).

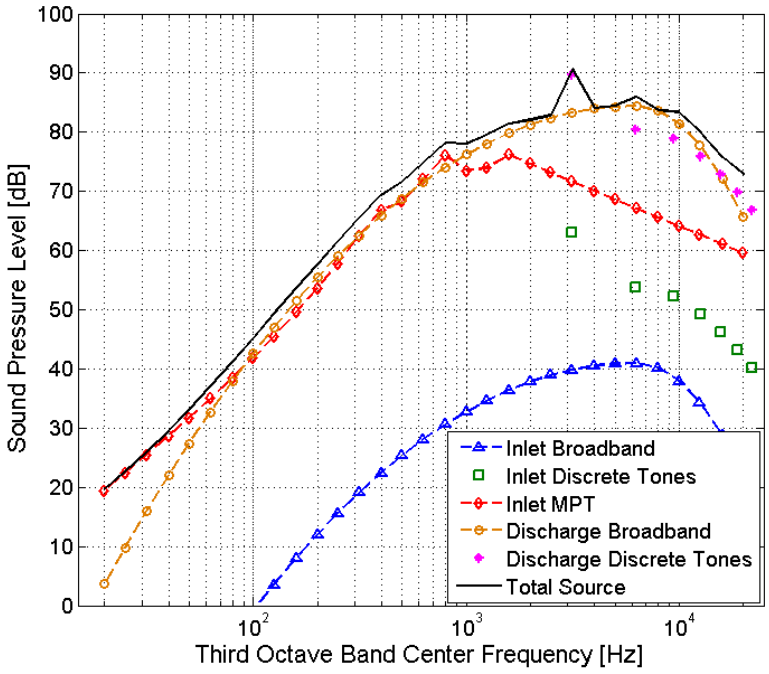

Figure 9. Heidmann Fan noise prediction in the rear arc for TECH977 engine at takeoff power setting, with a significant MPT component (87% power setting, 150° emission angle).

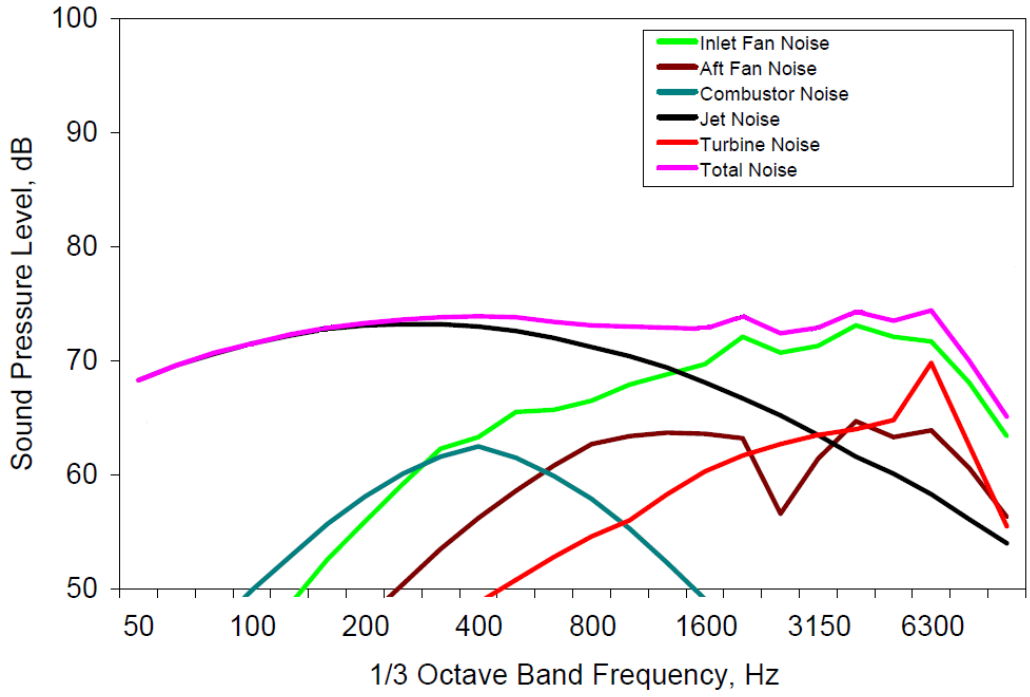

Figure 10. Total TECH977 ANOPP engine noise prediction, including total fan noise source (60% power setting, 60° emission angle). Adapted from [30].

2.4 EVNERT Experiment

The efforts to extract, analyze, and characterize short term fluctuations in fan noise were performed using an existing data set. The Engine Validation of Noise and Emissions Reduction Technology (EVNERT) tests were conducted jointly by NASA and Honeywell Aerospace from 2004 to 2007, and were designed "to evaluate several integrated technologies for noise reduction" [30]. A demonstrator engine was used for several of the tests, under the designation TECH977. Test conditions were intended to evaluate the noise reduction benefit of technologies such as inlet surface liners or sidewall C-ducts, relative to a baseline (unmodified) engine condition. Recordings of engine noise from the baseline configuration (number 19) were the focus of this investigation. A complete list of EVNERT test configurations can be found in Appendix A – EVNERT TECH977 Test Configurations.

Key performance parameters for the TECH977 engine can be found in Table 1. The TECH977 engine is a two-spool design, where the low-pressure shaft is designated as "N1" and the high-pressure shaft is designated "N2." The single stage fan, low-pressure compressor, and three-stage low pressure turbine (LPT) were all attached to the N1 shaft. The high-pressure compressor and corresponding two-stage high-pressure turbine were attached to the N2 shaft.

The TECH977 demonstrator engine was mounted in a static test stand; a photograph of the setup can be seen in Figure 11. An inlet flow control device was installed to minimize turbulence ingested by the engine which might affect the radiated noise, and it is also visible in the photograph. For the baseline engine test configuration, a wooden barrier was constructed around the engine discharge to shield aft-radiated sources from reaching the microphone array. That barrier is not shown in Figure 11. In addition, there was no inlet acoustic liner installed as there were on many other configurations.

Table 1. Key performance parameters of the TECH977 engine [31].

Parameter	Value	Units
Takeoff Thrust	7000	lb
Cruise Thrust	Rated to 1910	lb
Fan Diameter	34.2	in
Number of Fan Blades	22	--
Weight	1364	lb
Thrust to Weight Ratio	1.40	--
Engine Length	73	in
Pressure Ratio	28.7	--

Figure 11. Photograph of the TECH977 engine mounted in the test stand. An inlet flow control device can be seen mounted around the engine inlet [30].

As part of the EVNERT experiment, extensive data sets were collected from phased microphone arrays, rotating rakes, and far-field microphone arrays at a variety of test conditions. The far-field microphone array which was used to collect the data for the baseline configuration consisted of 32 microphones which were inverted on the ground in a 100 ft arc around the engine inlet. A diagram showing microphone array positions relative to the test stand is shown in Figure 12. Microphone #1 was placed five degrees off-axis from the engine inlet. Successive microphones were placed at five degree increments along the arc, until finally microphone #32 was placed at 160

degrees off-axis from the engine inlet. Pressure-time history recordings were made with the array at five power settings; they were 48, 54, 60, 71, and 87% of the engine design point for maximum fan (N1) shaft rotation speed. Each recording was sampled synchronously in all microphones at a rate of 32,768 samples per second for approximately 69.7 seconds. As a result of this data acquisition, a total of 160 calibrated pressure-time histories were obtained. Each pressure-time history was stored in units of Pascals.

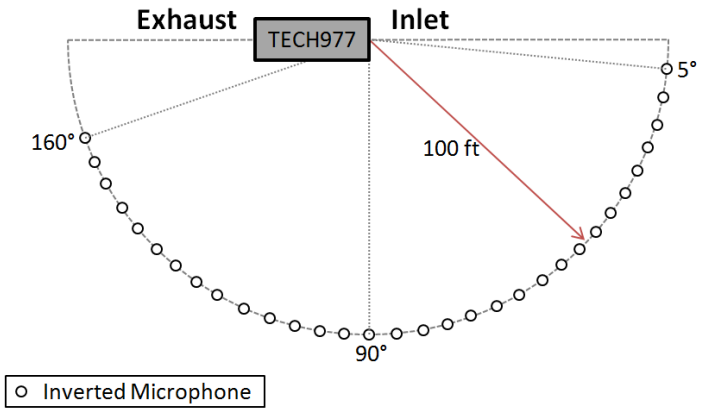

Figure 12. Diagram of the 32-microphone array used to capture recordings from the TECH977 engine.

The test log for configuration 19 is shown below in Table 2 and describes each run of data acquisition. Not shown are three runs whose data were not used in the current investigation, consisting of one acquisition of ambient noise and two acquisitions at maximum power setting. The fourth and fifth columns respectively show the rotation speed of the N1 (fan) and N2 (compressor) shafts in revolutions per minute (RPM). Rotational speeds in parentheses are in units of Hz. It should be noted that the entry for 48% power setting was later found to differ from the actual shaft rotation speed. The source of the discrepancy was unclear, but the N1 shaft rotation frequency as estimated from EVNERT measurements was 4,881 RPM (81.36 Hz). More information on the method for generating heuristic estimates of the N1 shaft rotation frequency can be found in Section 2.6.

Table 2. Test log showing relevant data acquisitions for EVNERT Configuration #19 (baseline).

Engine Condition, Power Setting	Date/Time	Thrust [lbs]	Physical N1 [RPM] (Hz)	Physical N2 [RPM] (Hz)	Engine Inlet Temp [F]
87%	9/28/05 3:27 AM	6007	8889 (148.15 Hz)	26340 (439.00 Hz)	87.5
71%	9/28/05 3:40 AM	3625	7250 (120.83 Hz)	24700 (411.67 Hz)	85.9
60%	9/28/05 3:50 AM	2470	6113 (101.88 Hz)	23470 (391.17 Hz)	85.6
54%	9/28/05 4:00 AM	1960	5520 (92.00 Hz)	22880 (381.33 Hz)	85.7
48%	9/28/05 4:09 AM	1515	4485 (74.75 Hz)	21880 (364.67 Hz)	85.9

2.5 Typical Recorded Spectra

A representative spectrum of the EVNERT recordings captured at low power settings can be seen in Figure 13. Spectra recorded in each microphone matched the expected general characteristics of fan noise as noted in Section 2.3. That is, the TECH977 engine noise displayed a significant tonal component at multiples of the blade passage frequency (BPF) at low fan power settings, with an underlying broadband noise source. One interesting feature of recorded spectra is the presence of a significant broadband component peaking near 400 Hz, most likely corresponding to the jet noise source. See Section 2.6 for a complete description of how various engine noise sources were identified and tied to spectral characteristics. Another feature evident from recorded spectra is the anti-aliasing filter used to ensure noise components above the acquisition Nyquist frequency were rejected. That filter can be seen to begin rolling off recorded spectra near 13,000 Hz.

Recordings made at high power settings contained MPT noise, though it was not completely dominant as expected. Instead, the MPT component was strong at angles near the engine inlet (about 5° to 50° off-axis), and dominant between angles of about 60° and 100° off-axis. Beyond that limit, all tonal noise was observed to roll off in amplitude. The spectrum shown in Figure 14 is representative of recordings captured at high-power settings where the MPT noise component was dominant. Shaft-order harmonics were observed over the entire recorded frequency range, though they decreased somewhat in amplitude as harmonic order increased. Broadband noise was also present in high-power recordings as expected, and the characteristic jet noise peak near 400 Hz was also present.

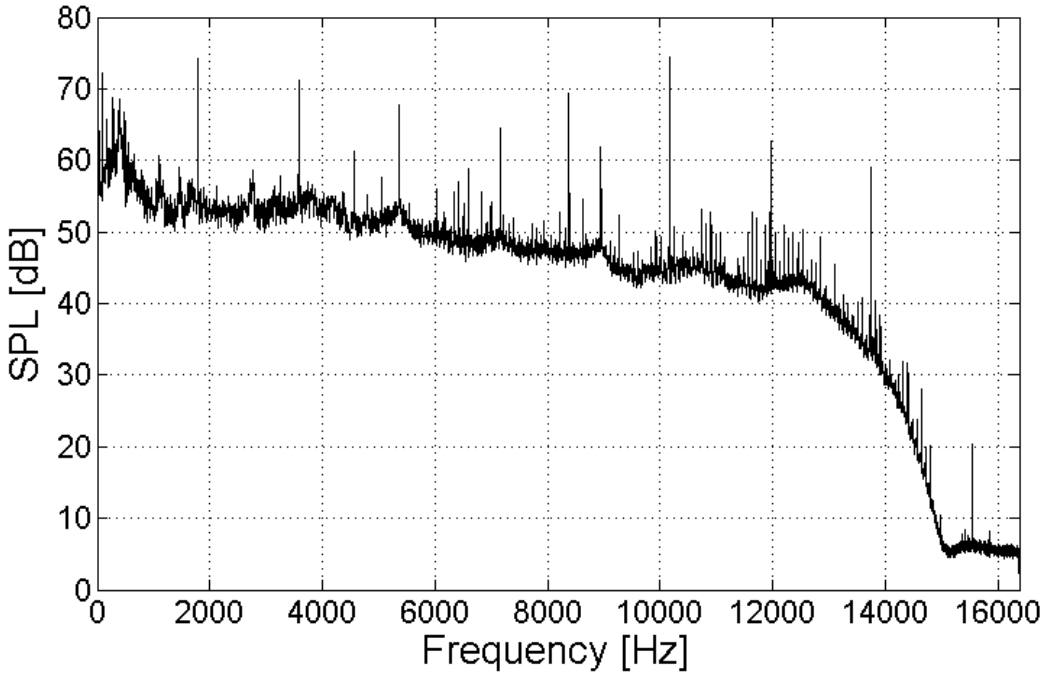

Figure 13. SPL spectrum of typical TECH977 recording at low power setting (48% power setting, 75° emission angle).

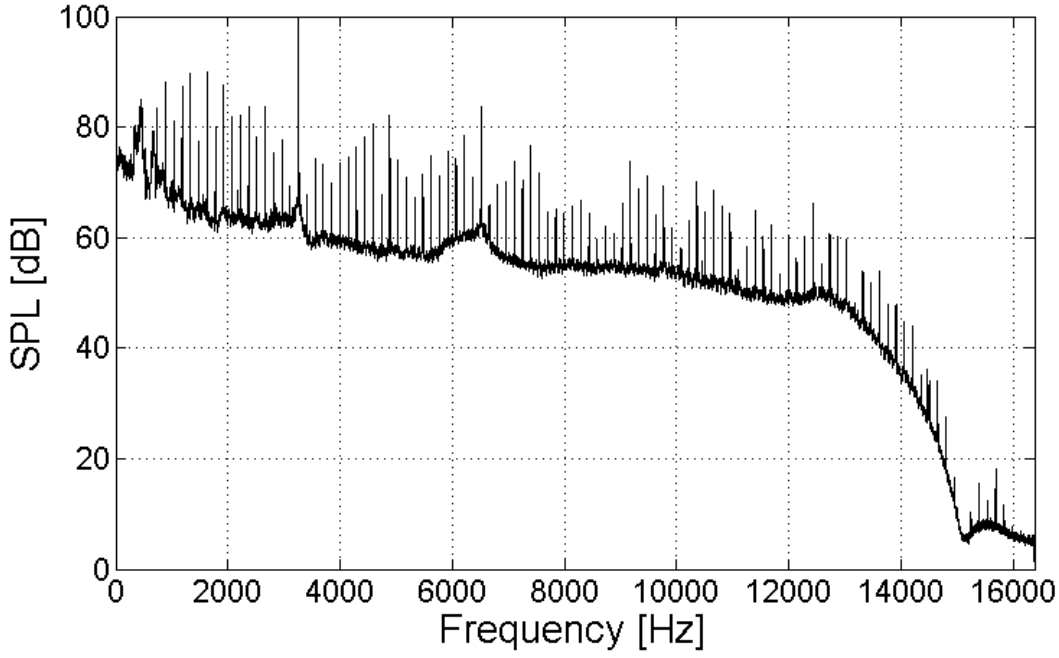

Figure 14. SPL spectrum of typical TECH977 recording at high power setting (87% power setting, 75° emission angle).

2.6 Heuristic Tonal Identification

Tonal signals may, in general, be identified using a variety of routines. The most common approach for blind tone identification is a peak-finding procedure applied to a representation of the signal energy as a function of frequency. However, knowledge of the geometry and operating conditions of the engine in a particular recording may be used to simplify the tonal identification procedure. Known generation mechanisms also play a role in defining expected locations of tones.

Blade passage frequencies were calculated simply by multiplying the appropriate shaft rotation frequency by the number of blades on the particular fan, compressor, or turbine stage of interest. Other generation mechanisms which transfer modal energy away from major sources are also responsible for tonal noise in a turbofan engine. For example, fan rotor-stator interaction tones arise at the fan blade passage frequency and at several multiples (harmonics). Additionally, at high power settings where the fan blade tips travel at supersonic speeds relative to the surrounding flow, tones arise at many harmonics of the fan (N1) shaft rotation frequency.

Knowledge of typical generation mechanisms was also used to predict the frequencies of tones which arose through interaction of several noise sources. Specifically, when the high pressure compressor tones propagated upstream and through the rotating fan blades, the resulting modulation generated sum-and-difference tones according to Equation (2.1)

$$f_{interaction} = BPF_{HPC} \pm N \cdot BPF_{FAN} \tag{2.1}$$

where $f_{interaction}$ are sum and difference frequencies in Hz arising from the interaction of compressor and fan tones, BPF_{HPC} is the blade passage frequency of the high pressure compressor in Hz, N is any positive integer, and BPF_{FAN} is the blade passage frequency of the fan in Hz.

Table 3 shows the results of estimating the BPF for the five major tonal generation mechanisms in the TECH977 engine. One problem was encountered, however, when identifying the fan rotor-stator interaction tone frequency in the 48% power setting recordings. The only significant tone apparent in the 1,500 to 2,000 Hz range in Figure 13 was evident at 1,790 Hz rather than the 1,644 Hz as implied by the N1 shaft rotation speed recorded in test logs. The reason for the discrepancy was not apparent. However, all subsequent analyses of recordings at 48% engine power setting were made on the assumption that N1 shaft frequency was actually 81.36 Hz as would be required to observe a 1,790 Hz fan BPF tone.

Table 3. Estimated BPF of several tonal generation mechanisms inside the TECH977 engine at acquisition power settings. Estimates not supported by observed spectra are shown in red text.

Performance Parameters			Estimated BPF [Hz]				
Power Setting [%]	N1 Shaft Rotational Speed [Hz]	N2 Shaft Rotational Speed [Hz]	Fan (N1) 22 blades	Compressor (N2) 23 blades	LPT 1 (N1) 56 blades	LPT 2 (N1) 62 blades	LPT 3 (N1) 74 blades
48	74.8	364.7	1644.5	8387.4	4186.0	4634.5	5531.5
54	92.0	381.3	2024.0	8770.6	5152.0	5704.0	6808.0
60	101.9	391.2	2241.4	8996.9	5705.3	6316.6	7539.1
71	120.8	411.7	2658.3	9468.4	6766.5	7491.5	8941.4
87	148.2	439.0	3259.3	10097.0	8296.4	9185.3	10963.1

The tonal analysis in the current investigation focused on inlet-radiated tones, as would be predicted by the ANOPP Heidmann fan module. Amplitude envelope and instantaneous frequency were not extracted for turbine, compressor, or compressor-fan interaction tones. However, identification of those tones was a useful exercise since their locations were used to refine other analyses. For example, the accuracy of the broadband analysis technique described in Section 3.2 was improved by ignoring bins known to contain tonal components from turbine, compressor, or compressor-fan interaction mechanisms.

Figure 15 shows a representative SPL spectrum of EVNERT recordings made at low power settings, along with significant noise sources identified. In the forward emission arc, the fan rotor-stator interaction and high-pressure compressor BPF tones were evident. Several harmonics of the fan rotor-stator interaction tones were also identified, and are denoted by dark blue arrows. Low pressure turbine tones from each stage were observed in the forward arc, albeit at levels approximately 15 dB below the fan rotor-stator tone BPF. Another significant tonal component observed, especially at low power settings, was the interaction source between the high pressure compressor and the fan. Those fan/compressor interaction tones were observed at evenly spaced intervals of the fan rotor-stator tone BPF, centered on the compressor fundamental as expected (green arrows). Another important component identified in recordings was due mainly to jet noise, and was dominant in the region below 500 Hz. Special consideration was given to this region in all subsequent analysis, synthesis, and evaluation stages. For example, jet and combustion noise were filtered out of recorded noises during presentation to listeners in subjective evaluations.

Overall, the turbofan source was much louder in each component at high power settings. At high power settings as shown in Figure 16, tonal noise generated by turbine, compressor, and

compressor/fan interactions was not dominant. Rather, the MPT source masked them. This was especially evident at turbine tone frequencies, which were predicted to arise at N1 shaft orders anyway. All energy in those tones was assumed to have been generated by the MPT source.

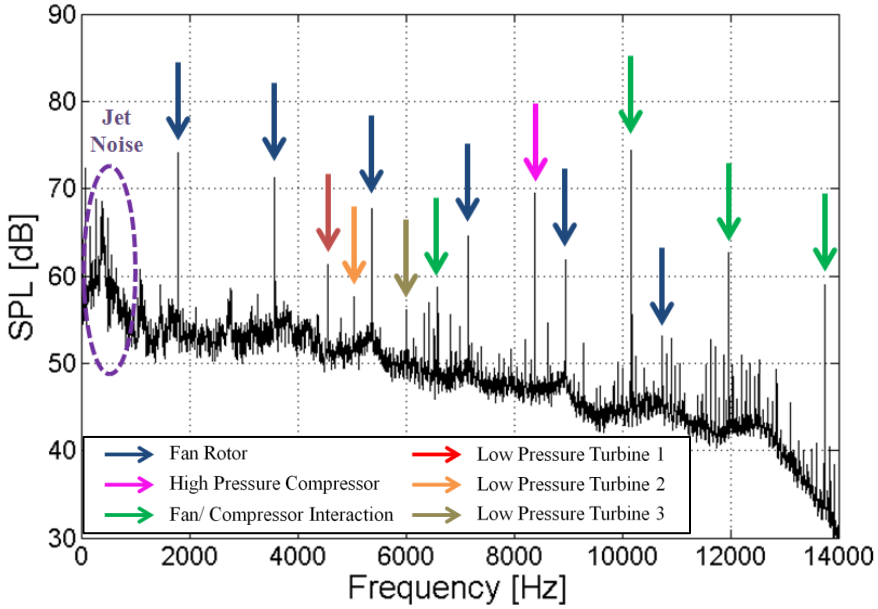

Figure 15. Recorded EVNERT spectrum with major noise sources identified (48% power setting, 75° emission angle).

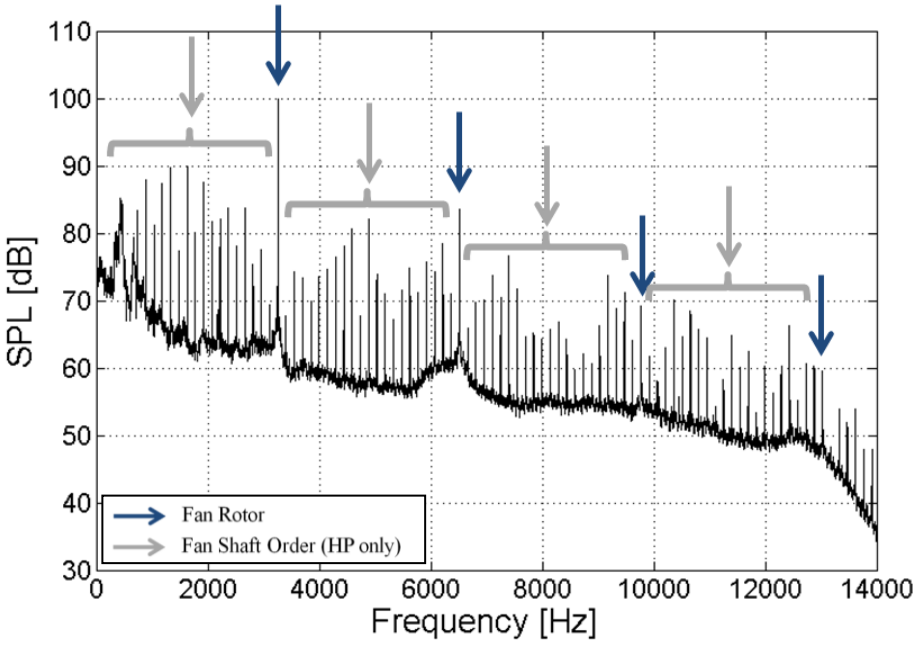

Figure 16. Recorded EVNERT spectrum with relevant noise sources identified (87% power setting, 75° emission angle).

Lastly, not all tones identified using the heuristic procedures were apparent in all measured spectra. Since predictions for which specific BPF or fan-order tones would be cut on at a specific operation point or emission angle were unavailable, some further work was performed to evaluate whether a predicted tonal location actually contained energy significantly above that of the background noise. This work, including estimation of a time-varying noise floor for each tone and post-processing to correct regions where tones fall below that noise floor, is discussed in Section 3.5.

Signals recorded from the EVNERT tests, when viewed as a time-frequency representation, also revealed important information. A noise source separation was performed by isolating the first three fan BPF tones in Figure 15. A spectrogram was then generated, and revealed that measured tonal noise was indeed fluctuating as a function of time. Amplitude fluctuations are visible in the peak of each tone of the spectrogram shown in Figure 17. The figure frequency scale does not have sufficient resolution to illustrate fluctuations in tonal frequency, though they are occurring. The presence of the fluctuations observed in tone-isolated noise is hypothesized to result in perceptual differences between recordings and prediction-based source noise synthesis. The remainder of this investigation is concerned with analyzing, characterizing, and synthesizing time-domain fluctuations observed in EVNERT data but not accounted for by time-averaged predictions.

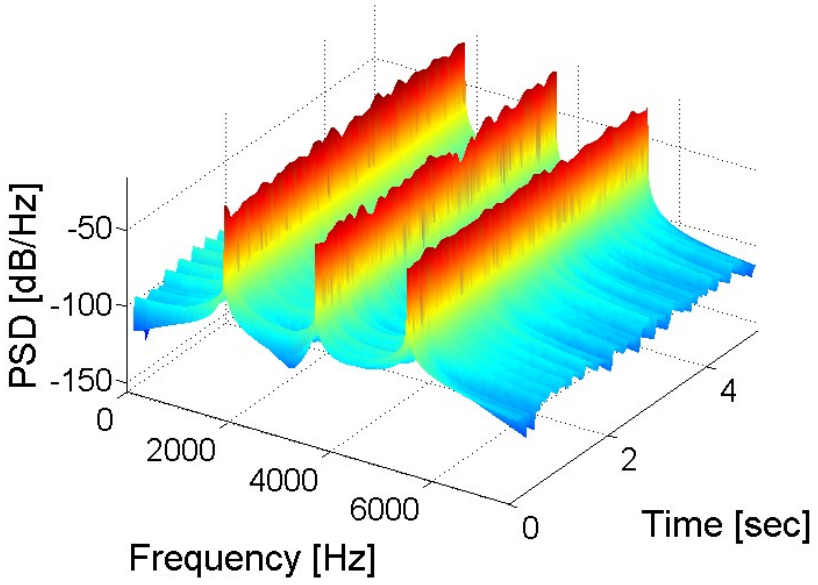

Figure 17. Spectrogram of BPF, 2BPF, and 3BPF tones isolated in the recording made at 48% power and 75° emission angle.

3 Signals Analysis

Analysis processes were developed to extract time-varying parameters for tonal and broadband components of measured turbofan noise. This chapter details analysis steps for each of those components. Broadband noise analysis proceeded using the Short-Time Fourier Transform, and provided estimates for third-octave band SPL as a function of time. Broadband analysis is described first in this chapter, since subsequent tonal analysis used the third-octave band representation as an estimate of the noise floor as a function of time.

To extract tonal fluctuations of interest, a heuristic tone-identification process was employed on the set of recordings from EVNERT test configuration 19, followed by three major analysis steps. Knowledge of tone-generation mechanisms inside the turbofan engine were combined with information about fan geometry and operation points to provide an estimate of frequencies where fan rotor-stator interaction tones and multiple pure tones (MPTs) would be found. These locations were verified using long term Power Spectral Density (PSD) estimates. In the first analysis step, each tone of interest was separated from other tonal information as well as the background broadband noise using passband filtering. Next, the complex-valued analytic signal was constructed from the real-valued tone-isolated recording. Finally, the magnitude and instantaneous frequency of the analytic signal were estimated to obtain the amplitude and frequency fluctuations of interest.

3.1 Representation of Recorded Signals

A simple representation of the signal recorded in each microphone at each power setting was created to facilitate analysis, and is shown for continuous time in Equation (3.1). Recordings generally consisted of a combination of tonal and broadband noise. The tonal source itself was a sum of many tones, which arose from a combination of the three mechanisms noted in Section 2.3. The representation for the total modeled signal is

$$s(t) = \sum_{k=1}^{K} s_k(t) + b(t) \tag{3.1}$$

where $s(t)$ is the total recorded source pressure-time history, K is the total number of modeled fan tones, $s_k(t)$ is the pressure-time history of the k^{th} tone, and $b(t)$ is time-varying broadband noise from several sources. Since $b(t)$ was complicated both temporally and spectrally, it was difficult to

represent its contribution with more accuracy. However, the noise contribution at a particular time in a particular spectral region was of interest to several analysis and post-processing steps detailed later. The structure of Equation (3.1) allowed each tone to be separated, analyzed, and characterized individually, while maintaining the ability to account for broadband noise sources. For example, the tonal component of Equation (3.1) only includes fan rotor-stator and shaft-order tones as predicted or inferred from a Heidmann Fan prediction. It does not include other generation mechanisms such as turbine, compressor, or fan/compressor interaction tones. The broadband noise source, too, was not intended to capture noise from sources other than the fan. For cases where jet noise was captured in the recordings, such as at low frequencies, filtering was applied to remove it.

Since data acquired during the EVNERT tests was sampled at discrete points in time, the representation of recordings was converted accordingly. Discrete time sequences of pressures were represented as uniformly sampled values of the continuous function described by Equation (3.1). The representation for the total recording in each microphone at each power setting was then

$$s[n] = \sum_{k=1}^{K} s_k[n] + b[n] \tag{3.2}$$

where *s[n]* is the total acquired recording at each sample index *n*, represented as the sum of *K* tones. Note that the conversion from the continuous time *t* used earlier to the sample index *n* shown in Equation (3.2) was obtained by

$$s[n] = s(t)\big|_{t=n\Delta t_s} = s\left(n\Delta t_s\right) \qquad n = 1, 2, ..., N \tag{3.3}$$

where Δt_s is the sampling interval of EVNERT data acquisition, or time between successive pressure samples, and *N* is the total number of samples obtained in a particular recording. Discrete-time representations are always denoted by brackets over a finite sequence of integer-valued indices.

Signals represented in discrete time at a fixed sampling rate (whether in the model stated above or in the EVNERT recordings acquired) may contain energy up to a certain limit, called the Nyquist frequency. The Nyquist frequency is directly related to the sampling rate of recordings by

$$F_{NYQ} = \frac{1}{2\Delta t_s} = \frac{F_s}{2} \tag{3.4}$$

where F_{NYQ} is the Nyquist frequency in Hz and F_s the sampling rate in Hz.

3.2 Analysis of Broadband Noise

As part of engine noise analysis, the time-varying broadband noise component *b(t)* was estimated on a third-octave band basis. The method used was derived from previous work which was geared toward the analysis and synthesis of jet noise sources [25]. Time-domain fluctuations in broadband noise spectra were extracted, but no model was generated for synthesis, as in the case of tonal noise. Instead, broadband noise was useful for creating a realistic analog of the total fan noise source during the synthesis and subjective testing efforts described in Chapters 4 and 5, respectively. This section describes how a narrowband estimate of the time-varying broadband noise content was calculated using the Short-Time Fourier Transform, then converted to a third-octave band basis.

3.2.1 Calculation of Short Time Fourier Transform

A Short Time Fourier Transform (STFT) method was used to analyze fluctuations in third-octave band levels of broadband noise. The STFT method used a sliding analysis block to isolate segments of noise in the time domain, and was implemented largely with the MATLAB *spectrogram* function. Each block isolated a portion of the input signal whose spectral content did not vary significantly within the segment. Each block of pressure-time history was then windowed to reduce spectral leakage due to discontinuities at window edges, and the power spectral density (PSD) of each block was calculated. The time-varying nature of the signal's spectrum was inferred by following frequency content in each successive (time-shifted) analysis block. The PSD at each block was converted to mean-squared pressure through multiplication by the PSD bin width.

A depiction of the STFT analysis process is shown in several parts in Figure 18. The top plot shows a "chirp" signal in black, whose frequency linearly increases from 0 to 200 Hz over one second. The input chirp has time-invariant amplitude of 1 Pa. Also shown are a series of successive STFT analysis blocks. The time history isolated by application of the red window is shown in the center left plot, and its corresponding PSD is shown in the bottom left plot. The analysis block is then shown sliding forward several more times in green. At each block, the PSD of the windowed signal is calculated, though the spectra are not shown in Figure 18. Another representative analysis window is then shown in blue, along with the windowed time history and the resulting PSD. The chirp frequency can be seen to increase in the time domain plots, though the effect becomes more apparent in the frequency-domain plots at the bottom of the figure.

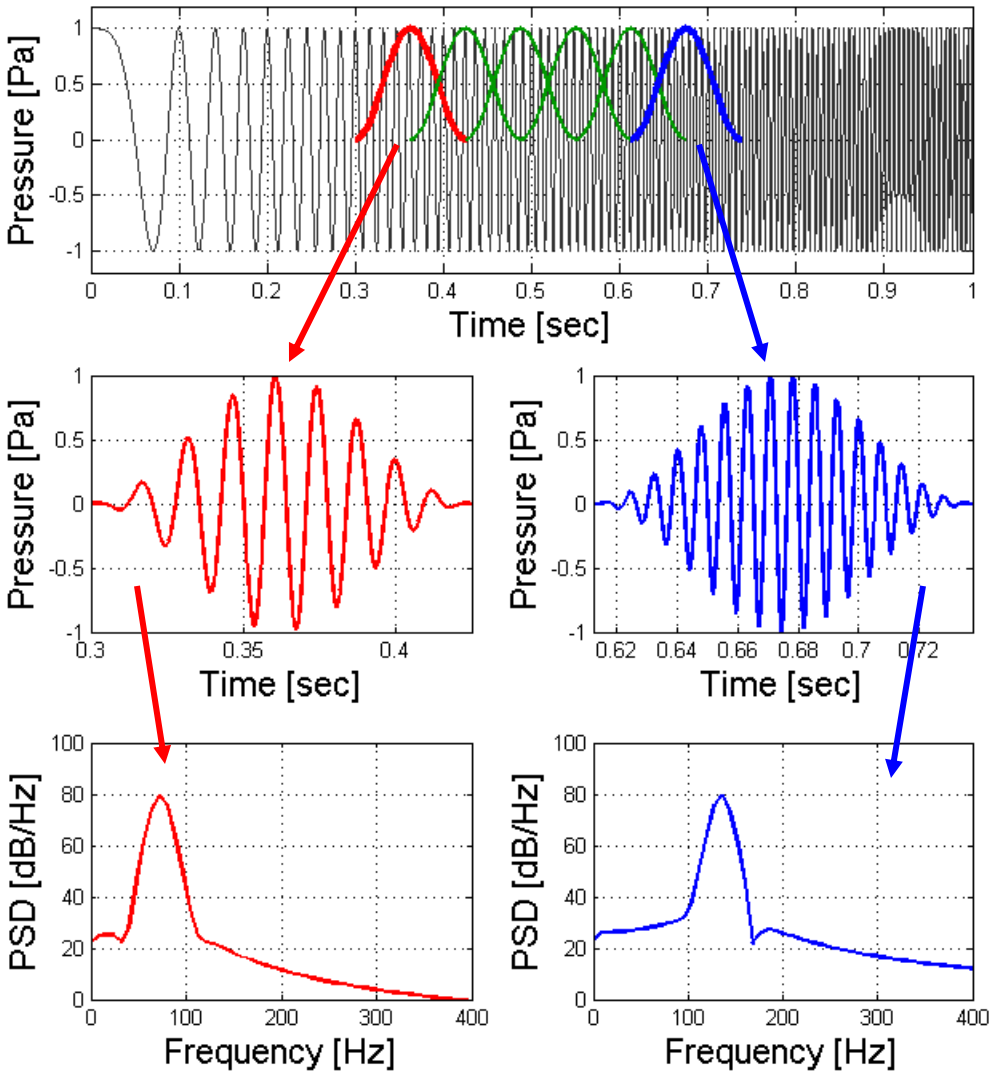

Figure 18. Depiction of STFT analysis as applied to a chirp signal. Analysis block length is 0.125 seconds and hop size is 0.0625 seconds.

The frequency resolution of the spectrum at each analysis block is inversely related to the block length, as

$$\Delta f_{STFT} = \frac{1}{T_B} = \frac{1}{N_B \Delta t_s} \tag{3.5}$$

In Equation (3.5), Δf_{STFT} is the frequency resolution of the spectrum at each block in Hz and T_B is the length of each block in seconds, which can also be represented as the number of samples N_B in each block times the recorded sampling interval Δt_s. The inverse relationship implies that an

inherent tradeoff exists in any STFT analysis, where increased spectral resolution at each analysis block requires a longer block length. However, a long block will average out the variations of interest. For that reason, the expected properties of the signal must be taken into account to arrive at an appropriate balance between time and frequency domain resolution. The block length used in Figure 18 was 0.125 seconds, and can be seen as the distance between the endpoints of each window.

Another parameter, called the overlap percentage, is important in STFT analysis. In order to increase the number of analysis segments available in a given pressure-time history (and thus the number of spectrum estimates), successive blocks may be overlapped. Overlapped blocks slide the window forward in time by an amount less than the full block length. The overlap factor is usually specified as a percentage of one block length. For example, 75% overlap means that successive blocks share 75% of the same samples. Often, the number of samples that the block slides forward is called the "hop size." By using some of the same pressure samples in more than one PSD estimate, the time domain resolution of the output can be increased. The time-domain resolution at which spectral estimates are obtained from the STFT as a function of the hop size is

$$\Delta t_{STFT} = \frac{N_{HOP}}{F_s} = N_{HOP}\Delta t_s \tag{3.6}$$

where Δt_{STFT} is the output time resolution of the STFT and N_{HOP} is the hop size between the beginning of successive blocks in samples. In Figure 18, the overlap percentage used was 50%. The hop size corresponding to that overlap percentage was 0.0625 seconds.

In the application of STFT analysis to the broadband fan noise component ($b(t)$ in Equation (3.1)), the values for block length and overlap percentage were chosen in the following way. A spectral resolution of two Hz was desired, so that tonal components could be resolved and ignored in the calculation of third-octave band levels at each segment. That process is described in Section 3.2.2. In addition, a relatively fine frequency resolution was necessary to avoid errors when lumping narrowband bin energy into third-octave bands later in the process. Those errors were expected to be more serious at lower frequencies, where the constant Δf bin width was a relatively larger proportion of third-octave band width. The relationship between block length and frequency resolution in Equation (3.5) showed that a block length of 0.5 seconds (N_B=16,384 samples) was required to obtain 2 Hz resolution at the recorded sampling interval of 1/32,768 seconds. Next, the hop size was calculated so that the STFT provided spectral estimates for the signal at a rate sufficient to resolve

fluctuations with a bandwidth of 20 Hz. A Nyquist frequency for STFT output samples could be calculated according to

$$F_{NYQ,STFT} = \frac{1}{2\Delta t_{STFT}} = \frac{F_{STFT}}{2} \tag{3.7}$$

where $F_{NYQ,STFT}$ is the Nyquist frequency of STFT output samples in Hz and F_{STFT} is the sampling frequency of STFT output samples in Hz.

For the broadband STFT analysis, the required sampling rate ($F_{STFT)}$ based on the desired $F_{NYQ,STFT}$ was 40 Hz. The time-frequency relationship means that a hop size of 0.025 seconds between blocks was required to resolve spectral energy in fluctuations below 20 Hz. The hop size was then decreased further to ensure that no fluctuations would occur above the Nyquist frequency. The final hop size was 0.01 seconds, rounded to an integer number of samples (328). Effectively, the final F_{STFT} implied by the hop size was 100 Hz. For 69.7 second EVNERT recordings, the analysis parameters of 16,384 sample block length and 328 sample hop size returned 8,193 narrowband frequency bins at each of 6,914 discrete time indices. A table summarizing input and output parameters for the STFT analysis applied to recordings can be seen in Table 4.

Table 4. Summary of inputs and outputs for calculation of the Short-Time Fourier Transform.

Parameter	Description	Value	Units
STFT Analysis Parameters			
	Window Shape	Hann	
N_B	Block Length	16,384	samples
N_{HOP}	Hop Size	328	samples
STFT Output			
Δf_{STFT}	Frequency Resolution	2	Hz
F_{STFT}	STFT Sampling Rate	100	Hz
$N_B/2+1$	Number of Frequency Bins	8,193	bins
	Number of Time Steps	6,914	steps

3.2.2 Conversion to Time-Varying Third-Octave Band SPL

Next, the narrowband mean-square pressure in each frequency bin was lumped together into third-octave bands at each analysis block. Nominal third-octave band frequency bounds were used to determine which narrowband bins fell into each third-octave band. A list of nominal third-octave band limits used can be found in Appendix B – 1/3 Octave Band Limits. The energies of all bins

falling into a particular band were summed to find the total energy in that band. When part of a bin overlapped the edge of a third-octave band, the proportion of overlap was calculated and the bin energy was divided among the appropriate bands. In practice, this partial distribution only influenced the very low frequency third-octave bands, which were not of interest for broadband fan noise synthesis or for tonal correction. Both of these processes were performed on higher third-octave bands.

Additionally, a correction was applied to bins which were predicted and observed to contain significant energy from one of the tonal generation mechanisms noted earlier. This correction was applied at each analysis block. Figure 19 shows all bins in the third-octave band with center frequency F_c = 2,000 Hz, as measured at a single STFT time step for the recording made at 45° emission angle and 54% engine power setting. The 1BPF tone at that power setting was predicted to occur at 2,024 Hz, which is within the depicted 2,000 Hz band. The appropriate bin and one bin on either side of it were all assumed to contain energy from that tone, whether due to small inaccuracy in the estimation, leakage from windowing during computation of the spectrum, or modulations in the amplitude and frequency of the tone. Bins predicted to contain tonal energy for those reasons are displayed in green, and were observed to contain energy significantly above the mean broadband level. The bins containing tonal energy, if included in the total sum for mean-squared pressure in the 2,000 Hz third-octave band, would artificially increase the estimate which was desired for the broadband component only. Thus, those frequency bins were replaced with the average mean-square pressure of other measured values in the third-octave band. The resulting (post-processed) third-octave band spectrum which was then used for calculation of SPL is shown in Figure 20. The total energy in each band was then calculated as the sum of all narrowband corrected mean-square pressures.

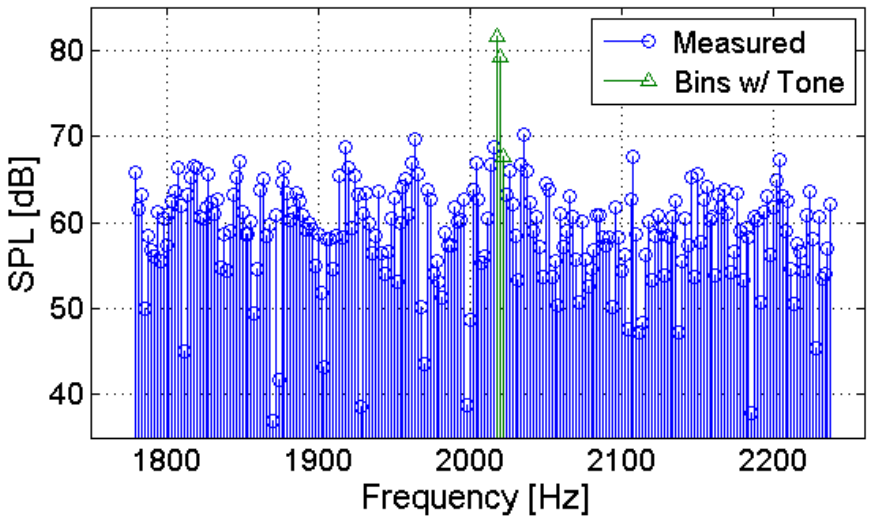

Figure 19. Narrowband bins as measured at one STFT time step at 54% engine power setting and 45° emission angle. Bins predicted and observed to contain tonal energy are noted in green.

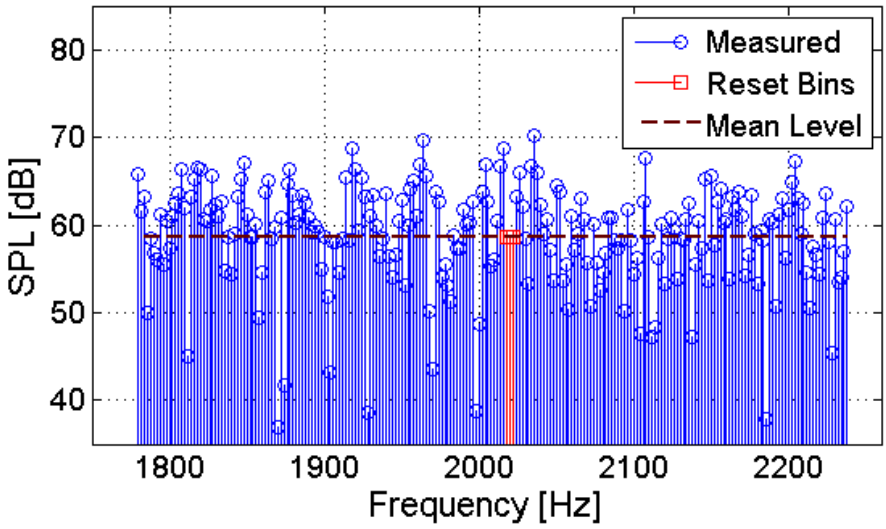

Figure 20. Corrected narrowband measurement at one STFT time step at 54% engine power setting and 45° emission angle. Band mean level and reset bins are shown in red.

The result of the narrowband to third-octave band lumping process was an estimate of the total energy in each band (in units of mean-square pressure) at each analysis block. Finally, the SPL of each third-octave band was calculated at each block as

$$SPL[m] = 10\log_{10}\left(\frac{p_{rms}^2[m]}{p_{ref}^2}\right) \tag{3.8}$$

where *SPL[m]* is the sound pressure level of the m^{th} block, p_{rms} is the root-mean-square pressure of the appropriate band at the m^{th} block in Pa, and p_{ref} is the 0 dB reference pressure. In this investigation, the reference pressure was 20 μPa.

The result of the entire process was the SPL resulting from broadband noise sources in each third-octave band at samples spaced 0.01 seconds apart for the length of each EVNERT recording. One set of tone-corrected third-octave band fluctuations was calculated for each of the 160 recordings. Figure 21 shows one such SPL fluctuation, returned for the third-octave band centered around 2,000 Hz in the recording made at 54% engine power setting at an emission angle of 40°. Also shown (in red) is the fluctuation in the same third-octave band which would have resulted if tonal energy from the BPF had been included in the broadband estimate. Eliminating bins known to contain primarily tonal energy changed the SPL estimate by an average of about 1.5dB over the time period displayed.

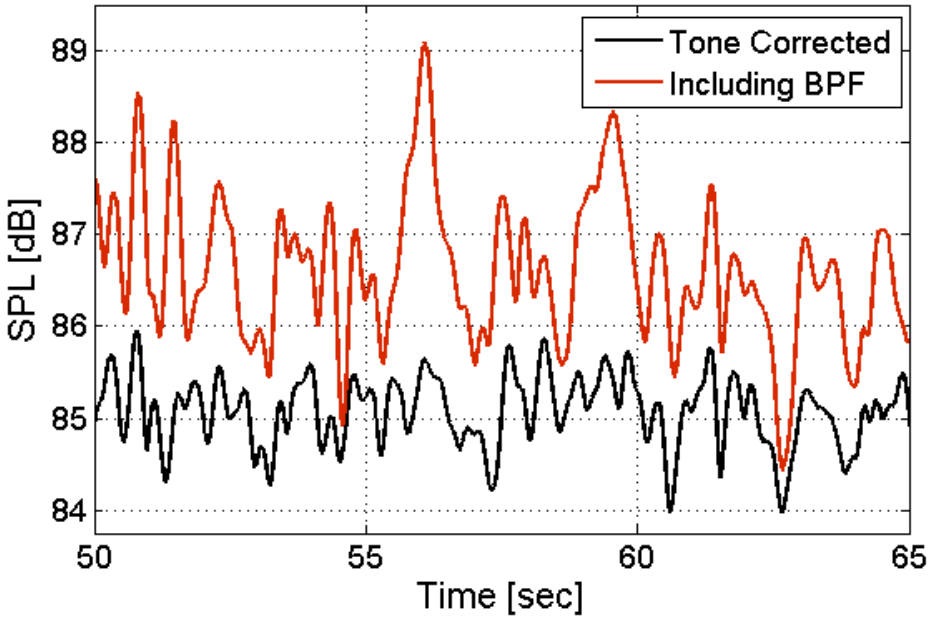

Figure 21. Comparison of fluctuations in third-octave band level vs. time when tonal energy is included or ignored (54% power setting, 40° emission angle, F_c = 2,000 Hz).

3.3 Review of Tonal Analysis Techniques

When considering various tonal analysis methods, a procedure was desired which would provide high resolution in both the time and frequency domains. Further, the procedure must produce reliable, unique estimations for each tonal parameter. Time resolution was important to resolve fluctuations with bandwidth less than 20 Hz, which are typically perceived as envelope variations rather than additional tonal components [4]. Frequency resolution was important to discriminate tonal energy from broadband energy as analyzed earlier. Two methods were initially investigated to analyze fluctuations in inlet-radiated tonal noise. Ultimately, these methods did not perform as desired for the current investigation. The benefits and drawbacks of those options are presented for reference in this section.

3.3.1 FFT/ Spectrogram

Previous attempts at tonal analysis work had proceeded using the Short Time Fourier Transform (STFT) [25]. By identifying the frequency-domain location of a target tone at successive time steps, a record of variations in both frequency and tonal amplitude could be constructed. However, the STFT suffers from the inherent tradeoff between time and frequency resolution which was noted in Section 3.2. That tradeoff was acceptable for broadband noise where a sum of many frequency bins was calculated to obtain the third-octave band representation. The specific difficulties associated with tonal analysis, however, made the time/frequency tradeoff unacceptable. Tones are highly localized in frequency, so high frequency resolution would be required to resolve them with sufficient confidence. However, that same frequency resolution necessarily comes at the cost of decreased time-domain resolution which serves to "smear" fluctuations of interest. To resolve tones with 1 Hz frequency resolution would have averaged out variations with period less than one second. For these reasons, a STFT analysis method was found unacceptable for tone tracking in the current investigation and new methods were considered.

3.3.2 Filter-Fit

An interesting method of tracking the frequency and amplitude of tonal sources as functions of time was pursued, but ultimately dismissed for much the same reasons as STFT analysis. This method was dubbed the "Filter-Fit" procedure, and was executed in the following way. It was first assumed that the tone of interest was not rapidly changing amplitude or frequency on some sufficiently small timescale, usually about 20 cycles. Each tone of interest was isolated with a narrow

bandpass filter. Next, the signal was buffered into short blocks. Each block alone would be too short to achieve any significant frequency domain resolution in the STFT method, so Filter-Fit displayed one advantage in that area. At each buffer block, a nonlinear least-squares fit routine was used to minimize the error between the observed tone and a prototype sine wave [32]. The fit method was allowed to vary the amplitude, frequency, and phase of the sinusoid in pursuit of minimizing deviation between the two time histories.

Once the fit routine had converged, the tonal parameters were output at each block. The Filter-Fit method eliminated the one major downfall of STFT tonal analysis; it removed the inherent time/frequency tradeoff through avoidance of frequency domain block processing. However, handling time-variations in the phase offset between blocks was ambiguous. The analysis technique implied that frequency and phase were independent parameters, when in fact they are not. A small increase in frequency over one block, for example, would correspond to a phase shift at the beginning of the next block. So, the underlying assumption that all three parameters (tonal amplitude, frequency, and phase) could be allowed to vary independently from block to block was incorrect. Too much ambiguity in tonal parameters was allowed by the Filter-Fit method; another method was then sought which could attach unique, reliable physical meaning to outputs.

3.4 Theory of Demodulation

The method eventually selected to extract the time-varying amplitude envelope and instantaneous frequency from tonal signals of interest avoided the pitfalls of STFT and Filter-Fit analysis described in the previous section. The analysis methods for amplitude and frequency stem from techniques which are more commonly defined in the context of signal processing for communications. For example, in radio transmission, a modulation in either amplitude or frequency is applied to a carrier tone with a time-invariant mean amplitude and frequency. The problem of the receiver in that case is to separate the modulated carrier tone from the surrounding noisy environment, and then to separate the modulation itself from the carrier. The problem of extracting the amplitude envelope and instantaneous frequency of a particular tone was approached from that perspective, through construction of the analytic signal.

The analytic signal is a unique complex representation of any real-valued signal [33-35]. As a complex representation, it offers the benefit of direct calculation of the magnitude and phase angle at each signal sample. This section describes analysis methods which were applied to recordings in

three steps for each fan-generated tone of interest, for which a top-level flow diagram can be seen in Figure 22. Each tone was isolated from other noise sources, used to construct the unique analytic signal, and finally processed to obtain the desired time domain fluctuations in tonal amplitude and frequency. Post-processing used time-varying estimates of broadband noise calculated in Section 3.2 to correct instantaneous frequency where tonal amplitude fell below a certain threshold.

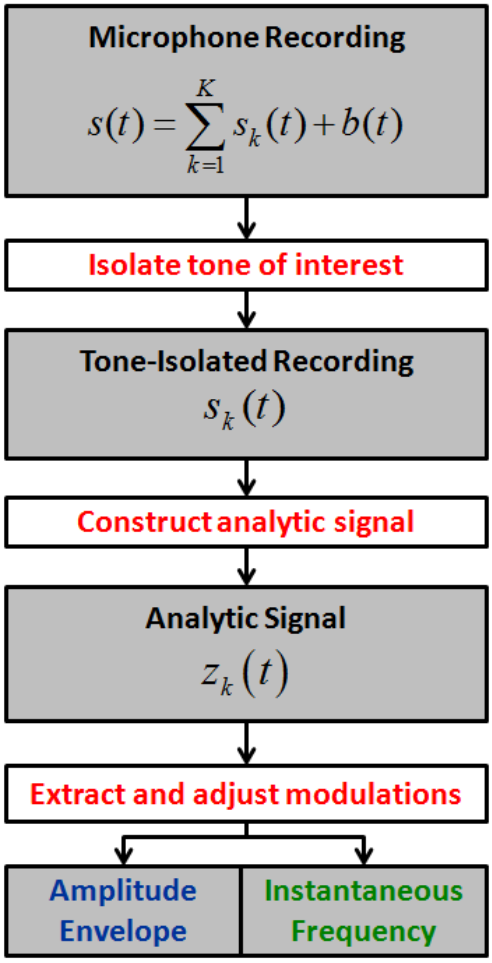

Figure 22. Flowchart describing overall process for extracting tonal fluctuations.

3.4.1 The Single-Tone Parametric Model

The pressure-time history of each tonal component of the combined tonal source was represented as an amplitude and frequency-modulated cosine wave, as in

$$s_k(t) = a_k(t)\cos\left(\phi_k(t)\right) \tag{3.9}$$

where $a_k(t)$ is the amplitude envelope of the k^{th} tone and $\phi_k(t)$ is the phase of the k^{th} tone in radians. According to Equation (3.9), each tone was characterized completely by two parameters; the amplitude and phase functions. The relationship of the time-varying frequency of the cosine term to the phase argument in the single-tone model is described by

$$\phi_k(t) = 2\pi \int_{-\infty}^{t} f_k(\tau)\, d\tau \tag{3.10}$$

where f_k is the instantaneous frequency of the k^{th} tone in Hz, and τ is a dummy variable of integration. It is important to mention that the frequency/phase relationship is responsible for the ambiguity which made the Filter-Fit method undesirable, but that it is handled inherently by the described model. Additionally, note that a tone of constant (time-invariant) frequency f will have a phase integral which becomes the familiar $2\pi ft$ argument of a simple harmonic oscillator. The instantaneous frequency may be obtained from Equation (3.10) by differentiating with respect to time as

$$f_k(t) = \frac{1}{2\pi} \frac{d\left(\phi_k(t)\right)}{dt} \tag{3.11}$$

Time variations in each of the cosine parameters (amplitude and frequency) were then represented as fluctuations around a time-invariant mean value according to

$$a_k(t) = a_{mean,k} + a_{mod,k}(t) \tag{3.12}$$

$$f_k(t) = f_{mean,k} + f_{mod,k}(t) \tag{3.13}$$

where $a_{mean,k}$ is the mean amplitude of the k^{th} tone, $a_{mod,k}$ is the amplitude modulation of the k^{th} tone around the mean value, $f_{mean,k}$ is the mean frequency of the k^{th} tone, and $f_{mod,k}$ is the frequency modulation of the k^{th} tone around the mean value. The corresponding discrete-time representation of each tone-isolated signal is given as

$$s_k[n] = a_k[n]\cos\left(\phi_k[n]\right) \tag{3.14}$$

The relationship between the phase function $\phi_k(t)$ and the instantaneous frequency function $f_k(t)$ which is represented by integration in continuous time must be approximated in discrete time. Since instantaneous frequency was not assumed to change rapidly enough to generate significant differences over successive samples, a simple rectangular approximation was used for the integral in

Equation (3.10). Thus, in discrete time, the relationship between the cosine argument for each tone and the instantaneous frequency was represented by

$$\phi_k[n] = 2\pi\Delta t_s \sum_{i=1}^{n} f_k[i] + \phi_{0,k} \tag{3.15}$$

where all quantities are as previously defined, except for the constant $\phi_{0,k}$ which was introduced to account for the initial condition of each phase vector. The initial condition $\phi_{0,k}$ is the first measured value of the phase of the k^{th} tone, in radians.

3.4.2 Construction of the Analytic Signal

The analytic signal is constructed from each tone-isolated signal to facilitate analysis of the target parameters. Certain operations (such as those involving magnitude and phase) are more convenient when performed on complex quantities rather than trigonometric functions such as cosines. This section presents the motivation for the construction of the analytic signal, and outlines its computational benefits. For a more complete summary of the theory and application of the analytic signal, the reader is directed to references [33-35].

It is well known that trigonometric functions have complex-valued analogs which can be described using Euler's formula

$$e^{j\phi} = \cos(\phi) + j\sin(\phi) \tag{3.16}$$

Equation (3.16) may be rewritten in terms of the cosine function as

$$\cos(\phi) = \frac{e^{j\phi} + e^{-j\phi}}{2} \tag{3.17}$$

This view represents a single harmonic oscillator as the sum of two counter-rotating vectors in the complex plane. Equation (3.17) may be generalized for the case where the phase argument of the cosine and its amplitude are changing as functions of time, that is,

$$a(t)\cos(\phi(t)) = a(t)\left(\frac{e^{j\phi(t)} + e^{-j\phi(t)}}{2}\right) \tag{3.18}$$

which holds true at each point. Two aspects of Equation (3.18) are very important. First, the left side represents the single-tone parametric model presented in Section 3.1, with the tonal index k omitted.

Use of Euler's formula has allowed the representation of a single amplitude- and frequency-modulated oscillator as two complex vectors which rotate in opposite directions. This matches the basic theory of the Fourier Transform, which represents signals in the frequency domain as having both positive and negative frequency components. The second important aspect is that the two complex vectors are identical except for the direction of rotation. The information contained in the vector which rotates in the negative direction is redundant – it has the same magnitude and frequency functions as the positive-rotating vector. Neglecting it does not destroy the original amplitude and phase functions of interest. The magnitude of the remaining positive-rotating vector is half of the original oscillator amplitude, and can easily be adjusted to match through multiplication by a factor of two.

Since the Fourier Transform describes *any* signal as the sum of many sinusoidal functions, the preceding idea may be generalized for all real-valued input functions. The analytic signal is thus generated by application of the following instruction in the frequency domain; "suppress the amplitudes belonging to negative frequencies, and multiply the amplitudes of positive frequencies by two" [33]. Practical implementation of that instruction can be summarized in a four-step algorithm, which was used in this investigation to calculate the analytic signal[4]. The algorithm is stated below, as adapted from MATLAB documentation[5] [36]:

1. Calculate the n-point fast Fourier transform of the entire tone-isolated input sequence, then store the result in a vector S_k
2. Create a vector h whose elements h[i] have the values:
    a. 1 for i=1 and i=(n/2+1)
    b. 2 for i=2,3,…,(n/2)
    c. 0 for i=(n/2+2),…,n
3. Calculate the element-wise product of S_k and h.
4. Calculate the inverse fast Fourier transform of the sequence obtained in step 3 and return the first n elements of the result.

[4] Note that (due to the periodicity of the Fourier Transform) the elimination of negative frequency content may also be viewed as the elimination of content above the Nyquist frequency. The MATLAB implementation uses the latter approach.

[5] The MATLAB function *hilbert()* was used in practice to generate the analytic signal. As the name suggests, construction of the analytic signal may also be motivated by the phase-shifting properties of the Hilbert transform.

The resulting analytic signal is then a complex-valued time-domain sequence which contains no negative frequencies. For the single-tone parametric model described earlier, it can be shown that the analytic signal is mathematically represented as

$$z_k(t) = a_k(t)e^{j\phi_k(t)} \tag{3.19}$$

where $z_k(t)$ is the complex-valued analytic signal, while $a_k(t)$ and $\phi_k(t)$ are the original amplitude and phase arguments. The problem of demodulation has now been transformed to one of calculating the instantaneous magnitude and phase of a single complex vector as a function of time. These are operations which are very conveniently performed on complex quantities.

Finding the magnitude of the analytic signal provides the amplitude envelope of the real-valued signal, as in

$$a_k(t) = |z_k(t)| = \sqrt{\mathrm{Re}\left(z_k(t)\right)^2 + \mathrm{Im}\left(z_k(t)\right)^2} \tag{3.20}$$

The mean value of the amplitude envelope is then removed to isolate the amplitude fluctuation of interest.

To find the instantaneous frequency of the tone-isolated signal from the analytic signal, several steps are applied. The analytic signal is first modulated by a complex exponential at the opposite of the carrier frequency. This modulation has the effect of shifting the deviations to "baseband" (centered on zero frequency) according to

$$\begin{aligned} z_{bb,k}(t) &= z_k(t)\exp\left(-2\pi j f_{mean,k}\right) \\ &= a_k(t)\exp\left(j2\pi\int_{-\infty}^{t}\left(f_{mean,k} + f_{mod,k}(\tau)\right)d\tau\right)\exp\left(-2\pi j f_{mean,k}\right) \\ &= a_k(t)\exp\left(j2\pi\int_{-\infty}^{t} f_{mod,k}(\tau)\,d\tau\right)\left(\exp\left(j2\pi f_{mean,k}t\right)\exp\left(-2\pi j f_{mean,k}\right)\right) \\ &= a_k(t)\exp\left(j2\pi\int_{-\infty}^{t} f_{mod,k}(\tau)\,d\tau\right) \end{aligned} \tag{3.21}$$

which represents the complex baseband analytic signal $z_{bb,k}$ of the k^{th} tone, and has frequency equal to the deviation from the original mean value. The instantaneous phase of the baseband-modulated tonal signal is then calculated by use of the inverse tangent function as

$$\phi_{bb,k}(t) = \tan^{-1}\left(z_{bb,k}(t)\right) \tag{3.22}$$

Finally, the instantaneous frequency is found by the time derivative of the phase angle. Division by 2π converts the angular frequency in radians per second to units of cycles per second, or Hz. So, the final representation for instantaneous frequency fluctuation is

$$f_{mod,k}(t) = \frac{1}{2\pi}\frac{d}{dt}\left(\phi_{bb,k}(t)\right) \tag{3.23}$$

where $f_{mod,k}(t)$ is calculated as the time derivative of the phase angle of the baseband-modulated analytic signal for the k^{th} tone, $z_{bb,k}(t)$.

3.4.3 Discrete-Time Representation

In analysis of the recorded (discrete-time) signals, time was replaced with sample indices. Use of the analytic signal provided values for the amplitude envelope and instantaneous frequency of a tone at each signal sample, which was another benefit over the spectrogram and filter-fit operations discussed earlier. Results at each sample ensured that measured fluctuations did not contain significant spectral energy above the acquisition Nyquist frequency, and thus were not aliased.

The analytic signal magnitude is calculated directly to find the amplitude envelope. The frequency modulation is found through analysis of the baseband-modulated analytic signal, given by

$$z_{bb,k}[n] = z_k[n] \cdot e^{-j2\pi f_{mean,k} n\Delta t_s} \tag{3.24}$$

where $f_{mean,k}$ is the estimated mean frequency based on the heuristic method described in Section 2.6. Note that Equation (3.24) is the discrete time representation of Equation (3.21). The discrete time representations of the amplitude envelope and the frequency modulations (shown for continuous time in Equations (3.20) and (3.23)) are shown below in Equations (3.25) and (3.26), respectively. Note that the estimation for instantaneous frequency is the time derivative of the phase of the baseband-modulated analytic signal.

$$a_k[n] = \left|z_k[n]\right| = \sqrt{\mathrm{Re}\left(z_k[n]\right)^2 + \mathrm{Im}\left(z_k[n]\right)^2} \tag{3.25}$$

$$f_{mod,k}[n] = \frac{\tan^{-1}\left(z_{bb,k}[n]\right) - \tan^{-1}\left(z_{bb,k}[n-1]\right)}{2\pi\Delta t_s} \tag{3.26}$$

One important implication of tonal analysis in discrete-time appears in the calculation of the time derivative of instantaneous phase (Equation (3.26)). Discrete-time representations imply that the

derivative cannot be exactly calculated, but must be approximated between samples. In this case, the derivative was approximated linearly between samples by finding the first-order backward-time difference. The previous value (*[n-1]*) of phase was subtracted from the n^{th} value, and the difference was scaled to the sampling interval Δt_s.

Lastly, note that while the zero-mean instantaneous frequency modulation $f_{mod,k}[n]$ is found directly from Equation (3.26), the entire amplitude envelope is returned. The mean value is calculated and removed from the output amplitude envelope to find the amplitude modulation in discrete-time, according to Equation (3.27)

$$a_{mod,k}[n] = a_k[n] - \frac{1}{N}\sum_{m=1}^{N} a_k[m] \tag{3.27}$$

where amplitude envelope and modulation are as previously defined, and the scaled summation term should be recognized as the mean value of the amplitude envelope over the length of the analyzed signal. Mean value calculations are guaranteed to be unbiased [37], and approach the true mean value as the number of calculation samples is increased.

3.4.4 Example Analysis of Chirp Signal

Figure 23 shows an example of the analytic signal described in Section 3.4.3 as constructed from a "chirp" test signal. The frequency of the test signal linearly increased from 1 Hz to 100 Hz over a five-second interval, while the amplitude remained constant at 1 Pa. The top plot in Figure 23 shows the pressure-time history of the chirp signal, whose frequency can be seen to increase as time progresses. The top-center plot shows the magnitude of the analytic signal generated for the chirp, and remains near one Pa as expected. The bottom-center plot shows the extracted phase argument $\phi(t)$ of the chirp, which increases with time squared. Finally, the bottom plot shows the derivative of instantaneous phase of the analytic signal, which is the instantaneous frequency. Instantaneous frequency can be observed to increase linearly from 1 to 100 Hz over the five-second chirp, as expected. Since the calculation of the analytic signal is essentially a filtering operation, small start and stop transients can be observed in tonal parameters.

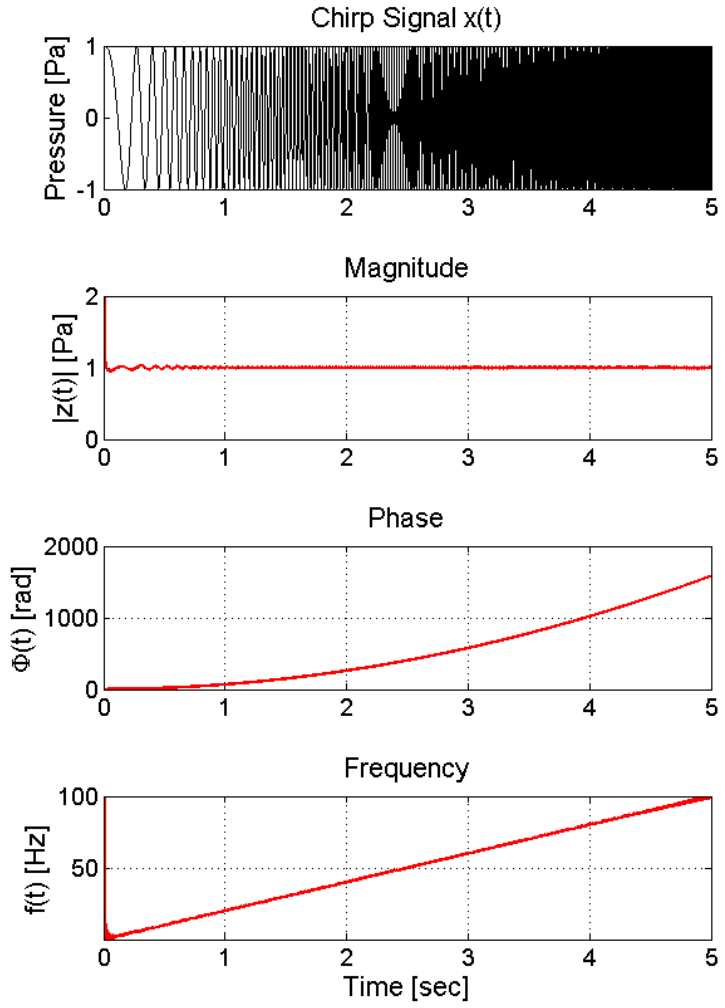

Figure 23. Example demodulation of a 1 Pa constant amplitude chirp signal with frequency which linearly increases from 0 to 100 Hz over 5 seconds.

3.5 Extraction of Fluctuations

A MATLAB tool was developed to obtain the amplitude envelope and instantaneous frequency of the tone-isolated recordings by utilizing the analytic signal according to the methodology outlined in the previous section. The analysis methodology described in earlier sections was applied to each of 6,016 tones of interest[6], described by Table 5. Four multiples of the BPF tone were analyzed in each of thirty-two microphones at the three low-power settings (48, 54, and 60%).

[6] 4 BPF tones in 32 recordings at each of three power settings, plus 88 fan order tones in 32 recordings at each of two power settings equals 6,016 tones analyzed.

Since the fan blade tips were supersonic at high power settings (71 and 87%), characterizations of the MPT noise were made from measurements at those conditions. The highest shaft-order tone analyzed was the 88th fan order, which also corresponded to the 4th multiple of the BPF. Theoretically speaking, fan order tones were predicted to continue at significant levels to even higher frequencies, but the anti-aliasing filter used in data acquisition limited the reliable frequency range to about 13,000 Hz.

This section details the functionality of tools developed to implement methods for isolating each tone of interest from other noise sources, extracting fluctuations from the analytic signal, and then using an estimate of the time-varying noise floor to improve the estimate of instantaneous frequency. The analysis tool was employed on tones of interest in each of the 160 EVNERT recordings described earlier.

Table 5. Description of fan-generated tones of interest from which amplitude and frequency fluctuations were extracted.

Power Setting [%]	Tone Types of Interest	Tones	Minimum Tone of Interest [Hz]	Maximum Tone of Interest [Hz]
48	BPF only	4 multiples of BPF	1790.1	7160.4
54	BPF only	4 multiples of BPF	2019.0	8076.0
60	BPF only	4 multiples of BPF	2241.4	8965.6
71	all Fan Orders	88 multiples of Fan Order	120.8	10630.4
87	all Fan Orders	88 multiples of Fan Order	148.1	13032.8

3.5.1 Tone Isolation

For each tone, the following analysis steps were applied. First, a bandpass filter with 15 Hz passband centered on the tone was designed and applied to the total source noise recording. The filter was a 3rd order Butterworth infinite-impulse response (IIR) filter design. Since Butterworth filters have maximally flat passband response, the impact of the tone isolation step was assumed to have minimal impact on the frequency content of the isolated signal and thus on the amplitude and frequency fluctuations of interest. Further, the filter was applied using the MATLAB *filtfilt()* command for zero-phase filtering [36]. The filtering operation essentially applied the designed filter in the forward-time direction, and then applied the filter again in the reverse-time direction. The

double application essentially doubled the filter order, further improving the rejection of unwanted noise sources during the filtering process. Application of the filter transformed the recorded signal which contained several tones as well as broadband noise into a single-tone signal which fit the parametric model presented earlier.

Figure 24 shows three stages of the tone-isolation process. The top plot shows the original spectrum of the 2BPF harmonic tone, as captured in the TECH977 engine recording at 48% engine power and 30° emission angle. The tone itself was predicted to occur at 5,370.8 Hz, which matched well with the observed spectral peak at 5,371 Hz. The center plot in Figure 24 shows the magnitude response of the 3rd order Butterworth bandpass filter which was designed to isolate the 2BPF harmonic tone. Finally, the bottom plot in Figure 24 shows an overlay of the original recorded signal spectrum and the tone-isolated signal spectrum. It verifies that the filtering process removed all other tonal energy and most broadband energy from the recorded signal. A small amount of broadband noise remained, and efforts to estimate the amount of noise captured in the filter passband are discussed in the Section 3.5.3.

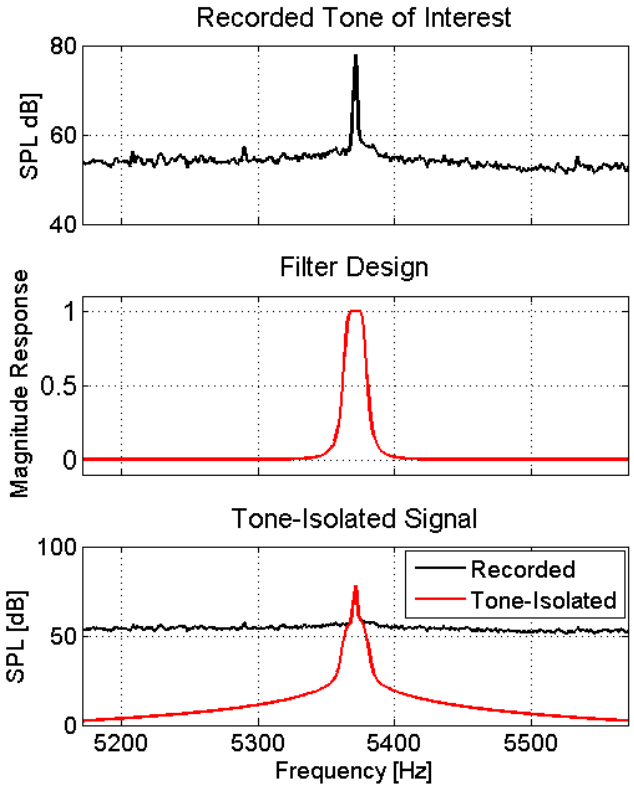

Figure 24. Recorded spectrum, filter design, and output spectrum from tone isolation process (Power Setting 48%, Microphone 6, 2BPF tone).

Figure 25 shows the original recorded pressure-time history captured at 48% power setting and 30° emission angle (gray), as well as the signal resulting from tone-isolation of the 2BPF harmonic (red). Note the different scales on the vertical axes, designed to highlight fluctuations in tonal amplitude. A significant amount of energy was removed from the recorded signal, and it is visually apparent from the figure that the tone-isolated signal did indeed contain fluctuations in amplitude. Frequency fluctuations were also present in the tone-isolated signal, but are not visible at the scale of Figure 25. Note also that only the first five seconds of the total 69.7 second time history are shown for clarity.

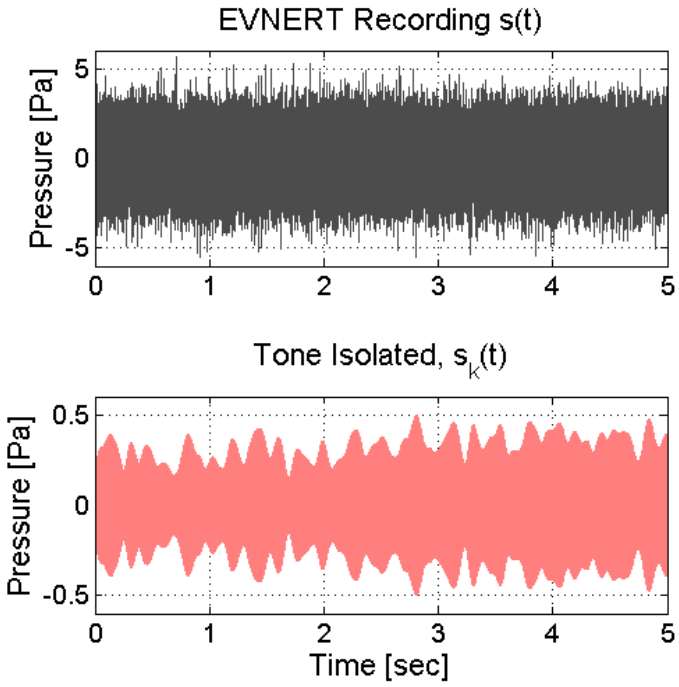

Figure 25. Pressure-time histories of the original recorded and tone-isolated signals for the 3BPF tone at 48% engine power and 30°emission angle.

3.5.2 Amplitude Envelope and Instantaneous Frequency

The MATLAB command *hilbert()* was used to generate the analytic signal, using removal of negative frequency information in the FFT as described in Section 3.4.2 [36]. The discrete-time amplitude envelope was then obtained by the magnitude of the tone-isolated analytic signal (Equation (3.25)). A plot of the extracted amplitude envelope from the BPF tone arising at 60% engine power setting and 30° emission angle can be seen plotted in Figure 26, along with the original recorded pressure-time history as well as the tone-isolated signal itself. Note that the time axis has

been zoomed to an arbitrary five-second window to show a detailed view of the extracted envelope. The amplitude envelope $a_k[n]$ which was extracted from the tone-isolated signal followed the contour of the pressure-time history, independent of frequency fluctuations, as expected. The extracted envelope had units of pressure. Each envelope extracted from a tone of interest was then shifted to zero-mean by removing the time averaged value over the 69.7 second recording.

Figure 27 shows the resulting amplitude fluctuation $a_{mod,k}$ which was obtained through the envelope of the analytic signal. One such amplitude fluctuation was generated for each tone of interest as enumerated by Table 5. The standard deviation of the observed fluctuation in tonal amplitude was 0.0964 Pa, which was about 45% of the mean observed amplitude in that tone. The standard deviation of amplitude variations observed across the entire EVNERT data set were almost always less than 60% of the mean tonal amplitude.

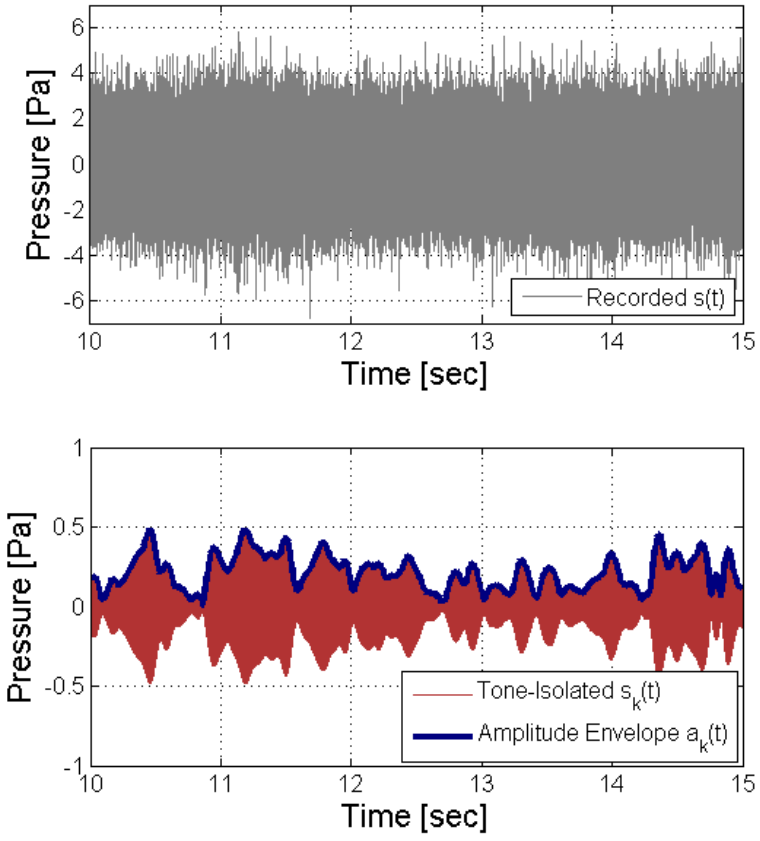

Figure 26. Extracted amplitude envelope of the BPF tone at 60% engine power setting and 30° emission angle.

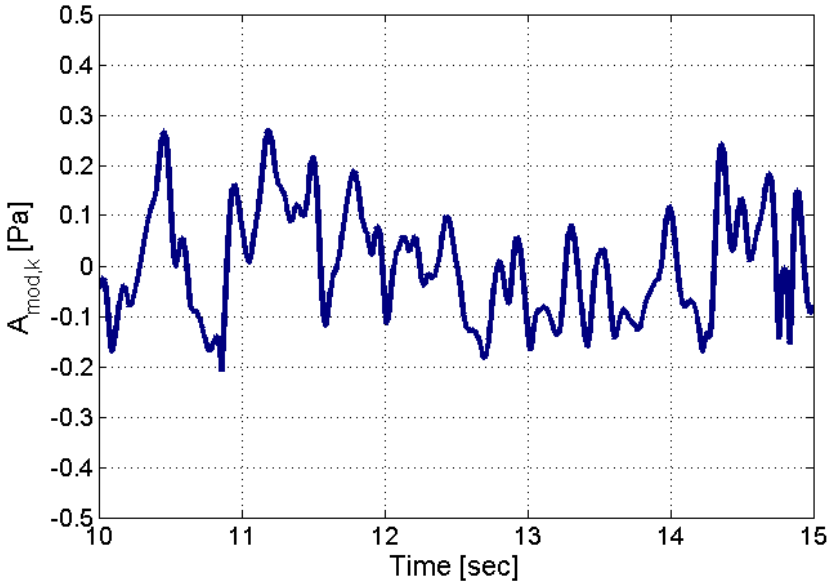

Figure 27. Extracted zero-mean amplitude fluctuation of the BPF tone at 60% engine power setting and 30° emission angle.

Just as amplitude modulations were calculated from the analytic signal, frequency modulations were obtained from the same MATLAB tool according to the method described in Section 3.4. The plot in Figure 28 shows an example of one such modulation, for the fan BPF tone as measured in the recording made at 54% power setting and 40° emission angle. The BPF tone in that recording was well above the broadband noise floor as estimated in Section 3.2. Departures from the mean frequency varied by tone, emission angle, and power setting, but in general were relatively small. Typical frequency departures observed were almost always less than 0.5% of the mean frequency.

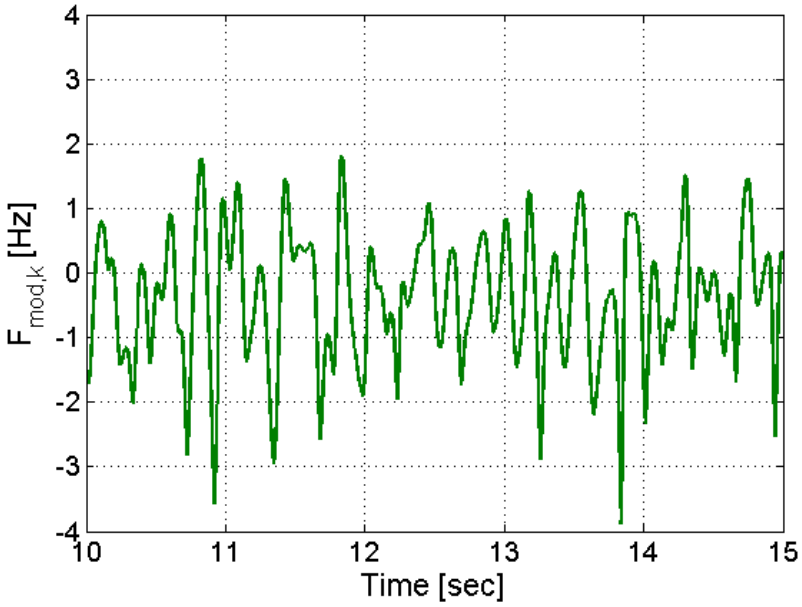

Figure 28. Extracted zero-mean frequency fluctuation in the fan BPF tone in the recording made at 54% power setting and 40° emission angle.

Since the estimates for mean tonal frequencies were based on the heuristic tonal identification procedure outlined earlier, they did not precisely correspond to the actual mean frequencies of analyzed tones. In this case, modulating each analytic signal to baseband did not entirely remove the carrier frequency as implied by the analytical representations. Instead, vestiges of the actual mean frequency remained in the baseband analytic signal. Vestigial carrier tones were removed by using a 3rd order lowpass Butterworth IIR filter with a cutoff frequency of 30 Hz on the corrected baseband frequency modulation.

3.5.3 Instantaneous Frequency Adjustment for Low SNR

In some cases observed tonal amplitudes were low relative to the surrounding broadband noise component, and were deemed to have poor signal to noise ratio (SNR). In regions where this occurred, the estimate of instantaneous frequency became unreliable [35]. A demonstration of such a case can be seen in Figure 29, where extracted tonal amplitudes and the corresponding frequency estimates are shown in the top and bottom plots respectively. Regions of low tonal amplitudes are shown in red rectangles. Though they generally only lasted for short periods of time, such excursions from zero-mean fluctuations would severely damage later modeling and synthesis processes, described in Section 4.2 and Section 4.3 respectively. For this reason, an estimate of the noise

captured inside the isolation filter passband was made as a function of time for each tone of interest, and the result was used to improve estimates of the instantaneous frequency where the tonal amplitude fell below the noise floor. No adjustments were made to extracted tonal amplitudes.

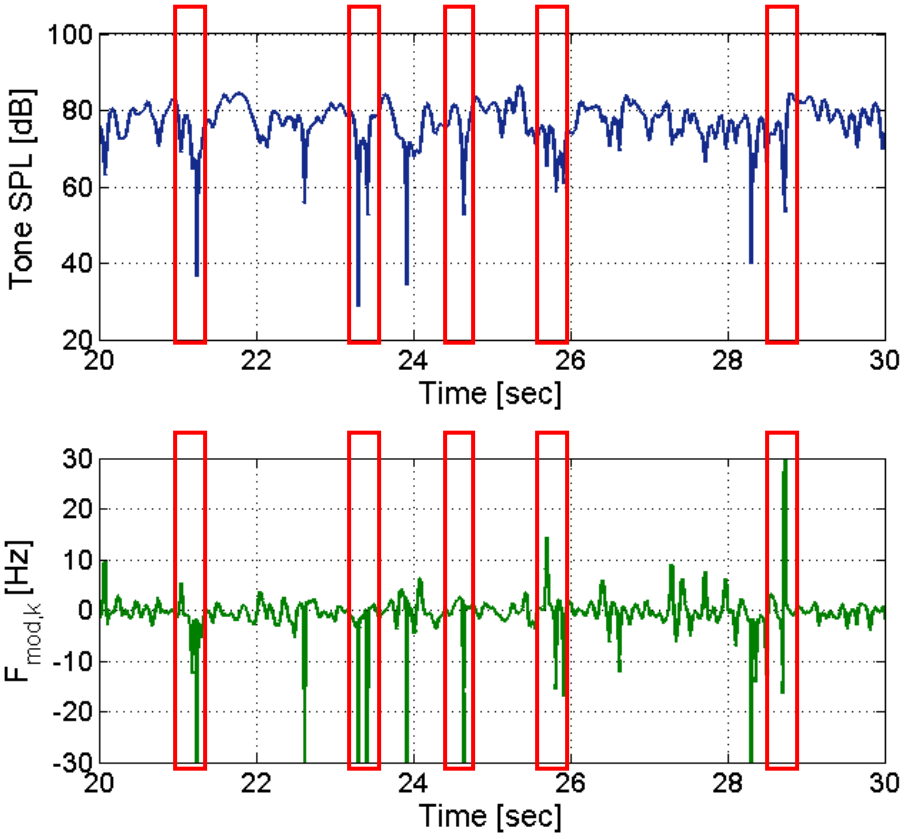

Figure 29. Extracted amplitude fluctuation and frequency modulation for a tone whose amplitude falls below the broadband noise component (60% power setting, 30° emission angle, 1BPF).

The procedure for post-processing a baseband frequency modulation to improve reliability was performed as follows. First, the broadband analysis tool outlined earlier was applied to the particular microphone recording captured at a certain power setting. This tool returned an estimate of the time-varying SPL in each third-octave band. A tone was associated with a particular third-octave band based on its mean frequency by calculating the appropriate band number according to

$$BN = \left\lfloor 10\log_{10}\left(f_{mean,k}\right) + 0.5 \right\rfloor \tag{3.28}$$

where BN is the integer-valued band number of the applicable third-octave band, $\lfloor \quad \rfloor$ indicates the floor function (round down), and the 0.5 serves to break ties in favor of the upper band. Note that the

third-octave band SPL calculated earlier was based on the total mean-squared pressure of the entire frequency range in the band, but that the tone-isolation filter eliminated most broadband energy. The average mean-squared pressure per bin was calculated by first converting the third-octave band SPL at each time step to total mean-squared pressure, then dividing that energy into the number of narrowband bins inside the band. That operation is represented by Equation (3.29)

$$p_{rms,avg}{}^2(t) = \frac{p_{ref}{}^2 10^{L_{third}(t)/10}}{N_{bins}} \tag{3.29}$$

where $p_{rms,avg}{}^2(t)$ is the average mean-squared pressure in each narrowband bin, $L_{third}(t)$ is the time-varying broadband noise SPL in the applicable third-octave band, and N_{bins} is the number of narrowband bins inside of the applicable third-octave band.

The noise floor was estimated as the sum of three bins of average mean-squared pressure which were assumed to be present inside of the tone-isolated signal. An expression for the estimated time-varying amount of mean-squared pressure due to broadband noise *b(t)* present in each-tone isolated signal is

$$p_{rms,noise}{}^2(t) = 3 p_{rms,avg}{}^2(t) \tag{3.30}$$

When the mean-squared amplitude envelope of each tone-isolated signal fell below the estimated noise floor, instantaneous frequency estimates were treated as unreliable and a correction was applied. In these cases, the last 'reliable' value of frequency was held until the tonal amplitude envelope rose above the estimated noise floor again. In this way, instantaneous frequency estimates that were the result of broadband noise *b(t)* rather than tonal energy $s_k(t)$ were avoided.

The estimation of low SNR and subsequent correction of the instantaneous frequency estimate are illustrated in Figure 30 and Figure 31. The tone of interest in those two figures is the 40th fan order multiple (5923.6 Hz), isolated from the recording made at 75° emission angle and 87% engine power setting. A five second region of the extracted amplitude envelope and instantaneous frequency is shown in Figure 30. The plot shows the SPL envelope of the extracted tone amplitude a_k in blue, relative to the estimated noise floor in gray. Regions where the tone falls below the noise floor are denoted in red. Four such regions are visible in the axis limits displayed, most notably near 63.8 and 64.2 seconds. In those regions, the instantaneous frequency (not shown) begins to diverge from reasonable estimates.

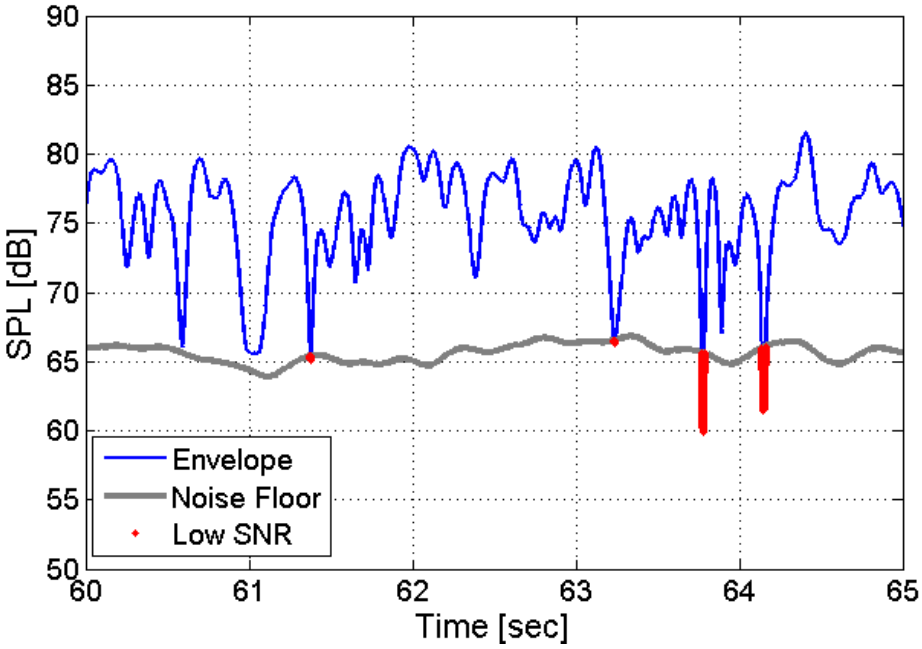

Figure 30. Five second zoomed time history of amplitude envelope, estimated noise floor, and corrected frequency fluctuations (87% power setting, 75° emission angle, 40 fan order tone (5923.6 Hz)).

Figure 31 shows a zoomed in view of the process as applied to the region near 63.8 seconds. Near the center of the time window, the tonal amplitude dips below the estimated noise floor, and the original instantaneous frequency estimate begins to diverge (gray dashed line). During post-processing, the last reliable estimate is held (red line), until the amplitude returns to a level above the estimated noise floor, at about 63.78 seconds. The filter which removes vestigial carrier harmonics then serves to smooth out sharp edges (high-frequency content) in the corrected IF estimate (blue).

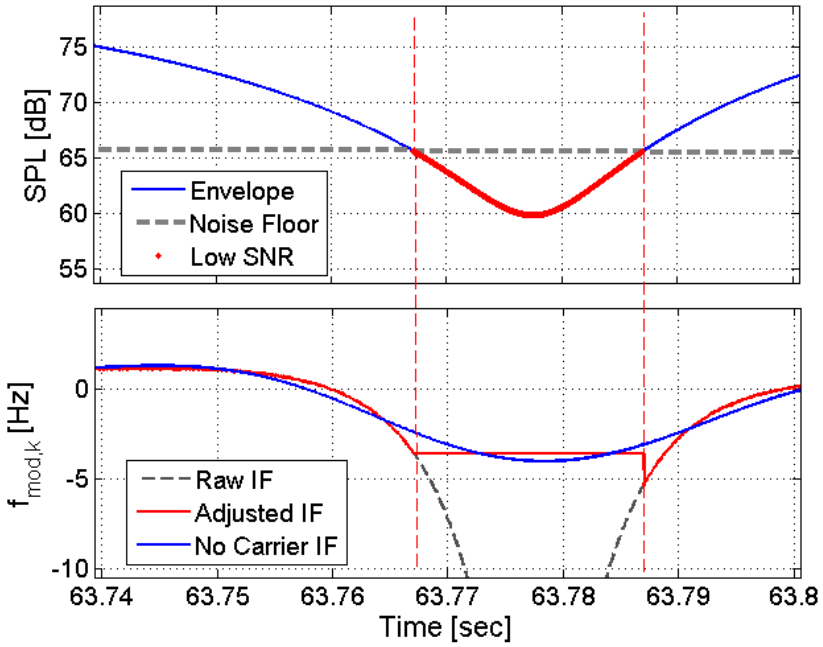

Figure 31. Extracted amplitude envelope, noise floor, and instantaneous frequency corrected for low SNR (87% power setting, 75° emission angle, 40 FO tone (5923.6 Hz)).

By using output of the broadband analysis stage in conjunction with the time-varying amplitude envelope of each tonal signal, a unique and reliable estimate of the instantaneous tonal frequency was obtained in this section. That tonal frequency was not allowed to diverge during regions of low signal-to-noise ratio. In this way, analysis methods which took advantage of the convenience of the analytic signal were implemented for many tones.

3.6 Analysis Summary

During the analysis stage, STFT methods were applied to available data to measure third-octave band fluctuations in broadband noise sources. These third-octave band levels were designed to ignore spectral regions known to contain significant tonal energy. Further, the goal of obtaining time histories for the amplitude and frequency fluctuations of each tone was met. Reliable extraction methods were developed using the tone-isolated analytic signal; where those methods performed poorly, post-processing was carried out using estimates of the signal-to-noise ratio. The arguments of the single-tone model were available, so that inlet-radiated tonal fan noise could be recreated as needed. However, it was desired to construct a general model which could be probed to provide

realistic tonal fluctuations away from power settings or emission angles where EVNERT measurements were available. After all, complete aircraft flyover simulations require calculating the source noise as emitted from a continuously time-varying emission angle. Chapter 4 details efforts to create general synthesis tools capable of accepting time-varying parametric inputs to create realistic fluctuations for arbitrary power settings or emission angles.

4 Synthesis Procedures

Analysis methods applied to tones of interest in EVNERT recordings generated discrete-time histories of the amplitude envelope and instantaneous frequency for each of 6,016 target tones. Likewise, time histories were obtained for measured variations in third-octave band levels of broadband noise. This chapter describes the development of a model which was designed to characterize fluctuations in tonal parameters as bandlimited random processes of specified variance. Synthesis methods are then detailed which use that model to synthesize new fluctuations for conditions and emission angles where EVNERT measurements were unavailable. The developed synthesis methods are able to probe fluctuation models to obtain synthesized tonal noise whose characteristics change over time. A synthesis method is also detailed which recreated the observed fluctuations in third-octave band broadband noise source. Finally, the capabilities of the synthesis tools will be demonstrated for synthesizing source noise corresponding to typical aircraft operations. Those operations may require time-varying emission angle (as in the case of a flyover with stationary observer), or power setting (as in the case of an engine spool-up).

4.1 Broadband Synthesis

The broadband noise component *b(t)* was recreated using the overlap-add method, essentially the reverse operation of a short-time Fourier Transform, using a custom MATLAB tool based on those found in Chapter 8 of ref. [38]. The MATLAB tool and an example function call are included as an attachment to this document as described in Appendix C – List of Attachments. Just as the parameters of frequency resolution at each block and time resolution between successive blocks was important in the STFT analysis, corresponding block lengths and hop sizes are important in overlap-add synthesis.

Instead of beginning with a pressure-time history, then windowing and transforming to the frequency domain to obtain samples of the time-varying spectrum, the overlap-add method begins with desired third-octave band spectra which are specified at many blocks. The inverse Fourier transform is applied to each block, and then the resulting pressure-time histories are windowed, overlapped, and summed in the time domain to obtain the output waveform. The overlap-add method allowed the noise spectrum to be defined independently at each block, thereby granting the ability to

reproduce observed short-term fluctuations in third-octave band levels. Either a third-octave band SPL spectrum or a narrowband pressure amplitude spectrum was defined at each synthesis block. For third-octave band SPL, the conversion to narrowband described in the next section was used. The ability to specify narrowband spectra allowed new fluctuations for tonal parameters to be created using the broadband synthesis tool and the modeled spectrum described in Section 4.2.

4.1.1 Conversion from Third-Octave Bands to Narrowband

Just as spectral estimates were converted from narrowband to third-octave band representations during broadband analysis, the broadband synthesis routine required a corresponding inverse operation. However, the transformation from third-octave band SPL to narrowband pressure amplitude did not require any special post-processing as in the case of the analysis stage. First, the measured total SPL in each third-octave band at each synthesis block was converted to mean-squared pressure by use of the equation

$$p_{rms}^2[k] = p_{ref}^2 \cdot 10^{(SPL[k]/10)} \tag{4.1}$$

where $p^2_{rms}[k]$ is the mean-square pressure in the band at the k^{th} synthesis block and $SPL[k]$ is the sound pressure level in the band of the k^{th} synthesis block. Next, the number of narrowband frequency bins in the third-octave band was calculated through knowledge of the relationship between block length and frequency resolution as stated earlier. The total mean-squared pressure was divided by the number of bins in the band to obtain the average mean-squared pressure in each narrowband bin. Finally, mean-square pressure in each frequency bin was converted to pressure amplitude, in preparation for the inverse Fourier Transform operation described in the next section. The division into average energy per bin represents somewhat of a simplification for synthesis.

A representative broadband SPL spectrum is shown in Figure 32, and the corresponding single-sided narrowband pressure amplitude is shown in Figure 33. Note that even though total third-octave band SPL shows an increasing trend as band number increases, this actually corresponds to a decrease in average energy per bin as frequency increases since the number of bins in each band grows exponentially. The peak energy displayed in measured spectra around 300 Hz due to the jet noise component is evident in the approximated narrowband spectrum.

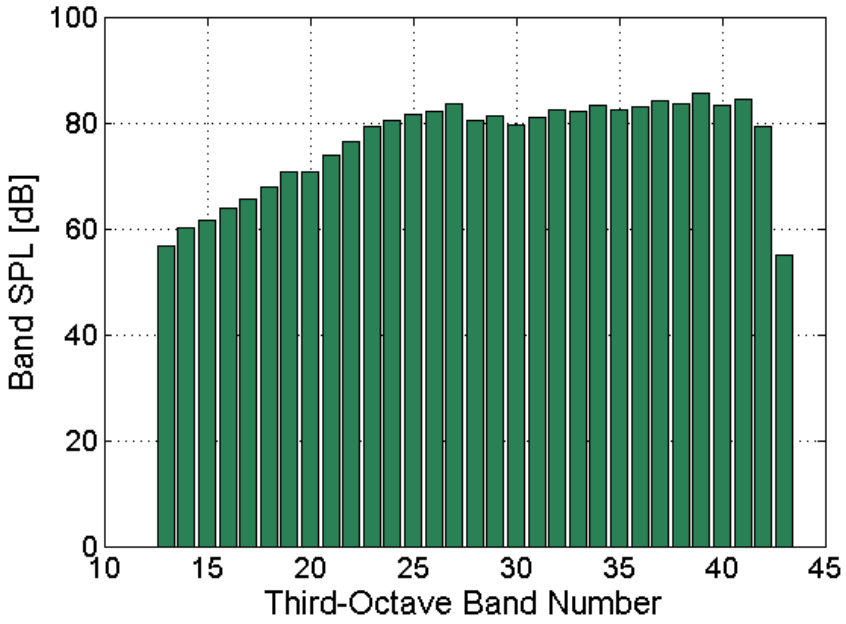

Figure 32. Third-octave band mean SPL vs. band number as input the broadband synthesis tool (measured from 60% power setting and 10° emission angle).

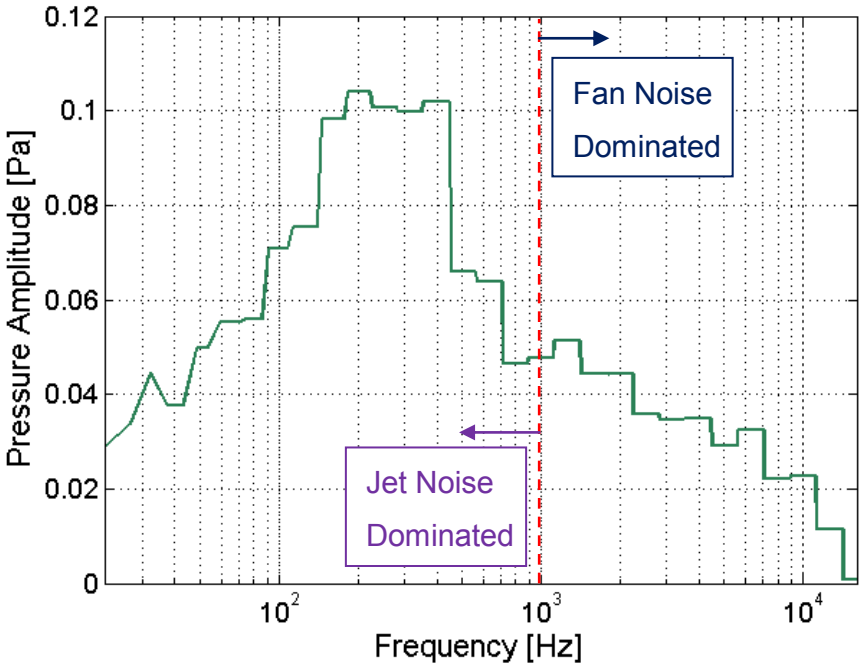

Figure 33. Narrowband pressure amplitude in Pa vs. narrowband frequency as synthesized at one block (approximation of measurement at 60% power setting and 10° emission angle).

4.1.2 Inverse Fast-Fourier Transform

Single-sided narrowband spectra were converted to two-sided filters, and then an Inverse Fast Fourier Transform (IFFT) was applied to obtain pressure-time histories at each synthesis block; those short pressure-time histories are known as "grains." The conversion form third-octave band to narrowband which was described in Section 4.1.1 returned *only* the pressure amplitude in each positive frequency bin, so missing phase information was assumed to be uniformly random in each bin. Real and imaginary parts of the complex frequency-domain spectrum for each block were then obtained by converting polar magnitude and phase to Cartesian coordinates according to Equations (4.2) and (4.3), respectively.

$$\mathrm{Re}\left(G_{SS}[kF]\right) = \left|G_{SS}[kF]\right| \cos\left(\tan^{-1}\left(G_{SS}[kF]\right)\right) \tag{4.2}$$

$$\mathrm{Im}\left(G_{SS}[kF]\right) = \left|G_{SS}[kF]\right| \sin\left(\tan^{-1}\left(G_{SS}[kF]\right)\right) \tag{4.3}$$

In Equations (4.2) and (4.3), $G_{ss}[kF]$ is the single-sided complex narrowband spectrum of the "grain" $g[n]$ at each frequency bin. The imaginary parts of the bins corresponding to zero Hz and the Nyquist frequency were set to zero, fulfilling one of the requirements for the IFFT to return a completely real-valued time history. Conjugate similarity about the Nyquist frequency is the second requirement for an all-real IFFT result. Real and imaginary parts were joined into the complex-valued single-sided spectrum, and then concatenated with the mirrored complex conjugate. The magnitude and phase of the filter which was generated for one synthesis block (corresponding to the pressure amplitude in Figure 33) can be seen in Figure 34. The mirrored similarity in both parameters about the Nyquist frequency is evident in the figure. The complex two-sided filter was then inverse Fourier transformed to obtain the time domain grain sequence g[n].

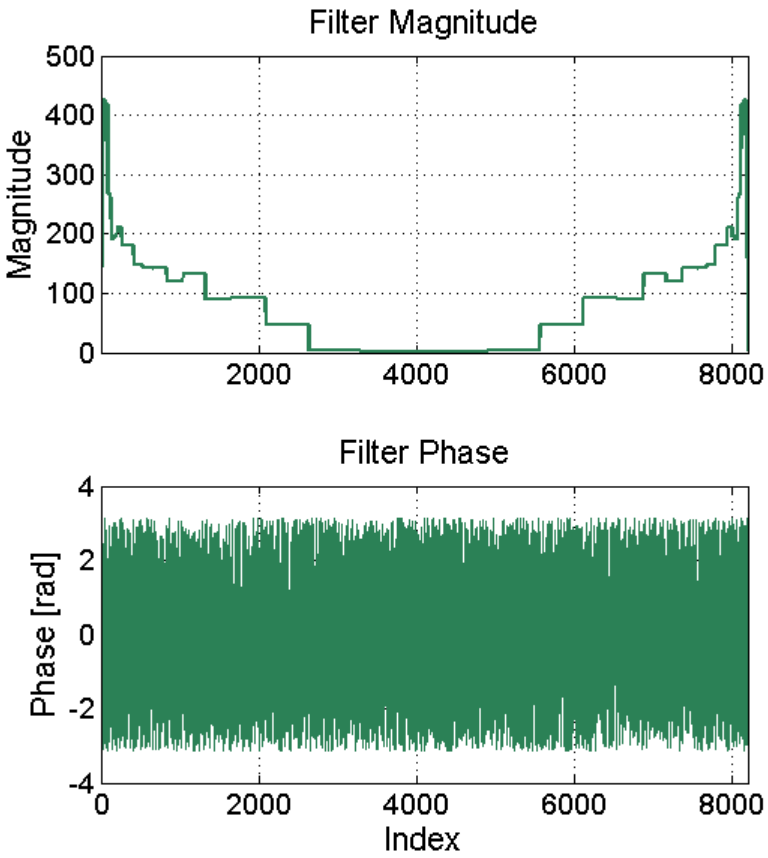

Figure 34. Magnitude and random phase of complex-valued filter designed to generate one output grain during broadband synthesis (approximation of measurement at 60% power setting and 10° emission angle).

4.1.3 Overlap-Add Process

The overlap-add process can be viewed as a moving synthesis buffer [38], where the current output grain *g[n]* is shifted forward in time, then added to existing output. A window was applied to the grain to minimize discontinuities at the block beginning and end. Finally, the block was shifted forward in time by the synthesis hop size, added on a sample-by-sample basis with the total output. The process was then repeated for each remaining synthesis block. Figure 35 shows four plots which summarize the overlap-add process. First, the IFFT is calculated to obtain the current output block (top). Next, the window is applied to the block (top middle). The windowed grain is then added to existing output samples (bottom two plots).

By providing mean values and fluctuations in third-octave band levels at each synthesis block, spectral characteristics may change with time in the broadband synthesis method described. Since fluctuations in those third-octave band levels were not modeled for broadband noise sources as

they were for tonal fan noise sources, the broadband synthesis program only reproduced time-variations which were observed in real data. This approach was successfully applied in the synthesis of jet noise in previous work [39]. Listening tests designed to evaluate perceived realism of model-based tonal fluctuations (described in Chapter 5) used reproduced broadband sources to investigate possible masking effects.

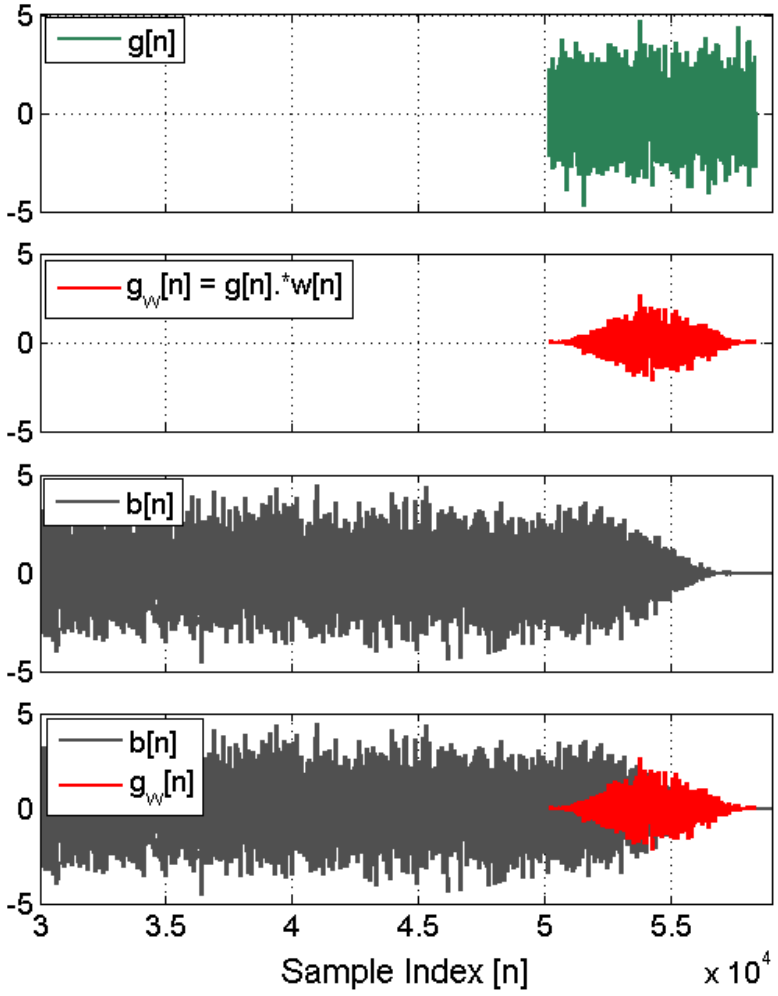

Figure 35. Summary of overlap-add process showing grain, windowed grain, current output, and the combination of windowed grain and total output.

4.2 Characterization of Short Term Fluctuations

A large library of extracted fluctuations was collected from the tonal analysis described in Chapter 3. Use of the extracted fluctuations directly in future simulations is undesirable for several

reasons. First; storage, recall, and simulation of measured tonal fluctuations is expensive in terms of both computation and memory. Second (and more importantly), direct use of measured fluctuations limits possible synthesis conditions to those where EVNERT measurements were taken, unless it can be assumed that one set of fluctuations can be applied to all conditions. That limitation is in direct conflict with the overall goal of flyover noise synthesis, which is to create perceptually realistic simulations for conditions where no measurements exist.

A method was then sought which could model the fluctuations in tonal amplitude and frequency, and could be used to create new fluctuations which are perceptually similar to those measured. The number of parameters and cost of implementation must be low, since random fluctuations must be generated for amplitude and frequency of about 100 tones when MPT noise is present. Additionally, the final model must be able to provide predictions for values where parameters were not directly measured.

4.2.1 Bandlimited Random Process

Psychoacoustic literature notes that humans tend to discriminate fluctuations based on two criteria; the rate (speed) of modulation, and the modulation depth [4]. Those two parameters make natural choices for a model of tonal fluctuations designed to match human perception. Observations of measured fluctuations in tonal parameters indicate that they display characteristics which correspond to the modulation rate and depth. The measured fluctuations contain energy below some limiting frequency, in accordance with expectations and analytic signal requirements. Further, they do not display definite periodicity on any observed timescale, as deterministic systems would. With these ideas in mind, the model chosen for tonal fluctuations was that of a bandlimited random process with a specified power spectral density (PSD).

Two parameters were of interest to represent each PSD estimate, and corresponded directly to the psychoacoustic parameters noted. The first PSD parameter was the cutoff frequency of a certain low-pass filter shape (developed in the next section), and the second was the variance of the fluctuation. An unbiased estimate of the sample variance was calculated according to

$$\hat{\sigma}^2 = \frac{1}{n-1}\sum_{i=1}^{n}\left(X_i - \bar{X}\right)^2 \tag{4.4}$$

where σ^2 is the sample variance[7] in mean-square pressure, n is the number of samples in the fluctuation record, X_i is the i^{th} observed value, and $\bar{X}$ is the sample mean of all recorded fluctuation values within the particular fluctuation signal being modeled [37]. The next section describes in detail the analysis steps taken to estimate the bandwidth of each fluctuation.

4.2.2 Method of Fitting Spectra

The bandwidth of spectral energy in a given fluctuation was estimated by calculating the cutoff frequency of a fitted filter. This process used several steps. The power spectral density of the zero-mean fluctuation was first calculated in units of dB/Hz. Next, the maximum value of the PSD was obtained as a rough estimate for the passband gain of the filter. A weighting vector was prepared whose value was '1' for all bins where the PSD was within 30 decibels of the maximum, and '0' everywhere else. The weighting vector was intended to ignore PSD bins with insignificant energy content. A 3rd order Butterworth filter magnitude response curve was chosen as the prototype for the spectral shape of the model. The weighted root-mean-square (RMS) deviation between the PSD of the measured fluctuation and the prototype filter was minimized as a function of the passband gain and cutoff (half-power) frequency. The RMS deviation between the measured power spectral density $S_{xx}(f)$ and the modeled power spectral density $\hat{S}$ was represented by

$$RMSD\left(S_0, f, f_c\right) = \sqrt{\sum_{m=1}^{M} \psi(f)\left(S_{xx}(f) - \hat{S}\left(S_0, f, f_c\right)\right)^2} \tag{4.5}$$

where the prototype filter magnitude response is given by

$$\hat{S}\left(S_0, f, f_c\right) = 10\log\left(\sqrt{\frac{S_0}{1+\left(\frac{f}{f_c}\right)^{2N}}}\right) \tag{4.6}$$

In Equation (4.5), *RMSD* is the root-mean-square deviation, M is the total number of frequency bins available in the PSD estimate, $\psi(f)$ is a weighting function to exclude low-energy bins, $\hat{S}$ is the modeled PSD shape in dB/Hz, f is the frequency at each bin in Hz, and f_c is the cutoff frequency of

[7] Also note that the variance may alternatively be obtained by calculating the autocorrelation $R_{xx}(\tau)$ of the fluctuation record evaluated at zero lags.

the prototype shape. In Equation (4.6), S_0 is the estimated DC gain of the prototype shape and N is the filter order (defined to be 3).

Figure 36 shows several plots which demonstrate the PSD weighting process. The top plot shows the original measured PSD of the frequency fluctuation of the 1BPF as measured at 48% power setting and 75° emission angle. The bandlimited characteristic is evident, where most energy is contained in the region below about 11 Hz, and the spectral energy decreases with increasing frequency. Above about 30 Hz, numerical noise begins to dominate, and the spectrum falls off steadily towards -100 dB. The maximum value near -5 dB is displayed, as well as the frequency corresponding to 30 dB down from the maximum. The center plot shows the weighting vector corresponding to that 30 dB down point, while the bottom plot shows only the PSD inside the fitted region.

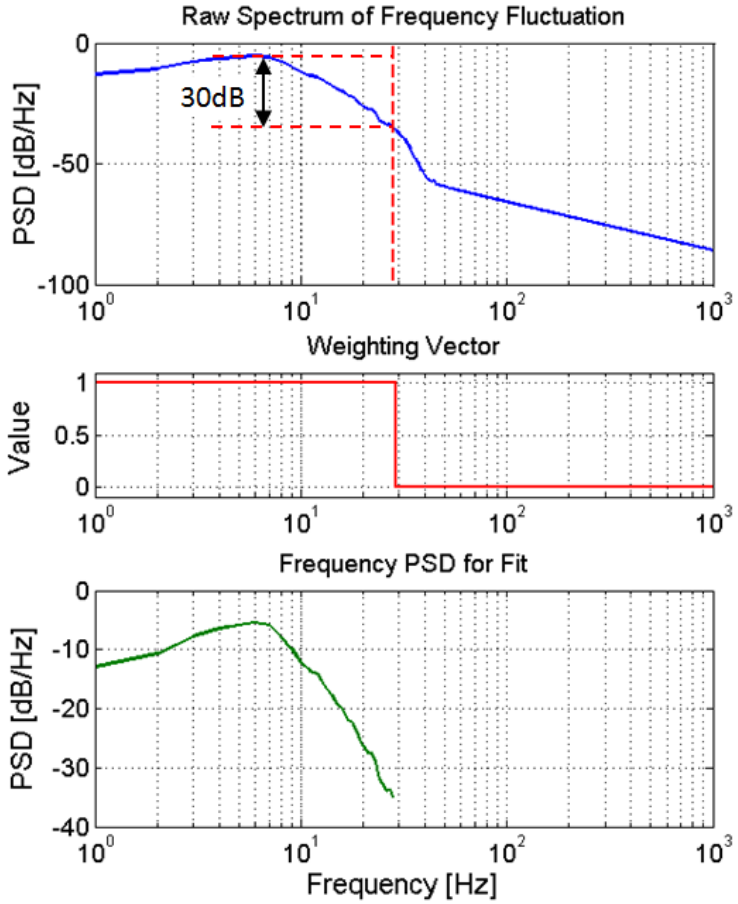

Figure 36. Original PSD of demodulated frequency fluctuation, weights, and weighted spectrum for RMSD minimization (48% engine power, 75° emission angle, 1BPF).

Minimization of the RMS deviation described by Equation (4.5) was performed using the MATLAB *'fminsearch'* function, which finds a local solution using the direct simplex method [40]. The result of the nonlinear fit routine was the cutoff frequency of a filter with minimum RMS error from the measured power spectral density. A graphic which displays a measured PSD and the resulting fit for the frequency fluctuation in the 1BPF tone at 48% power and 75° emission angle is shown in Figure 37. The original measured PSD is shown in solid green, while the fitted filter response is shown in dashed red. The filter matches the general trend in the measured fluctuation, up to the limit of the weighted region near 30 Hz. The cutoff frequency of the fitted filter (shown in pink), along with the calculated variance of the fluctuation, were then stored along with all other measurements. Those measurements were organized into useful surfaces as described in the next section.

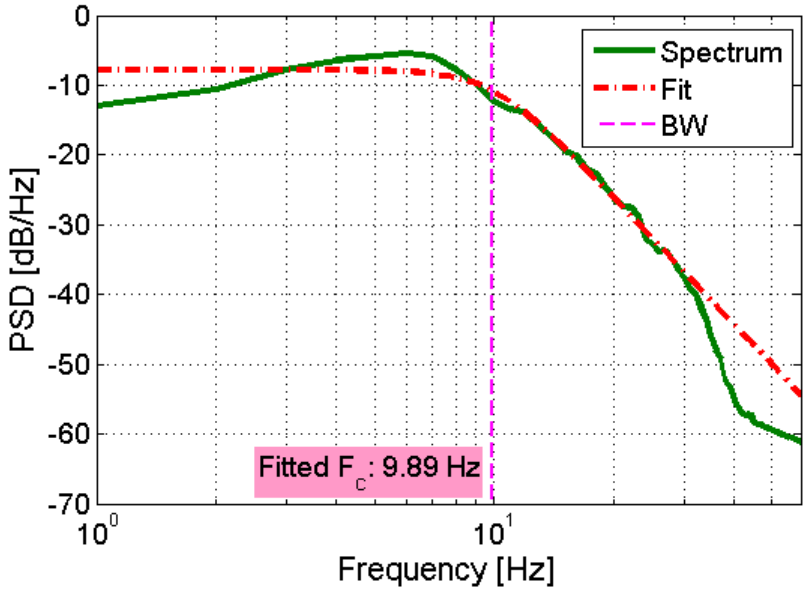

Figure 37. Results of the RMSD minimization for frequency fluctuations in the 1BPF tone at 48% engine power and 75° emission angle.

4.2.3 Surface Interpolation between Measurements

The result of modeling each fluctuation as a bandlimited random process resulted in the characterization of amplitude and frequency modulations for each tone in each microphone recording at each power setting. The total number of parameters stored was 24,064 – bandwidth and variance for the amplitude and frequency fluctuations of each of the 6,016 target tones. Each set of parameters

was visualized as a surface for each tone, where measured values were linearly interpolated as a function of engine power setting and emission angle.

Two-dimensional linear interpolation on each parameter resulted in four fit surfaces for each of the 88 tones analyzed. Figure 38 shows the bandwidth of amplitude fluctuations extracted from the 2BPF as measured in all available EVNERT data (in Hz). Figure 39 shows the variance of amplitude fluctuations in units of Pa^2. Figure 40 and Figure 41 show the corresponding model parameters for frequency fluctuations as measured for the same tone. Interpolated surfaces generated for each tone could then be probed to obtain an estimate of the model parameters at a point where no recording of the TECH977 engine was made. Inside of the measured regions for power setting and emission angle, linear interpolations were used as estimates between measurement points. Outside of the regions, the nearest measured value was used.

The lobed directivity of fan noise emission apparent from Figure 6, which is usually associated with mean amplitude values, is evident in several of the modeled surfaces (Figure 38 through Figure 41). It is especially apparent in emission angles ranging from 10° to 60° off-axis. It is hypothesized that emission angles greater than 110° begin to predominantly represent broadband noise characteristics rather than qualities of measured fan noise, since the barrier constructed for EVNERT configuration 19 served to block aft-radiated tonal noise from reaching the microphone array. This is thought to be the case since corrected regions in instantaneous frequency estimates outnumbered reliable estimates (especially for high-order, low-amplitude MPTs), further obscuring the calculated long term statistics. In addition, inlet-radiated tones become severely attenuated in aft microphone measurements. Fluctuation bandwidths did not change significantly over the measured range of engine power settings for either amplitude (4-11 Hz) or frequency (5.6-13 Hz). The variance of frequency fluctuations did not display a significant trend as power setting increased, but the variance of amplitude fluctuations did. The variance of amplitude fluctuations seemed to be larger in regions where the mean amplitude (not shown) was larger.

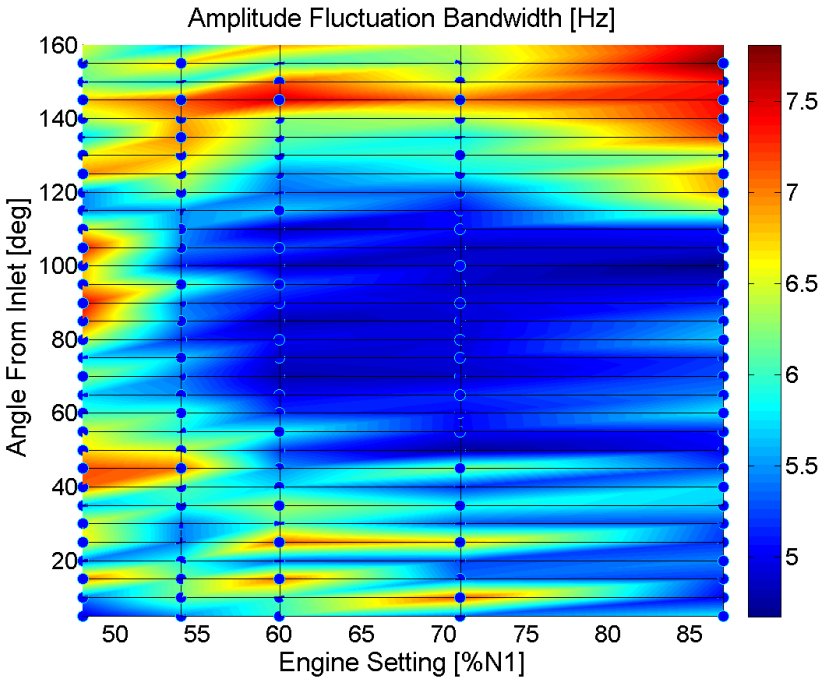

Figure 38. Interpolated surface for bandwidth [Hz] of amplitude fluctuations in the 2BPF tone in analyzed EVNERT recordings.

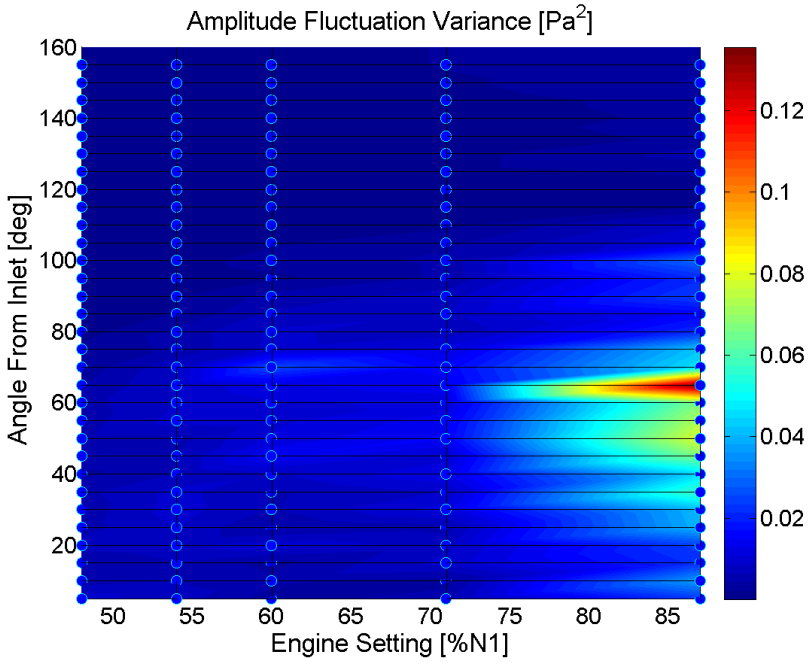

Figure 39. Interpolated surface for variance [Pa^2] of amplitude fluctuations in the 2BPF tone in analyzed EVNERT recordings.

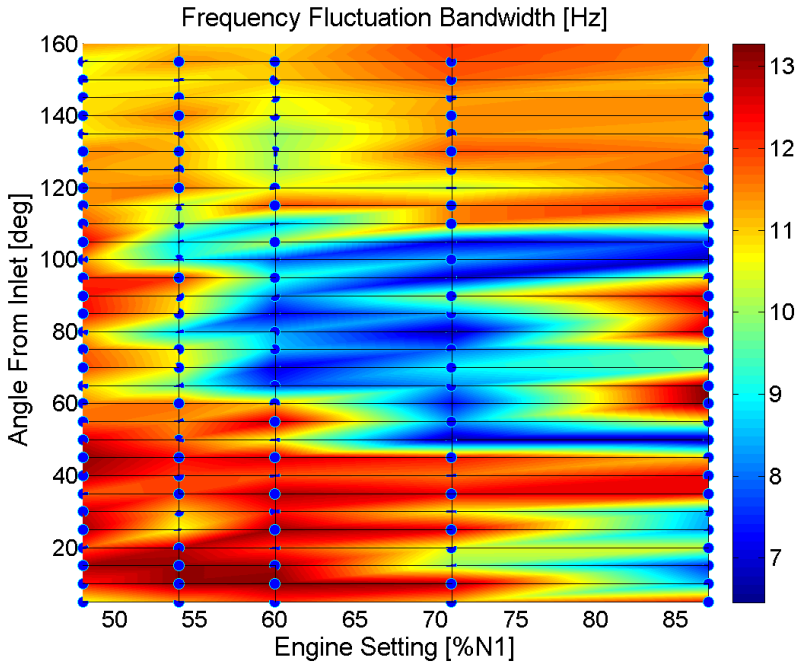

Figure 40. Interpolated surface for bandwidth [Hz] of frequency fluctuations in the 2BPF tone in analyzed EVNERT recordings.

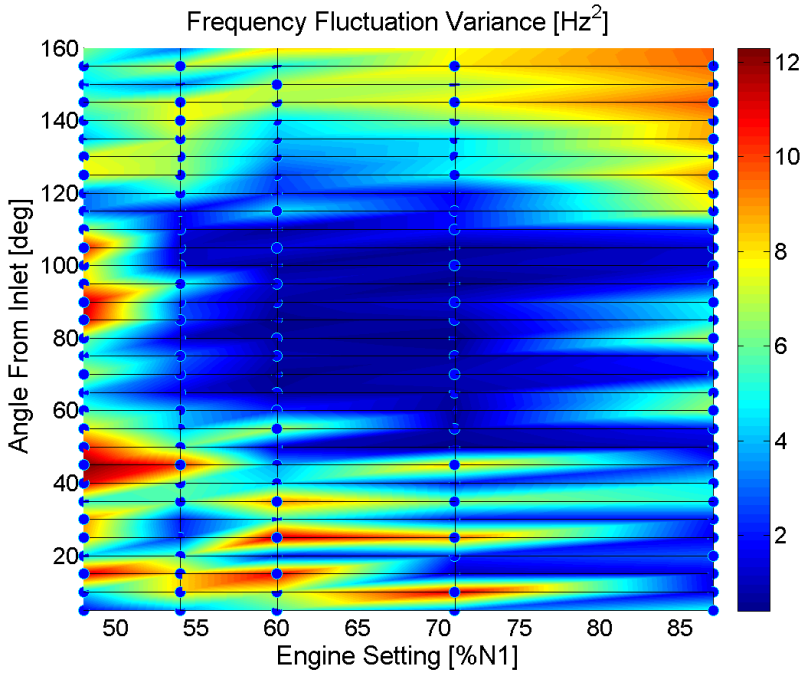

Figure 41. Interpolated surface for variance [Hz^2] of frequency fluctuations in the 2BPF tone in analyzed EVNERT recordings.

4.3 Tonal Synthesis

A tonal synthesis program was written in MATLAB to create new tonal noise based on the analysis and characterization steps detailed earlier. A copy of the tonal synthesis program and an example function call are included as attachments to this document, as described in Appendix C – List of Attachments. The synthesis program is able to synthesize either parametric inputs for fluctuation parameters in each tone as a function of time, or measured fluctuations directly. Synthesis is not handled in real time; instead time histories are generated for the entire requested record. Although analysis of each recorded tone was performed using the complex-valued analytic signal, new tonal noise was synthesized by directly supplying the amplitude and phase angle arguments of the single-tone model.

4.3.1 The Tonal Synthesis Approach

Multi-tone synthesis was performed by directly adding together many individual tones as

$$\hat{s}[n] = \sum_{k=1}^{K} \hat{s}_k[n] \tag{4.7}$$

where 'hats' denote synthesized pressure-time histories. Integration of instantaneous frequency to obtain the cosine argument was approximated during synthesis in the discrete time domain for the single-tone model. Specifically, each tone was generated by providing the amplitude envelope and instantaneous frequency directly to Equation (4.8)

$$\hat{s}_k[n] = \hat{a}_k[n]\cos\left(\frac{2\pi}{F_s}\sum_{i=1}^{n}\hat{f}_k[i] + \hat{\phi}_{0,k}\right) \tag{4.8}$$

Note the inclusion of the constant $\phi_{0,k}$ as the last argument of the cosine function. That constant of integration is carried over from analyses where it was the first value of the measured phase function, but lost when estimating the derivative to find instantaneous frequency. For cases where it was desired to directly synthesize an observed set of tonal fluctuations, that constant phase offset was important to ensure time alignment of the synthesis with the original measurement. When synthesizing tonal noise which was not supposed to mimic some measured set of fluctuations, the constant phase offset was set to random in the interval $[-\pi,\pi]$. The amplitude envelope and instantaneous frequency arguments of Equation (4.8) are given as

$$\hat{a}_k[n] = \hat{a}_{mean,k}[n] + \hat{a}_{mod,k}[n] \tag{4.9}$$

$$\hat{f}_k[n] = f_{mean,k}[n] + \hat{f}_{mod,k}[n] \tag{4.10}$$

Since mean values and fluctuations are specified separately, they may be obtained from different sources. Generally, mean values for fan noise synthesis are provided by some engine noise prediction, such as ANOPP. They may also be provided directly from measurement to make sure the time-averaged spectra match, while at the same time providing simulated fluctuations around those measured means.

Figure 42 shows original measured fluctuations in amplitude and frequency for an example tone, compared with those fluctuations as obtained from analysis of directly resynthesized noise. Measurement and analysis showed that the tonal synthesis routine generated a synthesized set of fluctuations which were in good agreement with the specific set provided. Some small differences are due to tonal energy leakage outside the analysis isolation filter window.

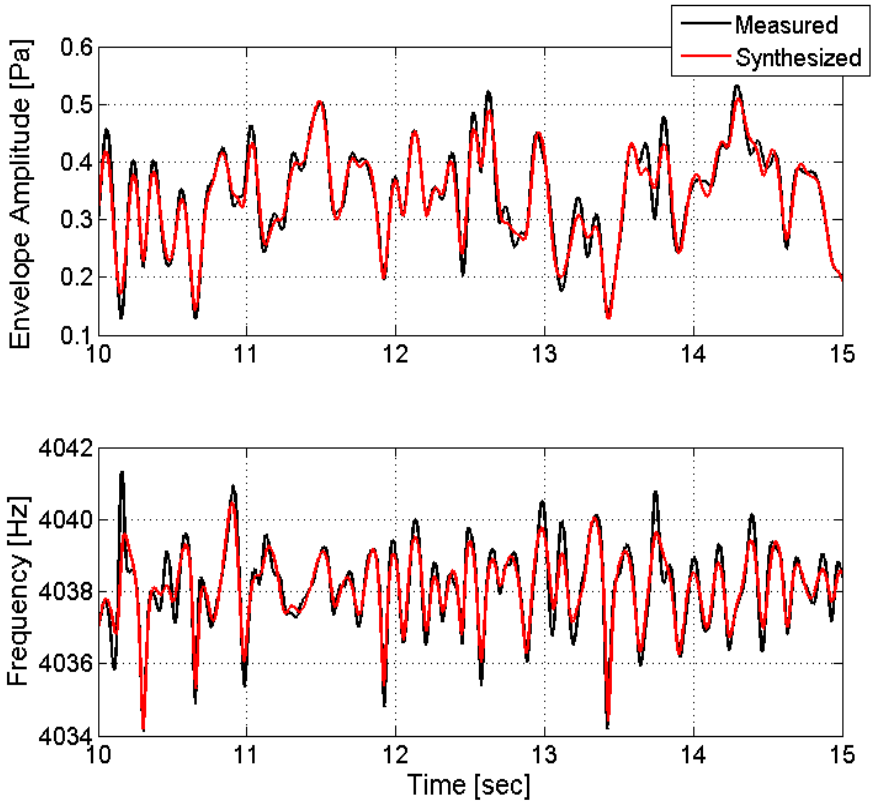

Figure 42. Comparison of measured and directly synthesized time histories for amplitude and frequency of the 2BPF tone at 48% engine power and 75° emission angle.

4.3.2 Generation of Fluctuations

One main objective of the work was to synthesize new tonal noise based on the parametric fluctuation model developed earlier. A top-level flowchart describing the process by which tonal fluctuations were generated for amplitude and frequency is shown in Figure 43. Modeled tonal fluctuations were generated by evaluating one realization of the corresponding bandlimited random process. The broadband synthesis tool developed earlier was used to obtain that realization, but rather than specifying time-varying third-octave band levels as input, narrowband spectra were directly provided at each synthesis block. Those narrowband spectra were simply the prototype spectral shape evaluated with the appropriate bandwidth and variance. Note that specification of fluctuation spectra at each synthesis block allowed model parameters to vary with time. That is, synthesis of tonal fluctuations could be performed for non-stationary bandwidth and variance. The capability to vary fluctuation model parameters as well as mean tonal amplitude and frequency proved to be useful for the ultimate goal of synthesizing realistic tonal noise in the context of an aircraft flyover.

Practically, fluctuation parameters were not specified at each synthesis sample, although the single-tone synthesis model required their eventual representation on that scale. Mean values for amplitude and frequency, as well as bandwidth and variance of amplitude and frequency fluctuations, were usually specified at several “waypoints” in time. Single-sided narrowband spectra were then generated at each waypoint for each fluctuation, corresponding to the model PSD function evaluated for the appropriate parameters. Mean parameters for amplitude and frequency were simply linearly interpolated at each tonal sample, while fluctuation spectra were linearly interpolated between waypoints at each broadband synthesis block. Specification in this way allowed the broadband synthesis program developed to also be used for generation of new, time-varying tonal fluctuations. Alternately, model parameters could be interpolated at each synthesis block. The single-sided narrowband spectra would then be generated directly from interpolated parameters rather than interpolated themselves.

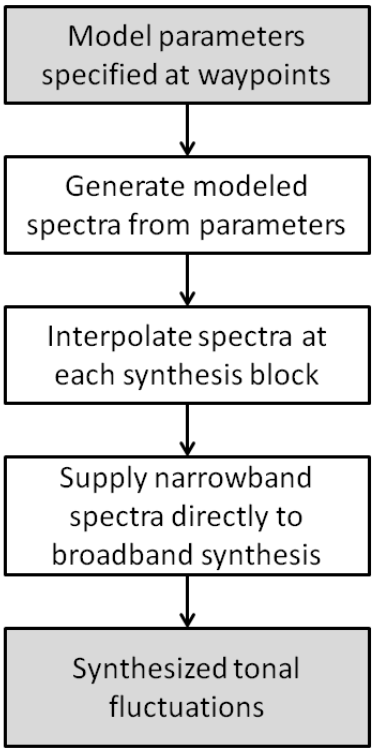

Figure 43. Flowchart describing process where broadband synthesis routine is utilized to create new a new tonal fluctuation based on model parameters.

4.3.3 Tonal Synthesis Demonstration

This section shows the effect that variation in each model parameter (mean, bandwidth, and variance) has on output time histories. It demonstrates that the modeling and synthesis methods developed have the ability to continuously vary parameters over time. To show those effects, a 1,000 Hz tone with time-invariant frequency was synthesized with several types of amplitude modulation. Only amplitude fluctuation parameters are varied in this demonstration.

Figure 44 shows the effect of linearly increasing the bandwidth of amplitude fluctuations from 1 Hz to 50 Hz over a period of 10 seconds. The 1,000 Hz tone had mean amplitude of 10 Pa, around which fluctuations were generated. Note that variance of fluctuations remains relatively constant over the 10 second synthesis time.

Figure 45 shows the effect of increasing amplitude fluctuation variance from 0 Pa^2 to 20 Pa^2 over ten seconds while holding the amplitude fluctuation bandwidth and mean steady. At zero seconds, there is no fluctuation whatsoever in tonal amplitude, while as the signal gets closer to ten seconds, the amplitude is fluctuating so wildly that it dips to zero (near the 9.5 second mark).

Lastly, Figure 46 shows how the mean amplitude term could be increased over time. Such an effect could occur during an increase in engine power up, or a change in emission angle to a region where the particular tone radiates more strongly. As the mean amplitude increases from 2 Pa to 20 Pa over ten seconds, the variance and bandwidth of fluctuations are held steady at 2 Pa^2 and 8 Hz, respectively.

Although the three figures show the effect of varying fluctuation bandwidth, variance, and mean of tonal amplitude over time, similar controls are available for tonal frequency. Since the same broadband synthesis routine is used to generate fluctuations, the performance is identical no matter the eventual use.

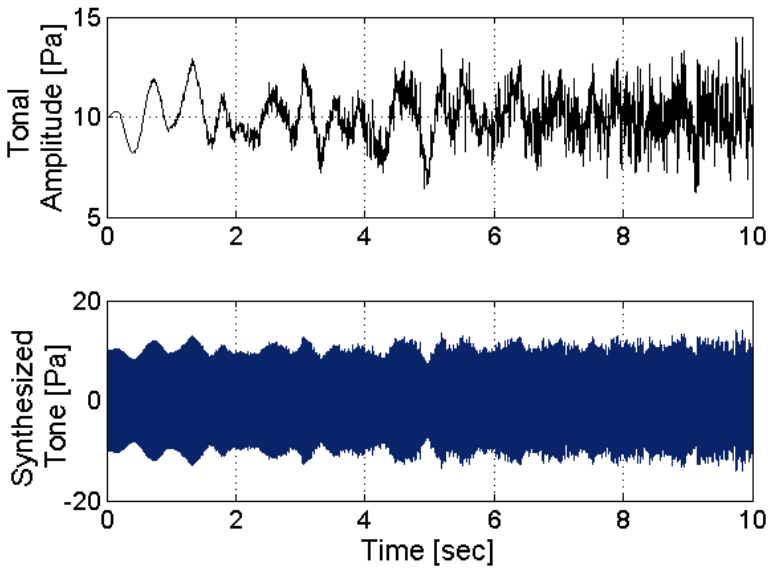

Figure 44. Demonstration of effects of increasing amplitude fluctuation bandwidth from 1 Hz to 50 Hz over a ten-second window.

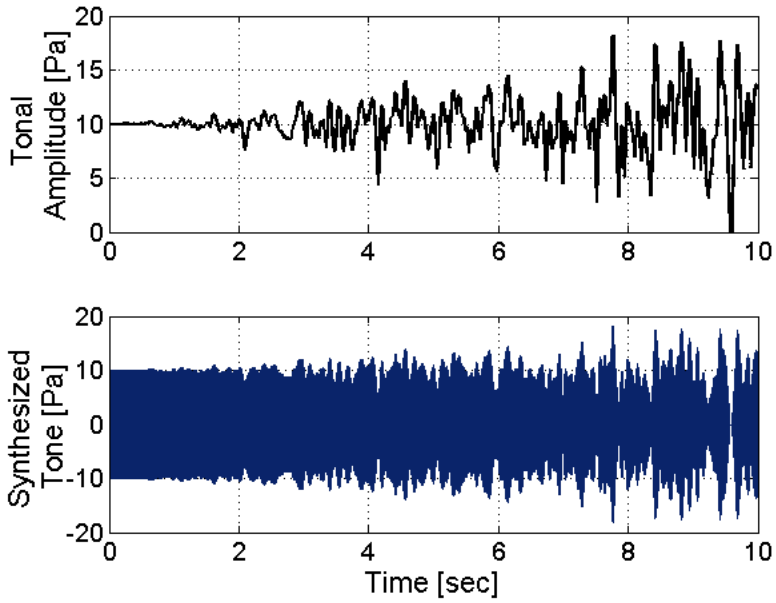

Figure 45. Demonstration of effects of increasing amplitude fluctuation variance from 0 Pa^2 to 20 Pa^2 over a ten-second window.

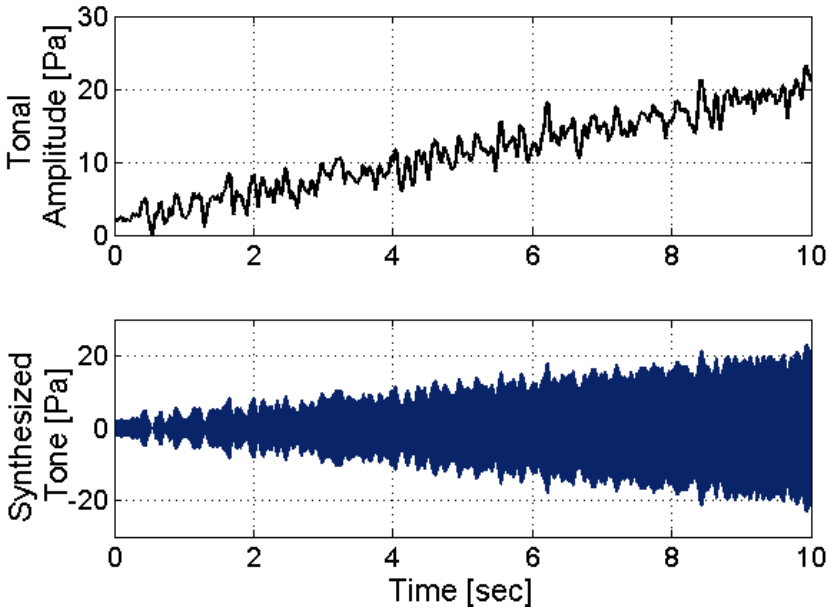

Figure 46. Demonstration of effects of increasing mean amplitude from 2 Pa to 20 Pa over a ten-second window.

4.4 Practical Synthesis Applications

The previous section demonstrated that the tonal synthesis method developed was able to reproduce arbitrary fluctuations in tonal parameters as a function of time. Since the ultimate goal of this work was the improvement of aircraft flyover noise simulation, this section describes how tonal synthesis methods may be utilized to create simulated measurements of practical TECH977 engine operations. For example, simulated aircraft flyovers for a fixed observer position require that source noise be created as if were radiating from a time-varying emission angle. Another simulated operation might require the power setting of the engine to change over time. The variation of engine performance parameters over time directly implies a variation in tonal fluctuation parameters over time. Such changes in simulated emission angle or engine power setting correspond to traversing trajectories over the interpolated model parameters as illustrated in Figure 38 through Figure 41.

4.4.1 Engine Spool-Up

One possible operation of interest when synthesizing tonal noise is that of an engine "spool-up," consisting of a continuous change in power setting as might be encountered before a takeoff. A WAV file of a synthesized engine spool-up is included with this thesis, as described in Appendix C – List of Attachments. During a spool-up, mean frequencies must increase while maintaining their harmonic relationship. MPT noise must also be accounted for, as it cuts on once the fan reaches a supersonic condition. Figure 47 shows a simulated TECH977 spool up at a constant emission angle of 45° which accounts for both characteristics. The engine power setting changes linearly between measured points, and once shaft-order tones were measured in the spectrum, they begin to cut on in the simulation as well (near 5 seconds).

Since mean amplitude and frequency were linearly interpolated at each tonal synthesis sample, care must be taken to provide a waypoint near the point where the supersonic transition actually takes place. That transition can be estimated as a function of inlet flow speed, fan rotational speed, and the speed of sound as a function of temperature. Figure 48 shows a notional example of the result when waypoints are specified too coarsely. If waypoints are too far apart, synthesized MPT noise will cut on at engine settings where it is not physically plausible. All that can be deduced from the data analyzed is that MPT cuts on somewhere between 60% and 71% engine power setting. This accounts for the ramp-up in MPT amplitude shown in Figure 47.

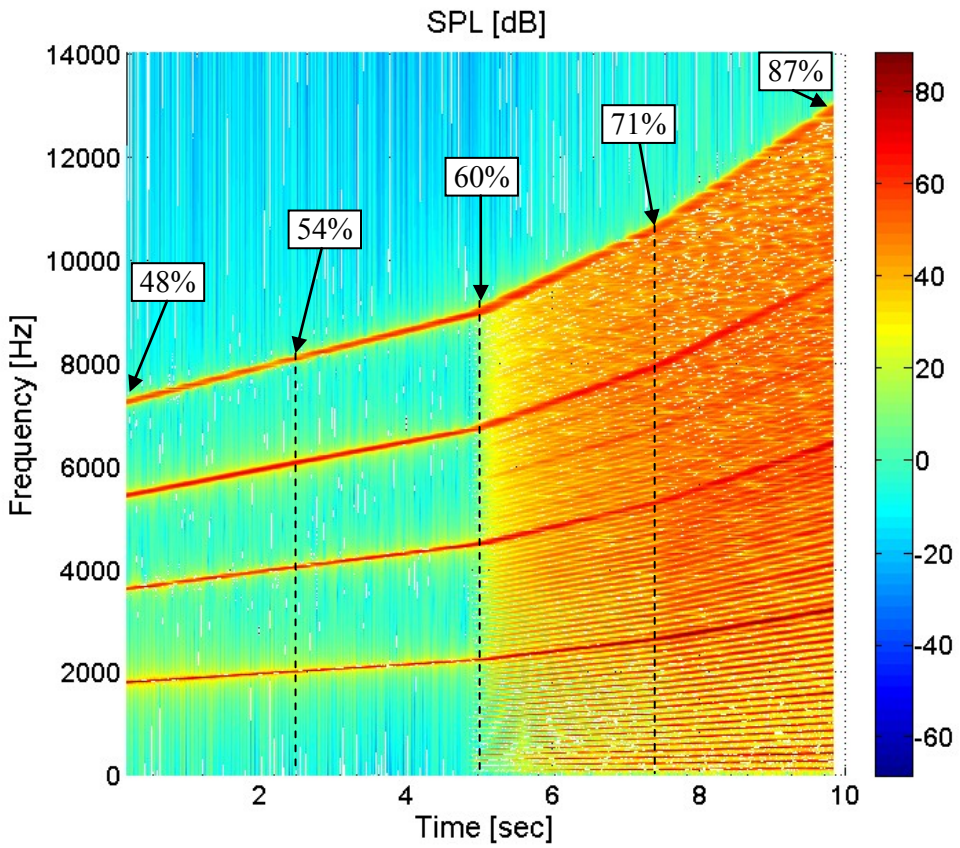

Figure 47. Simulated TECH977 engine spool up over 10 seconds using time-varying model parameters (stationary emission angle of 45°).

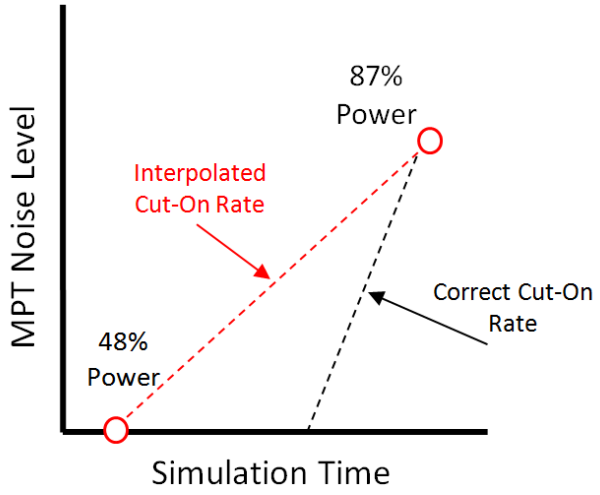

Figure 48. Notional example of non-physical synthesis result possibly caused by coarse waypoint specification during an engine spool-up.

4.4.2 Directivity Angle Change at Low Power

Another practical operation is to gradually change the emission angle from which source noise is synthesized. At low power, this operation would correspond to physically walking around the TECH977 engine from inlet to discharge while keeping power setting constant at an idle condition of 48%. Figure 49 shows the mean SPL of four synthesized multiples of the BPF versus time at the various input waypoints, which change level according to different regions of measured source directivity. Those waypoints are then interpolated at intermediate directivity angles during synthesis. A WAV file of this synthesized change in emission angle is included with this thesis as described in Appendix C – List of Attachments. Variance and bandwidth of fluctuations also change with respect to time. A spectrogram of the emission angle change can be seen in Figure 50, with SPL changes corresponding to those measured in EVNERT data.

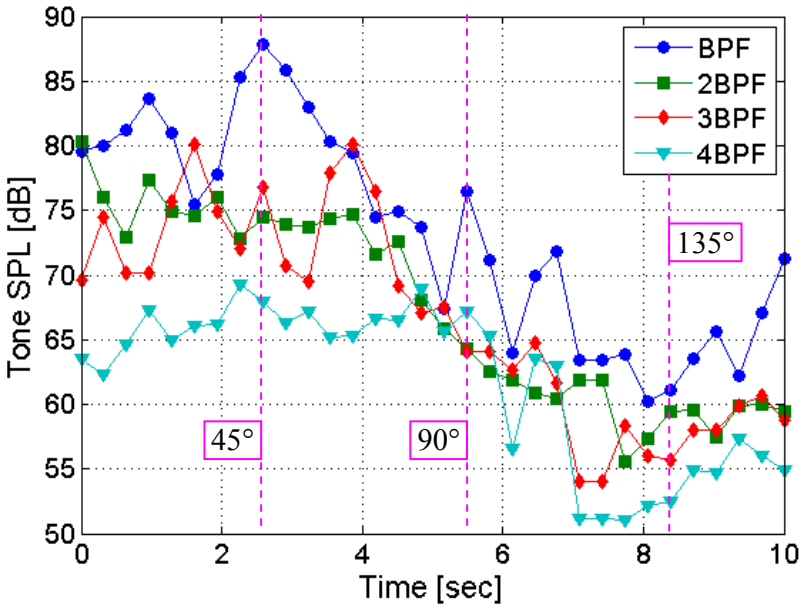

Figure 49. Mean SPL of four BPF multiples vs. time during simulated emission angle change at low engine power.

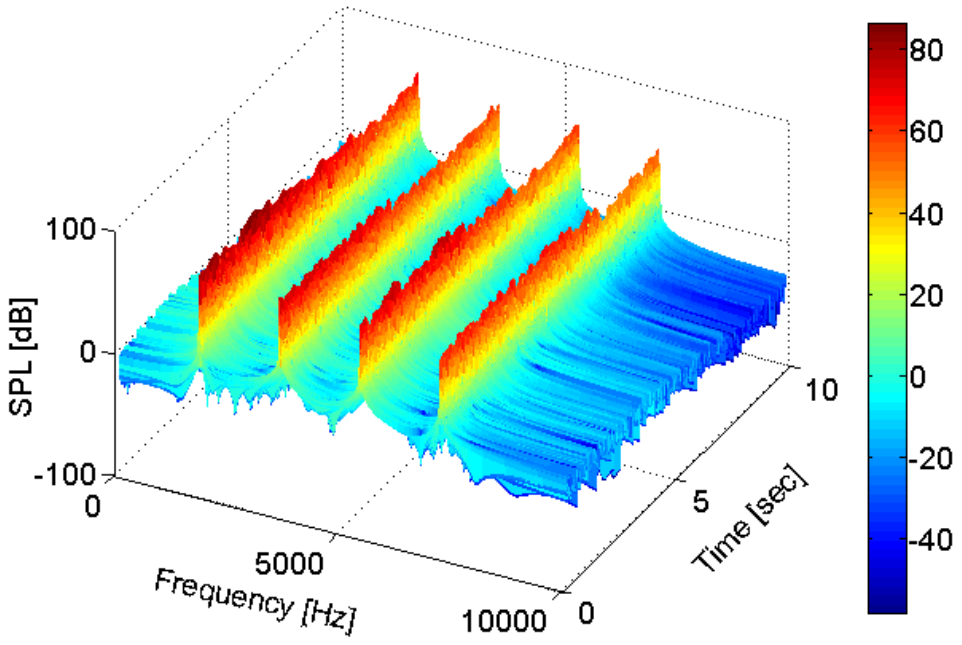

Figure 50. Simulated TECH977 emission angle variation from 5° to 160° off-axis over 10 seconds using time-varying fluctuation parameters.

4.5 Synthesis Conclusions

The results of this chapter show progress in two categories. First, a method was developed to realistically characterize measured fluctuations in tonal parameters. Second, a set of tools was created to synthesize general time-varying noise for both fan broadband and tonal sources. The model was developed based on important psychoacoustic parameters for rate and depth of modulation, which are related directly to the statistical properties of fluctuations: bandwidth and variance. The described tonal synthesis method allowed interpolated surfaces for each model parameter to be evaluated as a function of time with respect to both engine power setting and emission angle. That capability enabled the simulation of new TECH977 tonal noise for situations where measurements were not directly available, and for arbitrary engine operations where recordings were certainly not available.

5 Subjective Listening Tests

While quantitative comparisons showed good agreement, it was desired to gather data from human subjects to verify the perceptual similarity of synthesized and recorded fan noise. The goal of the work was ultimately to improve source noise modeling and synthesis methods for the tonal and broadband components of turbofan noise, so subjective listening tests directly evaluated several types of synthesized noise against recordings. Fan noise at two engine power settings and three emission angles was used to evaluate the subjective performance of the model for a variety of conditions. The broadband component was included in half of the test signals, and was synthesized using measured fluctuations according to the process detailed in Section 4.1.The following section describes the experimental design and results of subjective evaluations. It details expected sources of experimental bias, as well as how certain test design methods were utilized to minimize those biases. It also describes the Analysis of Variance (ANOVA) that was used to identify independent variables which had significant influence on subject responses.

5.1 Goals

The subjective evaluation conducted was structured to answer several questions about synthesis methods for fan source noise. The research questions (RQ) were:

RQ1. How similar to recorded noise is fan noise which is synthesized *with* short-term fluctuations in tonal amplitude and frequency?

   a. How does is this similarity change with respect to different engine power settings?

   b. How does this similarity change when a synthesized *time-varying* broadband noise component is added to time-varying tonal noise?

RQ2. What is the highest similarity score that a test constructed in the current manner can expect for a nominally identical[8] fan noise?

RQ3. How similar to recorded noise is fan noise which is synthesized *without* short-term fluctuations in tonal amplitude and frequency?

[8] 'Nominally identical' in this context means *having the same long-term statistical properties for mean values as well as those values which describe short-term fluctuations around the mean*. Practically, nominally identical segments are non-overlapping segments of the same recording.

a. How does this similarity change with respect to different engine power settings?

b. How does this similarity change when a synthesized *time-invariant* broadband noise component is added to the tonal source?

The research questions were focused on evaluating the increase in realism gained by including short term fluctuations in fan noise sources, rather than simulating directly based on time-averaged predictions. It was expected that (in general), including fluctuations in noise sources would increase the perceived realism of synthesized noise as in Figure 51. For a given rating scale whose minimum and maximum scales are outlined in black, the expected scores for several comparisons are shown. The lowest expected score, corresponding to the current state-of-the-art simulation methods, does not include fluctuations in either the tonal or broadband source. Due to experimental biases, it was not expected that listeners would assign the lowest possible score. Two other possible synthesis cases are shown in Figure 51, though they were not tested in these evaluations. They correspond to unlikely synthesis scenarios where only one component includes fluctuations. The next possibility corresponds to the synthesis methods developed here, which include time-domain fluctuations on both tonal and broadband noise sources. The final possibility is for recorded noise compared with itself, and represents the "perfect" score, for noise which is perceptually identical to recordings.

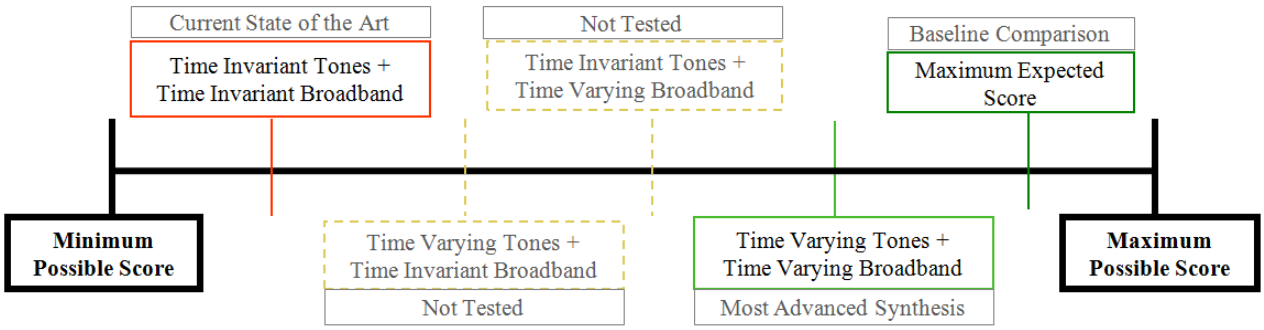

Figure 51. Expected results from subjective evaluations as a function of increasing simulation fidelity.

5.2 Experimental Design

Subjective evaluations were structured in a way to avoid expected sources of experimental bias. Various aspects of test design, such as duration, order of signal presentation, and noise characteristics were included in experimental controls. The following section describes how the

subjective listening tests were constructed to evaluate the realism of fan noise synthesized with time-domain fluctuations while eliminating or minimizing sources of bias.

5.2.1 Selection of Study Participants

The subjective evaluations discussed here were conducted in accordance with protocols approved by the Institutional Review Board (IRB) at NASA Langley Research Center[9]. Participants for the subjective evaluation were recruited from a pool of community volunteers through advertisements in local newspapers, colleges, and civic organizations. Subjects were required to be at least 18 years old, while no upper limit was specified. No affiliation, skills, or expertise was required of the subjects. The only requirement was that subjects with hearing loss more than 40 dB in either ear over the frequency range 500 to 8,000 Hz were not allowed to participate in the test.

Background material showed that for subjects who are not expected to have any familiarity with the types of noises presented, 24 to 36 subjects is an appropriate number [41]. Based on that information, thirty subjects were selected for this evaluation. Limitations on equipment available for playback required that subjects were divided into five groups of six participants each.

5.2.2 Paired Comparisons

For the average listener, realism of fan source noise is difficult to evaluate with no reference for comparison; typical experiences are with complete flyover events which include all propagation and listener effects noted earlier. Therefore, subjective testing presented listeners with paired noises and then requested a rating of the degree of similarity between them. Listeners were informed that the sounds they were hearing were aircraft noises, but were not informed that at least one noise was always a recording. When comparing a synthesized noise source with a recorded noise source, a high similarity rating was understood to mean that "the synthesized source sounds like a real source." In this way, a similarity score was used to imply the realism of synthesized noise rather than attempting to measure realism directly. One noise in each comparison was referred to as "A" and the other as "B" for clarity. A comparison in forward order was called "A-B" and a comparison in reverse order (as motivated by Section 5.2.4) was called "B-A."

[9] The NASA LaRC IRB title for the subjective evaluations was "Synthesized Engine Noise Test 1."

5.2.3 Description of Noise Comparisons

Using both recorded and synthesized fan noise at two power settings, three emission angles, and two spectral content types, 20 A-B comparisons were identified. These comparisons were each specifically designed to answer one or more of the research questions defined above. Three categories of comparisons are outlined in this section; they are referred to as "target," baseline," or "time-invariant."

Subjects were presented with twelve "target" pairs of fan noise to assess the potential effects of two independent parameters (power setting and spectral content) on the realism of synthesized fan noise. Each "target" pair consisted of one segment of a fan noise recording at a specified emission angle and power setting and one segment of synthesized noise whose tonal fluctuations were based on the model developed earlier. Table 6 summarizes the common characteristics of synthesized and recorded segments in each of the twelve target pairs. The research question addressed for each pair is indicated in the rightmost column. Several audio files which were played to subjects are included with this thesis as reference, and they are denoted by asterisks. A complete list can be found in Appendix C – List of Attachments.

Table 6. Configuration of fan noise "target" pairs, included to evaluate effect of independent variables on perceived realism.

Pair ID	Emission Angle [degrees]	Engine Power [%]	Spectral Content (synthesized sources are time-varying)	RQ
1	15	87	Tonal	1/a
2	15	87	Tonal + Broadband	1/a/b
3	15	48	Tonal	1/a
4	15	48	Tonal + Broadband	1/a/b
5*	50	87	Tonal	1/a
6*	50	87	Tonal + Broadband	1/a/b
7*	50	48	Tonal	1/a
8*	50	48	Tonal + Broadband	1/a/b
9	85	87	Tonal	1/a
10	85	87	Tonal + Broadband	1/a/b
11	85	48	Tonal	1/a
12	85	48	Tonal + Broadband	1/a/b

*WAV file included as attachment.

In addition to the twelve paired comparisons detailed in Table 6, four "baseline" comparisons were added, at conditions matching only one emission angle from the "target" comparisons. These baseline pairs were nominally identical, and consisted of two non-overlapping segments of the same recording. Thus, the addition of "baseline" pairs established a maximum expected score as a reference for similarity scores of target pairs at the same conditions. A description of the configuration of recorded segments included in "baseline" pairs is shown in Table 7.

Table 7. Configuration of "baseline" pairs, included to gauge the maximum expected similarity rating for a given combination of independent variables.

Pair ID	Emission Angle [degrees]	Engine Power [%]	Spectral Content (all sources recorded)	RQ
13*	50	87	Tonal	2
14*	50	87	Tonal + Broadband	2
15*	50	48	Tonal	2
16*	50	48	Tonal + Broadband	2

*WAV file included as attachment.

Finally, four pairs of fan noise were included, where each consisted of recorded noise compared against noise which was synthesized according to the current state of the art (without fluctuations in either the tonal or broadband component). A description of the configuration of the "time-invariant" pairs is included in Table 8. These pairs were intended to evaluate the increase in realism that accompanies the inclusion of time-domain variations in synthesized noise. These "time-invariant pairs" were also expected to add variability to paired comparisons, thereby avoiding listener fatigue.

Table 8. Configuration of "time-invariant" pairs included to evaluate improvement over the current state of the art and to avoid listener fatigue.

Pair ID	Emission Angle [degrees]	Engine Power [%]	Spectral Content (all sources time-invariant)	RQ
17*	50	87	Tonal	3/a/b
18*	50	87	Tonal + Broadband	3/a/b
19*	50	48	Tonal	3/a/b
20*	50	48	Tonal + Broadband	3/a/b

*WAV file included as attachment.

For cases where the total synthesized source (tonal and broadband) was required, broadband noise was synthesized using measured temporal fluctuations in each third-octave band, and then added to the synthesized tonal source. Fan-compressor interaction tones as described in Section 2.6 were removed from recordings using very narrow notch filters. For cases where tonal noise alone was required, narrow isolation filters as described earlier were applied to recordings to separate tones from broadband noise. All noise segments in all comparisons were high-pass filtered above 1,000 Hz to remove any influence of jet noise features which were dominant at low frequencies as predicted by ANOPP.

5.2.4 Elimination of Bias Effects

The order and presentation of paired comparisons were designed to address several sources of bias in test results. The following section details expected sources of bias, their expected effects on results, and the corresponding design factors which either eliminated or counterbalanced the effects.

When presented with a judgment scale, subjects tend to avoid the endpoints. This avoidance can be due to a desire to "save" extreme values for some hypothetical maximum judgment which the subject expects to encounter. It can also arise from a generally conservative approach to making judgments, where the subject does not expect that extreme ratings will actually be necessary. Bias due to avoidance was accounted for by inclusion of the 'baseline' comparisons, to identify the maximum score to be expected for nominally identical noise. For example, if subjects scored different segments of the same recording as 4.5 out of 5 on the similarity scale, then other analysis could use the 4.5 as a "perfect" rating rather than the scale maximum. A baseline score was calculated as a reference for each combination of power setting and spectral content.

Another well known source of error is called contraction bias [41]. Contraction bias arises because subjects tend to base the current judgment on previous judgments, and their impression of a particular noise is influenced by the impression of noises before it. A judgment directly after a very annoying noise, for example, is likely to be lower than it otherwise would have been as the subject expresses relief. In the current experiment, a judgment of a low power noise might be influenced by the high power noises before it, or evaluation of a very dissimilar pair might be influenced by the identical noise before it. Unfortunately, contraction bias is unavoidable since pairs must be presented to subjects in *some* order. For this reason, subjective testing methods were designed to *counterbalance* the effect of contraction bias by presenting each A-B comparison in reverse order at another time in the test. Any bias on a particular A-B comparison was expected to be opposite in

direction from the same bias on the B-A comparison, averaging out in the final analysis. The addition of reverse order comparisons doubled the total number of judgments to 40.

Subject learning and fatigue curves are other well-known sources of bias on subject judgments. Early in the test, subjects may enter inaccurate judgments due to unfamiliarity with the noises presented or the rating system. Later on in the test, response validity may be influenced as subjects grow accustomed to the test method or bored due to a tedious stimulus-response cycle. As the duration of a test increases, the more probable and severe the effects of fatigue bias become. Learning bias was eliminated in the current investigation by providing subjects with a training session before actual judgments were requested. Training sessions allowed subjects to become familiar with the noises presented, with the hardware in use, and with the rating scale available. Fatigue bias was avoided or minimized most significantly by creating a short test, and by splitting up the test into several sessions. The overall test consisted of four 15-minute sessions with short breaks in between, during which subjects were encouraged to leave their seats and walk around.

Learning and fatigue bias are not completely avoidable, so they were also counterbalanced by experimental design [41, 42]. A type of Balanced Latin Squares design was applied at the session level in the following way. Noises were divided into groups based on similar qualities (spectral content, power setting, source noise type), and equal numbers of each group were placed into four sessions (designated A, B, C, and D). Sessions were reordered to ensure that all comparisons in Session A, for example, were presented to some groups at the beginning of the test, to others near the end of the test, and to others in the middle. The design ensured that if one group's responses for a given session were influenced by learning or fatigue, then those effects were counterbalanced by the fact that other groups heard the same comparisons at a different part of the test. A table showing the order of sessions presented to each group is shown below in Table 9. Note that the addition of the last group required that the Latin Squares design be modified. A unique session presentation order was chosen and assigned to that group. The additional group meant that the experimental design was not perfectly balanced, but this was deemed acceptable in order to simplify and speed the experiment itself.

Finally, all test stimuli were presented to subjects at the same level (about 74 dB(A)), since the typical listener often uses that metric to discriminate sounds. WAV files were scaled to the same RMS value, and system gains were adjusted at several stages to achieve that goal.

Table 9. Presentation order of sessions A, B, C, and D to each group according to a modified Latin Squares design [42].

		Session			
		1	**2**	**3**	**4**
Group	**1**	A	C	B	D
	2	B	D	C	A
	3	C	A	D	B
	4	D	B	A	C
	5	A	D	C	B

5.3 Signal Presentation

Fan source noise segments were presented over headphones synchronously to all six subjects in each group. HEAD Acoustics headphone playback system (HPS) amplifiers were used for playback, each providing two headphone outputs. A photograph of several researchers posing as test subjects can be seen in Figure 52. In the rear of the room, an artificial head can be seen. The artificial head had microphones installed in its ears, and wore headphones to monitor the playback level during testing. A limiter system was employed on the signal as measured from the artificial head to ensure that test subjects would not be exposed to sound pressure levels in excess of 95 dB(A). The wiring diagram of the experimental hardware setup can be seen in Figure 53, and shows the signal path from the playback computer itself to the artificial head and each of the six subjects.

A preliminary investigation was conducted to assess whether the quality of subjects' responses improved when given the opportunity to hear a comparison more than once. Numerical results of the preliminary work showed significant effects only for tonal noise comparisons at low power settings when the pair was presented twice. For this reason, signals were presented in four second segments, with each pair presented twice in a row.

Figure 52. Six researchers posing as subjects in the testing room. The artificial head used to monitor signal levels can be seen behind the last row of seats. Photo by author.

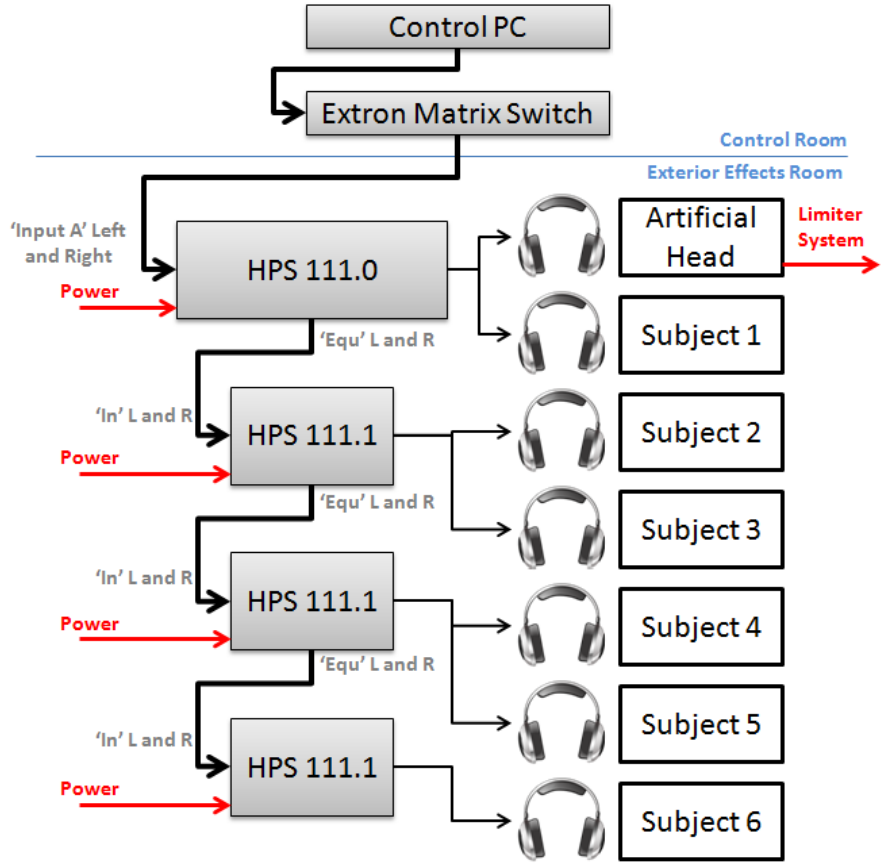

Figure 53. Wiring diagram of playback system for subjective evaluations. Test stimuli were presented simultaneously over headphones to six subjects.

Each comparison was presented to each of six listeners in a given group in the following manner. Tablet PC's were distributed to each study participant, and were running the CNoTE "Quizzer" application. First, a message appeared on each tablet screen with information about the upcoming comparison, as in Figure 54. Next, the first segment of the pair was played at the same time to all six listeners, while the image shown in Figure 55 was displayed. A one-second pause followed the first segment played, though communication delay over the wireless network often extended the time between segments to two or three seconds. After the pause between segments, the second segment was played to all six listeners while the image in Figure 56 was displayed. A two-second pause was inserted before repeating the same pair again, showing Figure 57 and Figure 58 at the appropriate times. At the conclusion of playback, the rating scale was presented to subjects. An image of the rating scale can be seen in Figure 59, along with the red tick mark used to verify the judgment. Subjects then entered their subjective judgment of the similarity between segments "A" and "B" on the tablet computers, using either their finger or a supplied stylus.

Figure 54. First Quizzer screen shown for each judgment during subjective testing.

Figure 55. Second Quizzer screen shown for each judgment during subjective testing.

Figure 56. Third Quizzer screen shown for each judgment during subjective testing.

Figure 57. Fourth Quizzer screen shown for each judgment during subjective testing.

Figure 58. Fifth Quizzer screen shown for each judgment during subjective testing.

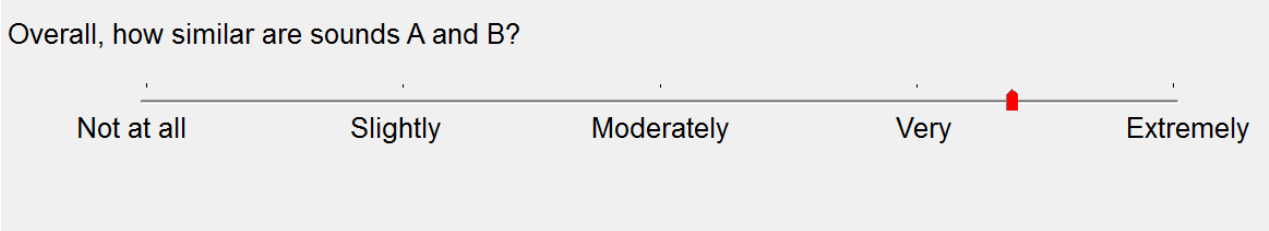

Figure 59. Quizzer screen with rating scale presented to listeners for each judgment during subjective testing.

To facilitate analysis, the verbal anchors on the rating scale were assigned numbers. The minimum score (corresponding to a similarity judgment of "Not at all") was 1, while the maximum score (corresponding to "Extremely") available on the scale was 5. Intermediate values were each anchored to integers, so "Slightly" corresponded to 2, "Moderately" to 3, and "Very" to 4. The total scale had 100 available divisions, and subjects were instructed that responses between verbal anchors were acceptable.

5.4 Results and Analysis

During the subjective testing, 30 subjects each made 40 judgments of the similarity between recorded and synthesized fan noise, for a total of 1200 responses. Analysis of numerical data focused on answering each of the three research questions outlined earlier. This section details calculation of mean response scores in each category, an ANOVA test conducted between response categories, and post-hoc analyses to further investigate significant observed differences.

5.4.1 Mean Similarity Response Scores

Recorded scores in each category were widely distributed over the available rating scale, but generally grouped around mean values. Mean scores for each category are summarized in Table 10. The results show that the mean judgment was 3.8 for recorded source tonal noise compared to synthesized tonal noise without fluctuations. When fluctuations were added to synthesized tones, the similarity score increased to 4.4. The 'baseline' score for tone-isolated recorded noise against another segment of the same recording was 4.5.

The bottom row of Table 10 describes mean similarity scores for comparisons when both the broadband noise and tonal components were included. For time-invariant pairs, no fluctuations were included on either the tonal component or the broadband noise third-octave band levels. The mean response for that category of comparisons was 4.1. When fluctuations in both tonal noise and third-octave band levels for broadband noise were included, the mean similarity score increased to 4.2. The baseline score for comparisons where a segment of recorded noise was compared to another segment of the same recording was 4.3.

Table 10. Summary of mean similarity scores for each comparison category

Spectral Content	Time-Invariant (fluctuations not included)	Target (time-varying; fluctuations included)	Baseline (nominally identical)
Tonal Only	3.8	4.4	4.5
Tonal + Broadband	4.1	4.2	4.3

5.4.2 Analysis of Variance (ANOVA)

Mean response scores did not give sufficient information to either describe the distribution of judgments or imply significant differences between them. Even considering departures from the baseline reference score by themselves did not give information about which sets of responses probably came from different populations. An ANOVA investigation was then conducted to gain confidence that differences observed in recorded means reflected differences in the underlying population responses to time-invariant and fluctuating noise.

Several one-way ANOVA tests were performed on results in each category of comparisons; for convenience, these categories are referred to as 'baseline', 'target', and 'time-invariant' comparisons. Each test compared the sample of judgments in one category against the sample of judgments in a different category with the same spectral characteristics. For example, one ANOVA

test sought to evaluate the hypothesis that "subjective judgments of target tonal comparisons do not have a significantly[10] different population mean than subjective judgments of baseline tonal comparisons." Each ANOVA test evaluated the hypothesis that categories elicited the same response, and returned a p-value which estimated the probability of measuring results at least as extreme as those observed (if the hypothesis was true). The p-value resulting from such an analysis is in the range from 0 to 1, where smaller values correspond to greater confidence that the population means are different.

In the subjective assessments discussed here, a 95% confidence threshold was used. Thus, when the ANOVA returned p-values less than 0.05, differences between the underlying populations of the categories compared were understood to be significant. Conversely, for p-values greater than 0.05, the underlying populations were said to be "not significantly different."

Comparison of each category against the others of the same spectral type generated the ANOVA results table in Table 11, where significantly different comparisons are denoted in red text. ANOVA results show that there were significant differences in the sample means of time-invariant and target pairs for tonal noise, as well as between time-invariant and baseline pairs for tonal noise. Notably, there were no significant differences ($p<0.05$) between target and baseline pairs for tonal noise, or between any two samples when the broadband source was included. The interpretation of these results is discussed in Section 5.4.4.

Table 11. Results of several one-way ANOVA analyses performed on the results of subjective evaluations.

Spectral Content	**Comparison of Responses**		**P-value**
	Category 1	**Category 2**	
Tonal Only	Time-Invariant	Target	0.006
	Target	Baseline	0.23
	Time-Invariant	Baseline	0.004
Tonal + Broadband	Time-Invariant	Target	1
	Target	Baseline	0.08
	Time-Invariant	Baseline	0.5

[10] "Significant" in this context refers to differences that are unlikely to arise between two samples from the same population, rather than differences of large magnitude.

5.4.3 Post-Hoc Analysis

To investigate the driving factors in each of the significant differences observed in ANOVA results in the previous section, a post-hoc analysis was conducted. The goal of post-hoc analysis was to find answers to research questions related to engine power setting (RQ 1a, RQ 3a). Each category in Table 11 was divided into subcategories which separated judgments made on low power settings from those made on high power settings. A summary of the results of post-hoc analyses can be seen in Table 12, where significant comparisons are shown in red. The results of post-hoc analysis show that significant differences in the sample means for both high and low power fan noises drive the observed differences. For the tonal and broadband source, no further significant differences were observed in post-hoc analyses.

Table 12. Summary of post-hoc ANOVA analyses to identify driving factors in significant differences between response categories.

Main Effects		**Multiple Pairwise Comparisons**		**P-value**
		Category 1	**Category 2**	
Tonal Only	High Power	Time-Invariant	Target	0.024
		Target	Baseline	1
		Time-Invariant	Baseline	0.04
	Low Power	Time-Invariant	Target	0.027
		Target	Baseline	0.4
		Time-Invariant	Baseline	0.013
Tonal + Broadband	High Power	Time-Invariant	Target	1
		Target	Baseline	0.09
		Time-Invariant	Baseline	0.24
	Low Power	Time-Invariant	Target	1
		Target	Baseline	0.46
		Time-Invariant	Baseline	1

5.4.4 Discussion of Subjective Evaluation Results

The comparison of *time-invariant* tonal noise against the baseline score indicated that subjects were able to confidently tell synthesized source noise from recordings. For tone-isolated fan noise, the mean score for judgments of the current (time-invariant) synthesis methods was significantly different and less than the mean score for baseline comparisons. That result indicated current synthesis methods without fluctuations in tonal parameters are *not* perceptually similar to recorded noise. The perceptual difference agreed with the hypothesis that average listeners can effectively discriminate noise which was synthesized without fluctuations from recordings.

The comparison of results for *time-varying* tonal noise against the baseline revealed that when modeled fluctuations in tonal amplitude and frequency were added, the resulting noise was not perceptually different from recordings. The mean score for time-varying synthesized noise (4.4) was only slightly less than the baseline (4.5), so that conclusion is supported.

When broadband noise was added, scores were much more uniformly distributed than those for the tonal source in isolation. The fact that no significant differences were found between responses for time-invariant tonal and broadband noise and time-varying tonal and broadband noise or between time-invariant tonal and broadband noise and the baseline comparisons shows that subjects were not able to hear differences. That is, there was no basis to conclude confidently that the mean scores for any comparisons of tonal and broadband noise came from different populations. In other words, the improvement in perceptual realism using the new time-variant synthesis method is reduced or eliminated by also including the broadband noise component.

The change in similarity ratings with the addition of broadband noise could be attributed to one of several sources. First, perhaps the tonal source simply wasn't the major discriminator for subjects in that context. The total fan noise source is complicated, so subjects could have been preoccupied with sorting out cues from broadband and tonal sources and didn't bother discriminating time variations in either component. Second, the broadband component might have masked fluctuations in tonal amplitudes or frequencies. Research is available to quantify the just-noticeable-differences (JND) for pure amplitude or frequency modulated tones [4]. Measured amplitude fluctuations were generally above the applicable JND for a 1 kHz pure tone, but the presence of the broadband noise source likely raised the minimum threshold to differentiate time-invariant from time-varying noise. Perhaps amplitude fluctuations which were often above the JND in isolation might not have been perceptible in the presence of significant broadband noise. Additional work is required to determine the threshold of broadband noise below which time-varying syntheses can be differentiated from time-invariant syntheses.

6 Discussion and Summary

The work summarized in this thesis sought to improve prediction-based fan noise synthesis methods by including short-term fluctuations. One major contribution of this work is the identification and implementation of useful methods for analyzing short-tem fluctuations in tone-dominated source noise. Broadband noise analysis methods were based on STFT techniques from previous work [25]. Secondly, this work developed a simple model for representing measured fluctuations according to two perceptually important parameters. Third, MATLAB tools were developed to synthesize general time-varying tonal and broadband noise sources. Those tools are capable of reproducing useful engine operations such as engine spool-ups or emission angle changes. The final contribution of this work is the completion of subjective listening tests to quantify the importance of including time-domain fluctuations in fan noise sources. Results from those tests may be used to justify the inclusion or exclusion of fluctuations from future simulations based on characteristics of the particular noise sources involved.

This chapter describes and evaluates the stated contributions with respect to the objectives detailed in Section 1.4. Where appropriate, methodological limitations and suggestions for future work are discussed.

6.1 Signals Analysis

The first objective of this work was the development of a reliable analysis methodology for extracting fluctuations in tonal amplitude and frequency as well as in third-octave band SPL of broadband noise. The analysis methodology generally performed well, and was aided by the ability to predict likely locations of tonal energy in the frequency domain. Knowledge of which tones were generated by fan mechanisms (and which were not) was an important part in several analysis stages. First, it dictated a correction applied to output from the broadband noise analysis stage where bins known to contain tonal energy were reset to more appropriate values. Second, it allowed tones generated by other mechanisms to be ignored during later synthesis stages and notched out of recordings during subjective evaluations.

The correction to instantaneous frequency in regions with low estimated SNR could be problematic for a source whose average tonal content is at or just above the surrounding level of

broadband noise. In this work, tonal measurements in the aft arc at all engine power settings contained significant regions of corrected instantaneous frequency. Fluctuation parameters measured in those regions might not apply well to recordings where a dominant tonal component was measured in the aft arc.

The analysis methods employed did not require that the signal be recorded from a turbofan engine. The analytic signal is a powerful representation of any real-valued signal, although the extracted instantaneous frequency only has a physical meaning when the signal only contains one component. That condition was met through application of the tone isolation filter before construction of the analytic signal.

It is important to note that the set of analysis tools was deliberately developed to be applicable to general aircraft source noise sets. For example, the same work could be performed on another component of turbofan-radiated noise (such as from the compressor or core), or on another vehicle source altogether. For example, simulation of other tone-dominated sources such as helicopters might benefit from the inclusion of short-term fluctuations. The only requirement is the availability of a clean set of recordings where fluctuations may be attributed to unsteady source characteristics rather than atmospheric or environmental uncertainties.

6.2 Characterization and Synthesis Methods

The second objective of this thesis was the development of synthesis tools capable of reproducing general time-varying tonal and broadband noise sources. Tonal synthesis was conducted by supplying parameters directly to the amplitude and frequency modulated model. The broadband synthesis method was designed to reproduce measured fluctuations in third-octave band levels using the overlap-add method. The two sources were then combined to obtain the total fan noise source. In order to synthesize the total turbofan engine source, the noise emission from multiple other generation mechanisms would have to be added. ANOPP could be used to supply predictions for mean parameters, and some assumptions could be made for using fluctuations based on the analysis summarized here.

In order to characterize the library of 6,016 extracted amplitude fluctuations and a matching number of frequency fluctuations, a simple model was developed. Psychoacoustic data which showed human response to the rate and depth of both amplitude and frequency was used to justify the model. Each fluctuation, regardless of its nature, was represented as a bandlimited random process.

The first parameter which characterized the process was the cutoff frequency of a fit filter response in the frequency domain, while the second was the measured variance of the fluctuation. The variance could have alternately been obtained by finding the value of the autocorrelation function evaluated at zero lags.

The choice of a 3rd order Butterworth filter magnitude response function as the prototype for the frequency domain fit was not motivated by any physical model of the generation mechanisms. Rather the power spectral density of observed fluctuations in both amplitude and frequency displayed a bandlimited shape, with a (generally) flat region up to about 12 Hz and a roll-off characteristic above that. These two facts motivated selection of the Butterworth filter due to its maximally flat passband and linear roll-off characteristics. In addition, the magnitude response was an intuitive and simple equation to implement in the minimization of RMS deviation between measured and modeled PSD shapes.

The measurements made and conclusions about the spectral shape of tonal fluctuations only apply to the EVNERT data set which was analyzed. It is not known if those characteristics will also describe other data sets, including other EVNERT conditions not analyzed e.g. configurations with liners. This uncertainty is partially due to the relative scarcity of high-quality recordings of full scale aircraft engines. Most available data consists of third-octave band spectra obtained from long term time averages. Often, far-field microphone array data measured in quiet environments for useful engine configurations is difficult to obtain. Second, the TECH977 engine was mounted in a test stand while recordings were obtained; the only flow through the engine was directly due to intake rather than the forward movement of the nacelle as would be typical at a flight condition. As a result, it is unclear if differences in blade loading or turbulent flow would induce tonal fluctuations of a different character. Until such data becomes available for analysis, conclusions are not possible. However, the analysis and characterization steps were designed to be easily adapted to new data sets.

Besides verification that measured fluctuations were indeed audible, no efforts were made to characterize *which* fluctuations were responsible for that impression. Just noticeable differences for amplitude and frequency fluctuation rate and depth could be important discriminating or generalizing factors for future models of fluctuating tonal noise. Further, it might be that the rate and depth of fluctuations are only perceptually important on a coarse scale. One value of bandwidth and variance each might be sufficient to characterize *all* measured modulations in frequency and amplitude. Additionally, the inclusion of other aircraft noise sources, such as broadband airframe noise, might further obscure fluctuations in tonal noise from the turbofan inlet during an actual flyover.

The current investigation used linear interpolations between measured model parameters as inputs for synthesis. Specification of parameters at several "waypoints" in time allowed the synthesis routines to create practically useful source noise simulations. Most flyover simulations use source noise simulation whose emission angle and/or power setting depend on time. It would be more useful in the future to calculate the bandwidth and variance of modeled fluctuations as a direct function of those operational conditions. That change would allow simulation programs more intuitive control over source noise synthesis for the fluctuating tones, rather than evaluation of models which provide only fluctuation parameters for input.

6.3 Subjective Listening Tests

The third and final goal of this work was to conduct subjective listening tests to verify that the inclusion of short-term fluctuations produced more realistic source noise. Overall, subjective listening tests indicated that tonal fluctuations are indeed an important part of perceived realism for tone-dominated sources, and that the developed analysis/ modeling/ synthesis chain is capable of producing realistic fluctuations. The tests revealed that synthesized tonal source noise without fluctuations is not perceptually realistic, a conclusion which is supported by noting the significant difference between subjective responses for time-invariant tonal noise and the baseline for that category. The tests also revealed that the presence of a broadband noise source (with or without measured fluctuations in third-octave band levels) created realistic source noise without regard to the inclusion of tonal fluctuations. It was hypothesized that either the total source was too complex for tonal fluctuations to be a discriminating factor, or the broadband noise source had some type of masking effect over tonal fluctuations. Perhaps the relative difference between levels of tonal and broadband noise might play a role. Identifying some threshold of broadband noise which masks tonal fluctuations would be useful as justification for either including or excluding fluctuations.

Several lessons were learned from difficulties in designing subjective tests. Realism proved to be a difficult quality to define, since most typical listeners do not have everyday experience with aircraft noise sources in isolation. The solution was to indirectly evaluate realism by posing the question "how similar is the synthesized noise to real noise?" Future subjective tests should take into account whatever practical experience subjects have with the noise in question. In the case of evaluating the realism of an entire flyover event, the question "how realistic does that sound" may actually be appropriate.

Further, the variable rating scale available to subjects proved to be a source of some difficulty. The varying association each subject made with the verbal anchors was unclear. Perhaps some listeners defined "not at all similar" as two wholly different noises, whereas other listeners defined it with reference to the range of stimuli presented. Leaving scale interpretation up to the subjects introduced an undesired element of variability into results. Perhaps future tests for realism should limit possible responses to binary values, or at least restrict them to definite, definable categories.

In the future it may be desirable to evaluate simulated source noise in the full context of a flyover event. The atmospheric effects noted earlier in that case would significantly alter the source noise that the listener hears. For example, propagation through the atmosphere tends to attenuate high frequency noises, an effect which increases significantly with distance. As a consequence, high-frequency cues would be less useful to the listener. High frequency tones will often be attenuated below the noise floor of the environment, so fluctuations in those tones would of course not be audible. It is proposed that the synthesis of realistic fluctuations in tonal noise would then become even less demanding – perhaps to the point that simply including *some* audible fluctuations is enough to convince the listener.

References

[1] FAA, "Part 36 - Noise Standards: Aircraft Type and Airworthiness Certification," in *14 CFR 36*, 2012.

[2] FAA, "Part 150 - Airport Noise Compatibility Planning," in *14 CFR 150*, 2012.

[3] Bennet, R.L. and Pearsons, K.S., "Handbook of Aircraft Noise Metrics," NASA CR-3406, 1981.

[4] Zwicker, E. and Fastl, H., *Psychoacoustics: Facts and Models*, 2nd Edition ed. Heidelberg, Springer-Verlag, 1999.

[5] Huff, D.L., "Noise Reduction Technologies for Turbofan Engines," NASA TM 2007-214495, 2007.

[6] Beranek, L.L., "Unsolved Military Noise Problems," *The Journal of the Acoustical Society of America*, Vol. 24, No. 6, pp. 769-772, 1952.

[7] Laurenzo, R., "Hushing the Roar of Air Traffic Growth," in *Aerospace America*: American Institute of Aeronautics and Astronautics, 2006, pp. 38-42.

[8] Hubbard, H.H., "Aeroacoustics of Flight Vehicles - Theory and Practice. Volume 2: Noise Control," NASA TR 90-3052, 1991.

[9] Nickol, C., "Environmentally Responsible Aviation (ERA) Project: Assessing Progress Toward Simulataneous Reductions in Noise, Fuel Burn and NOx," in *AIAA 2010 Conference*. Orlando, FL: National Institute of Aeronautics and Astronautics, 2010.

[10] Airbus, "Airbus Global Market Forecast 2011-2030," Blagnac Cedex, France 2011.

[11] "Global Traffic Forecast 2006-2025 ": Airports Council International, 2007.

[12] Boeing, "Boeing Current Market Outlook 2011-2030," 2011.

[13] Hubbard, H.H., "A Survey of the Aircraft-Noise Problem with Special Reference to its Physical Aspects," NACA-TN-2701, 1952.

[14] Sharland, I.J., "Sources of Noise in Axial Flow Fans," *Journal of Sound and Vibration*, Vol. 1, No. 3, pp. 302-322, 1964.

[15] Benzakein, M.J., Claes, H.P., Coward, W.E., Hochheiser, R.M., Kazin, S.B., and Knott, P.R., "Fan/Compressor Noise Research, Volume I - Detailed Discussion," Federal Aviation Administration, FAA-RD-71-85, 1971.

[16] Raney, J.P., "Research Needs in Aircraft Noise Prediction," NASA, NASA TM X-82787, 1975.

[17] Zorumski, W.E., "Aircraft Noise Prediction Program Theoretical Manual," NASA TM-83199, Part 1, 1982.

[18] Kontos, K.B., Janardan, B.A., and Gliebe, P.R., "Improved NASA-ANOPP Noise Prediction Computer Code for Advanced Subsonic Propulsion Systems " National Aeronautics and Space Administration NASA CR-195480, 1996.

[19] Lopes, L.V. and Burley, C.L., "Design of the Next Generation Aircraft Noise Prediction Program: ANOPP2," *17th AIAA/CEAS Aeroacoustics Conference*, Portland, OR, 6-8 June, 2011.

[20] McCurdy, D.A. and Grandle, R.E., "Aircraft Noise Synthesis System," National Aeronautics and Space Administration NASA TM-89040, 1987.

[21] Rizzi, S.A., Sullivan, B.M., and Sandridge, C.A., "A Three-Dimensional Virtual Simulator for Aircraft Flyover Presentation," *International Conference on Auditory Display*, Boston, MA, USA, 2003.

[22] Hubbard, H.H. and Powell, C.A., "Acoustic Facilities for Human Factors Research at NASA Langley Research Center," NASA TM-81975, 1981.

[23] Pulkki, V., "Virtual Sound Source Positioning Using Vector Base Amplitude Panning," *J. Audio. Eng. Soc.*, Vol. 45, No. 6, pp. 456-466, 1997.

[24] Shepherd, K.P., "The Effect of the Duration of Jet Aircraft Flyover Sounds on Judged Annoyance," NASA CR-159132, 1979.
[25] Grosveld, F.W., Sullivan, B.M., and Rizzi, S.A., "Temporal Characterization of Aircraft Noise Sources," in *Aerospace Sciences Meeting and Exhibit*. Reno, Nevada, 2004.
[26] "Tfan-schematic-kk-20050816.png," 2005. Khan, K., Retrieved 04-12-2012,<http://upload.wikimedia.org/wikibooks/en/8/84/Tfan-schematic-kk-20050816.png>. Reproduced under terms of the GNU Free Documentation License.
[27] Heidmann, M.F., "Interim Prediction Method for Fan and Compressor Source Noise," NASA TM X-71763, 1979.
[28] Hough, J.W. and Weir, D.S., "Aircraft Noise Prediction Program (ANOPP) Fan Noise Prediction for Small Engines," NASA CR-198300, 1996.
[29] Hubbard, H.H., "Aeroacoustics of Flight Vehicles - Theory and Practice. Volume 1: Noise Sources," NASA TR-90-3052, 1991.
[30] Weir, D., ed., "Engine Validation of Noise and Emission Reduction Technology Phase I," NASA CR-2008-215225, 2008.
[31] Weir, D.S. and Mendoza, J.M., "Baseline Noise Measurements from the Engine Validation of Noise and Emissions Reduction Technology Program," *14th AIAA/CEAS Aeroacoustics Conference*, Vancouver, British Columbia Canada, 5-7 May, 2008.
[32] MathWorks, "Curve Fitting Toolbox User's Guide," The MathWorks, Inc., Natick, MA 2012.
[33] Gabor, D., "Theory of Communication. Part 1: The analysis of information," *Journal of the Institution of Electrical Engineers - Part III: Radio and Communication Engineering*, Vol. 93, No. 26, pp. 429-441, 1946.
[34] Costain, J.K. and Coruh, C., *Basic Theory of Exploration Seismology*. Oxford, Elsevier, 2004.
[35] Boashash, B., "Estimating and Interpreting the Instantaneous Frequency of a Signal - Part 1: Fundamentals," *Proceedings of the IEEE*, Vol. 80, No. 4, pp. 520-538, 1992.
[36] MathWorks, "Signal Processing Toolbox User's Guide," The Mathworks, Inc., Natick, MA 2012.
[37] Leon-Garcia, A., *Probability, Statistics, and Random Processes for Electrical Engineering*. Upper Saddle River, NJ, Pearson Prentice Hall, 2009.
[38] Zolzer, U., ed., *DAFX: Digital Audio Effects*. West Sussex, England, John Wiley & Sons, 2002.
[39] Rizzi, S.A. and Sullivan, B.M., "Synthesis of Virtual Environments for Aircraft Community Noise Impact Studies," *11th AIAA/CEAS Aeroacoustics Conference*, Monterey, CA, 2005.
[40] MathWorks, "MATLAB Mathematics," MathWorks, Natick, MA 2012.
[41] Bech, S. and Zacharov, N., *Perceptual Audio Evaluation: Theory, Method and Application*. West Sussex, England, John Wiley & Sons, 2006.
[42] Montgomery, D.C., *Design and Analysis of Experiments*, 5 ed. Hoboken, NJ, John Wiley & Sons, 2001.

Appendix A – EVNERT TECH977 Test Configurations

Table 13. Test conditions for which TECH977 engine noise was recorded. The baseline configuration (19) analyzed in this investigation is highlighted in green.

Config	Date	Engine				Acoustic Sensors			Barrier	
		Name	Fan	Inlet	Bypass	32-mic, 100-ft	16+7-mic, 100-ft	internal+8 -mic	Covers Inlet	Covers Exhaust
13	9/21/2005 and 9/23/2005	Tech977	Baseline	15 Rayl	Full Treatment	X	X			
14	9/23/2005	Tech977	Baseline	15 Rayl	Full Treatment	X	X			X
15	9/24/2005	Tech977	Baseline	10 Rayl	Full Treatment	X	X			X
16	9/24/2005	Tech977	Baseline	10 Rayl	Full Treatment	X	X			
17	9/26/2005	Tech977	Baseline	aft 2/3 - 10 Rayl	Full Treatment	X				X
18	9/28/2005	Tech977	Baseline	aft 1/3 - 10 Rayl	Full Treatment	X				X
19	9/28/2005	Tech977	Baseline	Hardwall	Full Treatment	X				X
20	9/29/2005	Tech977	Baseline	15 Rayl	Full Treatment	X			X	
21	9/29/2005	Tech977	Baseline	15 Rayl	all CD trt, HW Nzl	X			X	
22	9/30/2005	Tech977	Baseline	15 Rayl	fwd 1/2 CD Trt, HW Nzl	X			X	
23	9/30/2005	Tech977	Baseline	15 Rayl	HW CD, HW Nzl	X			X	
24	Not Used									
25	10/1/2005	Tech977	Baseline	Hardwall	HW CD, HW Nzl	X	X			
26	10/1/2005	Tech977	Baseline	port side 1/2 - 15 Rayl	Full Treatment	X	X			X
27	10/3/2005	Tech977	Baseline	15 Rayl	Full Treatment	X	X			X
28	10/3/2005	Tech977	Baseline	15 Rayl	Full Treatment	X	X			

Appendix B – 1/3 Octave Band Limits

Table 14. List of nominal third-octave band limits used for broadband analysis.

Nominal Third-Octave Band Limits [Hz]			
Band Number	**Lower Limit**	**Center Frequency**	**Upper Limit**
9	7.1	8	8.9
10	8.9	10	11.2
11	11.2	12.5	14.1
12	14.1	16	17.8
13	17.8	20	22.4
14	22.4	25	28.2
15	28.2	31.5	35.5
16	35.5	40	44.7
17	44.7	50	56.2
18	56.2	63	70.8
19	70.8	80	89.1
20	89.1	100	112
21	112	125	141
22	141	160	178
23	178	200	224
24	224	250	282
25	282	315	355
26	355	400	447
27	447	500	562
28	562	630	708
29	708	800	891
30	891	1000	1122
31	1122	1250	1413
32	1413	1600	1778
33	1778	2000	2239
34	2239	2500	2818
35	2818	3150	3548
36	3548	4000	4467
37	4467	5000	5623
38	5623	6300	7079
39	7079	8000	8913
40	8913	10000	11220
41	11220	12500	14130
42	14130	16000	17780
43	17780	20000	22390

Appendix C – List of Attachments

Table 15. List of files associated with this thesis document. ID numbers correspond to those used during subjective listening tests.

Filename	Description
Spool_Up_45_deg.wav	Power setting changes from 48% to 87% over 10 seconds. Modeled fluctuations included.
Dir_Change_48_pct.wav	Emission angle changes from 5° to 160° over 10 seconds. Modeled fluctuations included.
ID5_TV_87_pct_Tonal.wav	Tonal synthesis at 87% power setting, 50° emission angle. Modeled fluctuations on tonal noise.
ID6_TV_87_pct_Tonal_Plus_Broadband.wav	Tonal synthesis at 87% power setting, 50° emission angle. Modeled fluctuations on tonal noise, measured fluctuations on broadband noise.
ID7_TV_48_pct_Tonal.wav	Tonal synthesis at 48% power setting, 50° emission angle. Modeled fluctuations on tonal noise.
ID8_TV_48_pct_Tonal_Plus_Broadband.wav	Tonal synthesis at 48% power setting, 50° emission angle. Modeled fluctuations on tonal noise, measured fluctuations on broadband noise.
ID13_Rec_87_pct_Tonal.wav	Tone-isolated recording at 87% power setting, 50° emission angle.
ID14_Rec_87_pct_Tonal_Plus_Broadband.wav	Recording at 87% power setting, 50° emission angle.
ID15_Rec_48_pct_Tonal.wav	Tone-isolated recording at 48% power setting, 50° emission angle.
ID16_Rec_48_pct_Tonal_Plus_Broadband.wav	Recording at 48% power setting, 50° emission angle.
ID17_TI_87_pct_Tonal.wav	Tonal synthesis at 87% power setting, 50° emission angle. No fluctuations on tonal noise.
ID18_TI_87_pct_Tonal_Plus_Broadband.wav	Synthesis at 87% power setting, 50° emission angle. No fluctuations on tonal or broadband noise.
ID19_TI_48_pct_Tonal.wav	Tonal synthesis at 48% power setting, 50° emission angle. No fluctuations on tonal noise.
ID20_TI_48_pct_Tonal_Plus_Broadband.wav	Synthesis at 48% power setting, 50° emission angle. No fluctuations on tonal or broadband noise.
TonalSynthesis.m	MATLAB file used to synthesize tonal noise with or without fluctuations
BroadbandSynthesis.m	MATLAB file used to synthesize broadband noise with or without fluctuations in third-octave band levels.
Synthesis_Functions.zip	Several low-level functions needed to run BroadbandSynthesis.m and TonalSynthesis.m
Example_BroadbandSynthesis_Call.m	MATLAB script which describes inputs and outputs for BroadbandSynthesis.m
Example_TonalSynthesis_Call.m	MATLAB script which describes inputs and outputs for TonalSynthesis.m